Journal of Nonlinear Science (2020) 30:2613–2669
https://doi.org/10.1007/s00332-020-09631-y

Journal of Nonlinear Science

Spike-Adding Canard Explosion in a Class of Square-Wave Bursters

Paul Carter[1]

Received: 20 May 2018 / Accepted: 18 April 2020 / Published online: 14 May 2020

Abstract
This paper examines a spike-adding bifurcation phenomenon whereby small-amplitude canard cycles transition into large-amplitude bursting oscillations along a single continuous branch in parameter space. We consider a class of three-dimensional singularly perturbed ODEs with two fast variables and one slow variable and singular perturbation parameter $\varepsilon \ll 1$ under general assumptions which guarantee such a transition occurs. The primary ingredients include a cubic critical manifold and a saddle homoclinic bifurcation within the associated layer problem. The continuous transition from canard cycles to N-spike bursting oscillations up to $N \sim \mathcal{O}(1/\varepsilon)$ spikes occurs upon varying a single bifurcation parameter on an exponentially thin interval. We construct this transition rigorously using geometric singular perturbation theory; critical to understanding this transition are the existence of canard orbits and slow passage through the saddle homoclinic bifurcation, which are analyzed in detail.

Keywords Bursting oscillations · Spike-adding · Canards · Geometric singular perturbation theory · Saddle-homoclinic bifurcation

Mathematics Subject Classification 34C25 · 34E17 · 34D15 · 37G15 · 92B25

1 Introduction

The phenomenon of bursting has been widely studied in models of neurons and neuroendocrine cells, as well as other excitable media, including physical systems such as semiconductor lasers (Al-Naimee et al. 2009; Ruschel and Yanchuk 2017), or in chemical reactions (Rinzel and Troy 1982). These solutions are characterized by alternation

Communicated by Paul Newton.

✉ Paul Carter
pcarter@umn.edu

[1] School of Mathematics, University of Minnesota, Minneapolis, USA

between slow quiescent phases and active bursting phases comprised of a sequence of action potentials or spikes and can be time periodic or aperiodic. One of the earliest models was introduced by Chay and Keizer (1983) to describe bursting dynamics in pancreatic beta cells, which formed the basis in Rinzel (1985), Rinzel (1987) for analyzing the bursting phenomenon in the context of singularly perturbed, or fast–slow, ordinary differential equations. This has since been a primary mathematical formulation for understanding bursting in numerical and analytical studies. In this context, bursting solutions can frequently arise as periodic orbits, in which the active phase is governed by oscillations on the fast timescale, and the quiescent phase is associated with drift along a slow manifold.

A feature which is prevalent in many bursting models is that of spike-adding, in which variation in system parameters can result in additional spikes during the bursting phase. This has been demonstrated and analyzed numerically in a variety of bursting models (Desroches et al. 2016a, 2013; Guckenheimer and Kuehn 2009; Linaro et al. 2012; Nowacki et al. 2012; Osinga and Tsaneva-Atanasova 2010; Tsaneva-Atanasova et al. 2010). In particular, these studies find that bursting solutions with different numbers of spikes can exist in nearby parameter regimes and furthermore that different branches of spiking solutions can be connected, so that a bursting orbit with N spikes can be continuously deformed into one with $N + 1$ (or more) spikes upon parameter continuation. Spike-adding has been shown to occur when varying the location of an equilibrium (Desroches et al. 2013; Osinga and Tsaneva-Atanasova 2010), or when varying the singular perturbation parameter itself (Guckenheimer and Kuehn 2009; Lee and Terman 1999; Terman 1991; Tsaneva-Atanasova et al. 2010). In many cases, this behavior has been intimately linked to the phenomenon of canards (Dumortier and Roussarie 1996; Eckhaus 1983; Krupa and Szmolyan 2001b): For instance, canard dynamics have been analyzed in relation to spike-adding in square-wave neuronal bursting models with one slow variable, such as the Morris–Lecar–Terman model (Guckenheimer and Kuehn 2009; Morris and Lecar 1981; Rinzel and Ermentrout Rinzel and Ermentrout; Terman 1991) and the Hindmarsh–Rose model (Hindmarsh and Rose 1982, 1984; Linaro et al. 2012), in which a canard explosion of periodic orbits is responsible for the onset of spike-adding (Desroches et al. 2013, §III). In systems with two slow variables, the role of folded singularities and their associated canard dynamics have been analyzed in relation to spike-adding in parabolic bursting models such as the Plant model of bursting in the Aplysia ganglion R15 cell (Desroches et al. 2016a; Plant and Kim 1975) and in the study of mixed-mode bursting oscillations (Desroches et al. 2013).

In many contexts, canard solutions provide a mechanism whereby small parameter changes can produce continuous transitions between globally distinct solutions, for example in the classical planar canard explosion (Krupa and Szmolyan 2001b), or in transitions between different traveling pulse solutions in the FitzHugh–Nagumo system of nerve impulse propagation (Carter and Sandstede 2018). In this spirit, this paper aims to rigorously analyze the link between canard explosion and the spike-adding phenomenon in an example class of square-wave bursting models and identify general techniques which can be used in the analysis of similar global transitions in singular perturbation problems. We focus on one of the simpler, well-studied geometric descriptions of square-wave bursting with one slow variable, introduced and

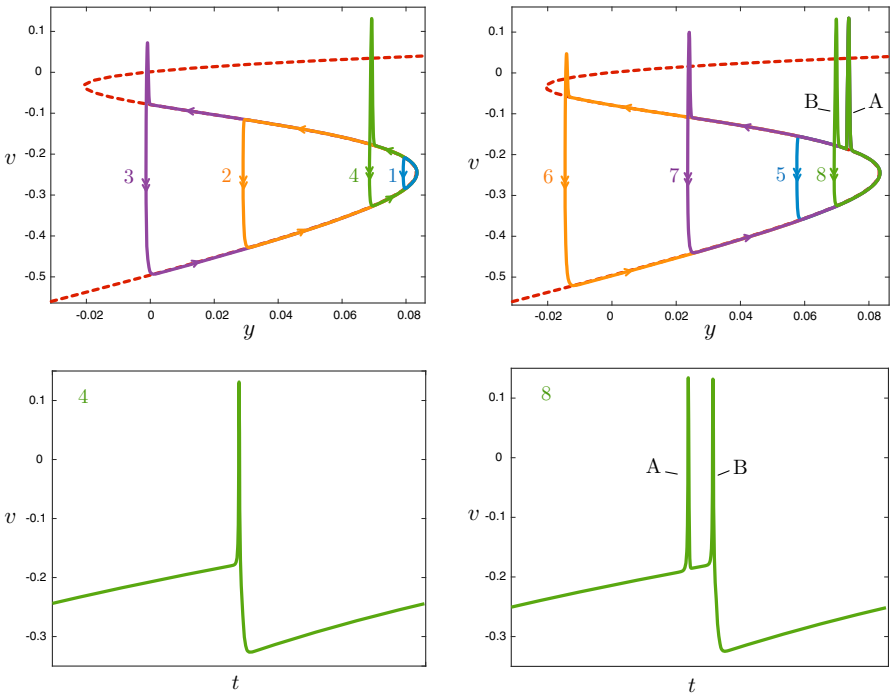

Fig. 1 Shown is the continuous spike-adding transition in (1.1) for $\varepsilon = 0.001$ obtained in AUTO; all solutions exist for values of $k \approx -0.0002$ on an interval of width $\mathcal{O}(e^{-1/\varepsilon})$. The upper left panel shows the transition sequence labeled 1–4 from small-amplitude canard orbits (blue label 1) to a 1-spike bursting solution (green label 4), and the critical manifold $\mathcal{M}$ is shown in dashed red. The lower left panel depicts the v profile for the 1-spike solution. The upper right panel shows the transition sequence labeled 5–8 from a 1-spike bursting solution to a 2-spike bursting solution (green label 8). The solutions labeled 5–8 all traverse the spike labeled A. The second spike is grown from right to left until reaching the upper fold $\mathcal{F}^{\ell}$, where it turns back (see solution with orange label 6) and continues from left to right to solution 7 before finally being deposited at the spike labeled B, culminating in a 2-spike bursting solution (green label 8); the v profile for the 2-spike solution is shown in the lower right panel (Color figure online)

analyzed by Terman (1991), which includes the Morris–Lecar model below as a primary motivating example. Our interest lies in the spike-adding process that is induced by a canard explosion when adjusting a parameter which controls the location of an equilibrium of the system. Although we are concerned with Terman's geometric formulation in this work, we note that square-wave bursters with different geometries, such as the Hindmarsh–Rose model, exhibit a similar transition from canard explosion to spike-adding bursting oscillations (Desroches et al. 2013).

The Morris–Lecar system (Morris and Lecar 1981)

$$\begin{aligned}\dot{v} &= y - 0.5\,(v + 0.5) - 2w\,(v + 0.7) - m_*(v)\,(v - 1)\\ \dot{w} &= 1.15\,(w_*(v) - w)\,\tau(v)\\ \dot{y} &= \varepsilon(k + \bar{k}_r - v)\end{aligned}$$

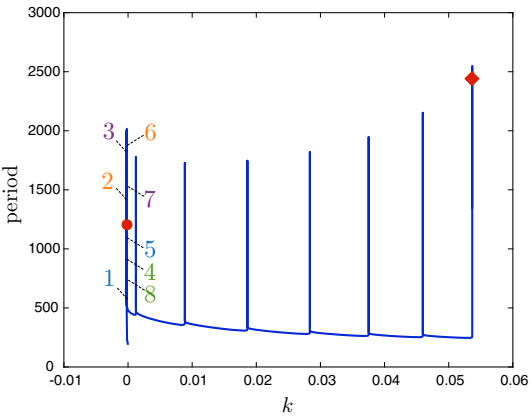

Fig. 2 Bifurcation diagram of spike-adding sequence of bursting oscillations, obtained numerically in (1.1) for $\varepsilon = 0.001$. Here, the period is plotted versus the bifurcation parameter k, along with the locations of the bursting orbits from Fig. 1 labeled 1–8, as well as the orbit from Fig. 5 (red circle) and the orbit from Fig. 6 (red diamond) (Color figure online)

$$w_*(v) = \frac{1}{2}\left(1 + \tanh\left(\frac{v-0.1}{0.145}\right)\right), \quad m_*(v) = \frac{1}{2}\left(1 + \tanh\left(\frac{v+0.01}{0.15}\right)\right),$$
$$\tau(v) = \cosh\left(\frac{v-0.1}{0.29}\right), \tag{1.1}$$

was originally proposed as a model of electrical activity in barnacle muscle fibers. In that context, v is interpreted as membrane potential, w is fraction of open potassium ion channels, and y is related to the near-membrane calcium concentration. The quantity $k + \bar{k}_r$ determines the equilibrium potential corresponding to potassium conductance. We identify (1.1) as being among the simplest examples of onset of spike-adding of bursting oscillations through canard explosion. Figure 1 depicts the transition from local canard explosion to large-scale bursting oscillations, obtained numerically in (1.1) for $\varepsilon = 0.001$. The lower panels show the v-profiles of bursting oscillations with 1 and 2 spikes in bursting phase; all solutions along the transition from local canard explosion born at a Hopf bifurcation to large-amplitude bursting oscillations were found along the same branch in parameter space and were obtained in the numerical continuation software AUTO upon varying the parameter k for fixed $\varepsilon = 0.001$. Figures 2 and 3 depict numerically computed bifurcation diagrams of the spike-adding process, labeled with the locations of the orbits from Fig. 1. We note that all of these orbits occur at very nearby (exponentially close) values of the parameter k.

In Terman (1991), Terman developed general assumptions in a class of three-dimensional ODEs which ensure that the geometry of the equations is qualitatively similar to that of (1.1). This formed the basis for the analysis of bursting solutions of the system (1.1) in Lee and Terman (1999), Terman (1991), Terman (1992) using geometric methods, and later using Conley index techniques (Kinney 2000, 2008). See Fig. 4 for a visualization of the singular limit geometry. The primary features are a cubic critical manifold $\mathcal{M}$ with three branches: an attracting bottom branch $\mathcal{M}^b$, a saddle-type middle branch $\mathcal{M}^m$, and upper branch $\mathcal{M}^u$ (typically repelling). In the fast layer dynamics for a value of $y = \bar{y}_{\mathrm{h}}$, the system undergoes a saddle homoclinic bifurcation along the middle branch, from which bifurcates a family $\mathcal{P}$ of periodic orbits

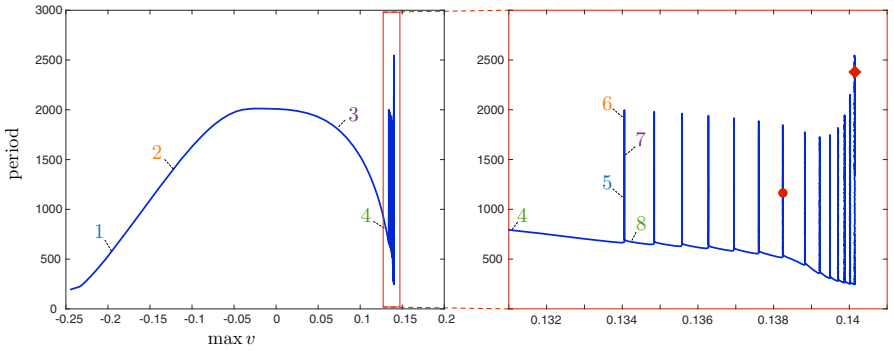

Fig. 3 (Left) Bifurcation diagram of spike-adding sequence of bursting oscillations, obtained numerically in (1.1) for $\varepsilon = 0.001$. Here, the period is plotted versus the maximum v value obtained over one period. The period wiggles back and forth as max v increases, as each spike is continually added along the transition. A zoom of the upper portion of the spike-adding bifurcation curve is plotted in the right inset. Also shown are the locations of the bursting orbits from Fig. 1 labeled 1–8, as well as the orbit from Fig. 5 (red circle) and the orbit from Fig. 6 (red diamond) (Color figure online)

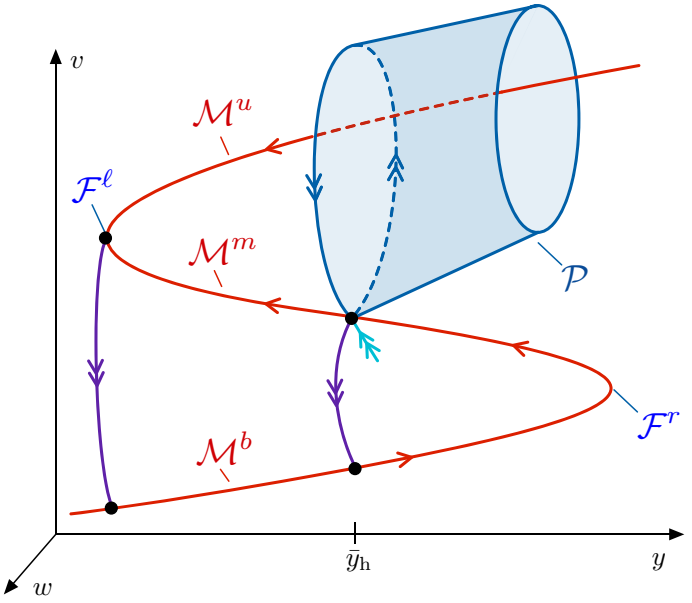

Fig. 4 Shown is the singular limit geometry for the class of square-wave bursting models considered by Terman (1991). The cubic critical manifold admits three branches: $\mathcal{M}^u$ (repelling), $\mathcal{M}^m$ (saddle-type), and $\mathcal{M}^b$ (attracting). There are two folds: $\mathcal{F}^\ell$ (classical fold) and $\mathcal{F}^r$ (canard point). In the fast layer dynamics, there is a saddle homoclinic bifurcation at $y = \bar{y}_\mathrm{h}$, which results in a family of periodic orbits $\mathcal{P}$ for $y > \bar{y}_\mathrm{h}$

for $y > \bar{y}_\mathrm{h}$. The cubic critical manifold also admits two fold points: one of classical fold type ($\mathcal{F}^\ell$) and one of canard type ($\mathcal{F}^r$); in (1.1), the constant $\bar{k}_r$ denotes the v-coordinate of the fold $\mathcal{F}^r$, which can be approximated numerically as $\bar{k}_r \approx -0.2449$.

The fold points and the saddle homoclinic bifurcation are the key pieces (and main technical challenges) to understanding the spike-adding transitions in this setting.

The spike-adding sequence is then generated as follows (Fig. 1 for sample periodic orbits along the transition in the Morris–Lecar system (1.1) obtained using AUTO). At the lower right fold, $\mathcal{F}^r$ are born small-amplitude canard orbits; see, for example, the blue orbit in the left panel of Fig. 1. As the parameter k is varied on an exponentially thin interval, the orbits grow into large-amplitude canards until reaching the upper left fold $\mathcal{F}^\ell$, though when continuing along the repelling upper branch $\mathcal{M}^u$, eventually they begin to interact with the family $\mathcal{P}$ of periodic orbits. The number of spikes in a given bursting solution is determined by the number of excursions around the upper branch $\mathcal{M}^u$, and the family of periodic orbits $\mathcal{P}$ allows for many such excursions. In particular, passing near the saddle homoclinic bifurcation allows for a fast spike which follows the singular homoclinic orbit to be "deposited," while the growth continues back along the middle branch $\mathcal{M}^m$ toward the fold, and back to the saddle homoclinic bifurcation to deposit another spike, and so on. Figure 5 depicts a bursting solution obtained numerically in (1.1) after many such spike-adding events by continuing numerically in parameter space from the local canard explosion at the fold $\mathcal{F}^r$. The fact that the slow portion of the bursting orbits passes near the lower fold from an attracting slow manifold to a saddle slow manifold (i.e., along a canard segment) is what allows each successive spike-adding event to take place within an exponentially thin interval of the parameter k; this also explains the proximity of these solutions in the bifurcation diagram in Fig. 2.

Remark 1.1 If the manifold $\mathcal{P}$ extends beyond the fold point $\mathcal{F}^r$—as is the case in (1.1)—then outside the canard regime, that is, once the equilibrium has moved up onto the middle branch, Terman showed in Terman (1991) that the system admits relaxation-type bursting oscillations which follow the bottom branch $\mathcal{M}^b$ and then jump off the fold point $\mathcal{F}^r$ up to the manifold $\mathcal{P}$, completing excursions around $\mathcal{P}$ until finally jumping back down to $\mathcal{M}^b$; see Fig. 6 for an example bursting orbit in this regime computed numerically for (1.1). In fact, numerical studies have demonstrated that spike-adding persists in this regime (Guckenheimer and Kuehn 2009); see also the bifurcation diagrams in Figs. 2 and 3, in which all of the bursting orbits, including the relaxation-type bursting oscillations as in Fig. 6, are contained on the same continuous spike-adding branch, though no longer at exponentially close values of the parameter k, as these orbits lie outside the canard explosion regime. Such orbits, however, do still contain "canard-like" segments along the saddle-type middle branch $\mathcal{M}^m$ of the slow manifold.

The aim of this work is to analyze the canard explosion regime in detail for $0 < \varepsilon \ll 1$ and rigorously construct the spike-adding sequence from small-amplitude canard cycles to bursting solutions with an $\mathcal{O}(1/\varepsilon)$ number of spikes. We will show that this transition occurs along a single continuous branch under exponentially small variations in the single bifurcation parameter k for fixed ε. The primary technical challenges relate to analysis near the fold points $\mathcal{F}^{\ell,r}$ as well as tracking solutions near the saddle homoclinic bifurcation. We present a detailed analysis of slow passage near the saddle homoclinic bifurcation in order to understand how solutions behave

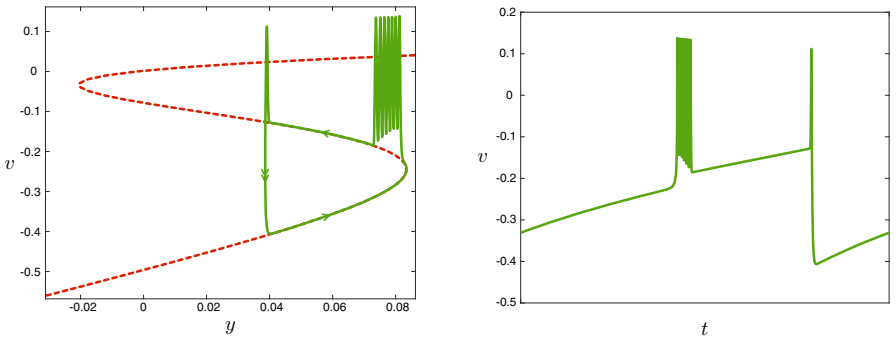

Fig. 5 Spikes are continuously added to the bursting oscillations along the spike-adding transition, achieving an $\mathcal{O}(1/\varepsilon)$ number of spikes. The left panel depicts a bursting solution of (1.1) along the transition from 7 to 8 spikes, and the right panel depicts the corresponding v-profile. The solution was obtained in AUTO for $\varepsilon = 0.001$ and $k \approx 0.0002$

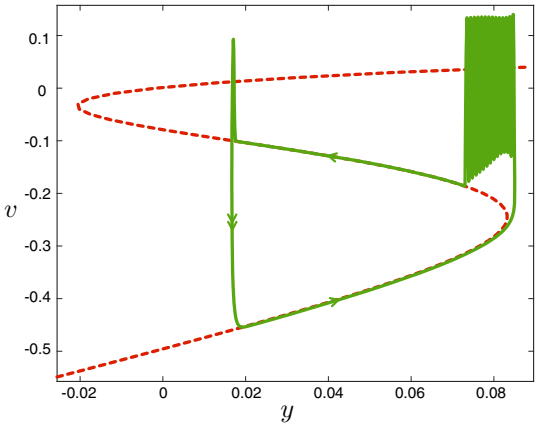

Fig. 6 Shown is a bursting solution obtained in (1.1) for $\varepsilon = 0.001$ and $k \approx 0.0539$. Note that this parameter regime is away from the canard explosion, and the solution no longer follows a canard trajectory along $\mathcal{M}_\varepsilon^m$ after passing the fold $\mathcal{F}^r$, but rather jumps directly from $\mathcal{F}^r$ to the periodic manifold $\mathcal{P}_\varepsilon$

in this region; this analysis is critical in showing how branches of periodic orbits with different numbers of spikes are connected.

The remainder of this paper is outlined as follows. The general setup and assumptions are detailed in Sect. 2, as well as the statement of the main result, Theorem 2.2. The proof of Theorem 2.2 is given in Sect. 3, followed by a brief discussion in Sect. 4.

2 Setup

The model system under consideration is a three-dimensional singularly perturbed ordinary differential equation with two fast variables and one slow variable, which we write in the form

$$\begin{aligned} \dot{v} &= f_1(v, w, y, k, \varepsilon) \\ \dot{w} &= f_2(v, w, y, k, \varepsilon) \\ \dot{y} &= \varepsilon g(v, w, y, k, \varepsilon), \end{aligned} \tag{2.1}$$

where $\dot{} = \frac{\mathrm{d}}{\mathrm{d}t}$, k is a bifurcation parameter, $\varepsilon > 0$ is a small parameter, and f_1, f_2, g are C^{r+1}-smooth functions of their arguments for some $r \geq 3$. We refer to (2.1) as the fast system. By rescaling $\tau = \varepsilon t$, we obtain the corresponding slow system

$$\begin{aligned} \varepsilon v' &= f_1(v, w, y, k, \varepsilon) \\ \varepsilon w' &= f_2(v, w, y, k, \varepsilon) \\ y' &= g(v, w, y, k, \varepsilon), \end{aligned} \tag{2.2}$$

where $' = \frac{\mathrm{d}}{\mathrm{d}\tau}$. These two systems are equivalent for any $\varepsilon > 0$, though the dynamics are best understood by perturbing from the distinct singular limits obtained by setting $\varepsilon = 0$ in each of (2.1), (2.2). We outline hypotheses with respect to each of these limits in Sects. 2.1 and 2.2, respectively. Assumptions on the slow/fast geometry of this system which guarantee bursting orbits were formulated by Terman in Terman (1991), and these form the basic setting in which we shall work. In some places, stronger hypotheses are required and we outline these in detail. Lastly, we describe additional assumptions regarding the nonhyperbolic fold points in the system in Sect. 2.3, and we state the main result in Sect. 2.4.

2.1 Layer Problem

Setting $\varepsilon = 0$ in (2.1) results in the *layer problem*

$$\begin{aligned} \dot{v} &= f_1(v, w, y, k, 0) \\ \dot{w} &= f_2(v, w, y, k, 0) \\ \dot{y} &= 0, \end{aligned} \tag{2.3}$$

which we consider for $k \in [-k_0, k_0]$ for some $k_0 > 0$. The dynamics are restricted to planes $y =$const, and this system admits a manifold of equilibria

$$\mathcal{M}_0 := \{(v, w, y) : F(v, w, y, k, 0) = 0\}, \, F(v, w, y, k, \varepsilon) := \begin{pmatrix} f_1(v, w, y, k, \varepsilon) \\ f_2(v, w, y, k, \varepsilon), \end{pmatrix} \tag{2.4}$$

which is called the *critical manifold*. For simplicity we assume $\mathcal{M}_0$ can be written as a graph over the v-coordinate. We also assume the following (Fig. 4).

Hypothesis 1 (S-shaped critical manifold) We assume the critical manifold is S-shaped, consisting of three branches; that is, we assume there exists $\bar{y}_r, \bar{y}_\ell$ such that the layer problem (2.3) admits a single equilibrium $p_b(y)$ for $y \in (-\infty, \bar{y}_\ell)$, three equilibria $p_b(y)$, $p_m(y)$, $p_u(y)$ for $y \in (\bar{y}_\ell, \bar{y}_r)$ and a single equilibrium $p_u(y)$ for $y \in (\bar{y}_r, \infty)$, with two equilibria colliding at saddle-node bifurcations at each of $y = \bar{y}_\ell, \bar{y}_r$ with $p_\ell := p_u(\bar{y}_\ell) = p_m(\bar{y}_\ell)$ and $p_r := p_b(\bar{y}_r) = p_m(\bar{y}_r)$.

We denote the fold points by

$$\mathcal{F}^{\ell,r} = (\bar{v}_{\ell,r}, \bar{w}_{\ell,r}, \bar{y}_{\ell,r}). \tag{2.5}$$

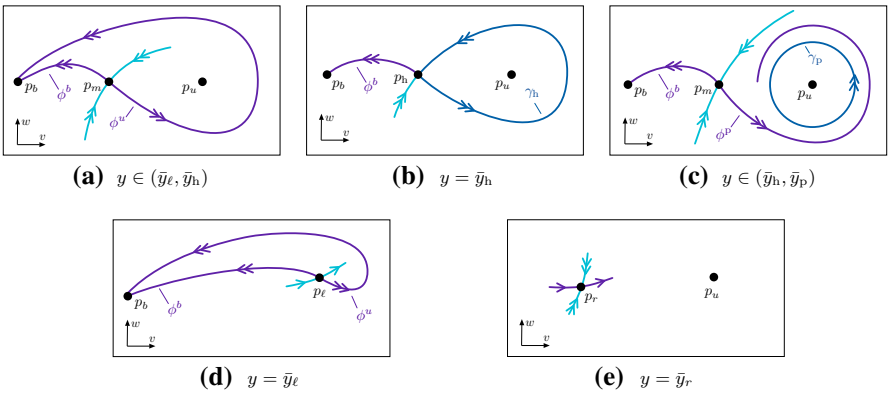

(a) $y \in (\bar{y}_\ell, \bar{y}_h)$ **(b)** $y = \bar{y}_h$ **(c)** $y \in (\bar{y}_h, \bar{y}_p)$

(d) $y = \bar{y}_\ell$ **(e)** $y = \bar{y}_r$

Fig. 7 Shown is the structure of the layer problem (2.3) in the cases: **a** $y \in (\bar{y}_\ell, \bar{y}_h)$, **b** $y = \bar{y}_h$, and **c** $y \in (\bar{y}_h, \bar{y}_p)$, as well as **d** $y = \bar{y}_\ell$ and **e** $y = \bar{y}_r$ corresponding to the layer problems which contain the fold points $\mathcal{F}^{\ell,r}$. Pictured in each phase portrait for $y \in (\bar{y}_\ell, \bar{y}_p)$ are the heteroclinic orbits $\phi^u(y)$, $\phi^b(y)$, $\phi^p(y)$; note that for $y = \bar{y}_h$, the orbit $\phi^u(y)$ coincides with the homoclinic orbit γ_h. In (c), also pictured are the periodic orbits $\gamma_p(\cdot; y)$ which bifurcate from γ_h for $y > \bar{y}_h$

We can therefore decompose $\mathcal{M}_0$ as

$$\mathcal{M}_0 = \mathcal{M}_0^b \cup \mathcal{F}^r \cup \mathcal{M}_0^m \cup \mathcal{F}^\ell \cup \mathcal{M}_0^u, \tag{2.6}$$

where the three branches $\mathcal{M}_0^{b,m,u}$ (bottom, middle, upper) are contained in the regions $\{-\infty < y < \bar{y}_r\}$, $\{\bar{y}_\ell < y < \bar{y}_r\}$, $\{\bar{y}_\ell < y < \infty\}$, respectively. We will sometimes write $\mathcal{M}_0^*(y_1, y_2)$, for $* = b, m, u$ to refer the intersection $\mathcal{M}_0^* \cap \{y_1 \le y \le y_2\}$.

Hypothesis 2 The bottom and middle branches of the critical manifold $\mathcal{M}_0$ satisfy the following.

(i) The bottom branch $\mathcal{M}_0^b$ is normally attracting, that is, $D_{(v,w)}F|_{\mathcal{M}_0^b}$ has two eigenvalues with negative real part.
(ii) The middle branch $\mathcal{M}_0^m$ is of saddle type, so that $D_{(v,w)}F|_{\mathcal{M}_0^m}$ has one positive and one negative eigenvalue.

Crucial to the spike-adding process in (2.1) is a saddle homoclinic bifurcation in the layer problem which occurs along the middle branch $\mathcal{M}_0^m$.

Hypothesis 3 (Saddle homoclinic orbit) There exists $y = \bar{y}_h(k) \in (\bar{y}_\ell, \bar{y}_r)$ such that (2.3) admits a homoclinic orbit $\gamma_h(t) = (v_h(t), w_h(t))$ bi-asymptotic to the saddle equilibrium $p_h := p_m(\bar{y}_h)$; further, the homoclinic orbit $\gamma_h(t)$ surrounds the equilibrium $p_u(\bar{y}_h)$ (Figs. 4 and 7).

We now consider the dynamics for nearby values of y. In order to construct a continuous spike-adding transition, we require some nondegeneracy with respect to the saddle homoclinic bifurcation. We first consider the linearization of the layer problem (2.3) about the equilibrium p_h, which by Hypothesis 2 admits one positive and one negative eigenvalue, which we denote by $\lambda_h^\pm$, respectively.

We next linearize (2.3) about $\gamma_{\rm h}$, which results in the system

$$\dot{\Phi} = D_{(v,w)}F(v_{\rm h}(t), w_{\rm h}(t), \bar{y}_{\rm h}, k, 0)\Phi. \tag{2.7}$$

The associated adjoint equation is given by

$$\dot{\Psi} = -D_{(v,w)}F(v_{\rm h}(t), w_{\rm h}(t), \bar{y}_{\rm h}, k, 0)^T\Psi, \tag{2.8}$$

which admits a unique bounded solution $\Psi_{\rm h}(t)$ (up to multiplication by a constant). We assume the following regarding the bifurcation of periodic orbits from the homoclinic orbit $\gamma_{\rm h}$ (Fig. 7).

Hypothesis 4 (Periodic manifold) The saddle quantity $\nu_{\rm h} := \lambda_{\rm h}^+ - \lambda_{\rm h}^-$ associated with the equilibrium $p_{\rm h}$ satisfies $\nu_{\rm h} < 0$ and the Melnikov integral

$$M_{\rm h} = \int_{-\infty}^{\infty} D_y F(v_{\rm h}(t), w_{\rm h}(t), \bar{y}_{\rm h}, 0, 0) \cdot \Psi_{\rm h}(t)\mathrm{d}t \neq 0, \tag{2.9}$$

is nonzero so that $\gamma_{\rm h}$ breaks transversely as y is varied near $y \approx \bar{y}_{\rm h}$ (Lin 1990). Therefore, from the homoclinic orbit $\gamma_{\rm h}$ bifurcates a family of attracting periodic orbits (Homburg and Sandstede 2010) for either $y < \bar{y}_{\rm h}$ or $y > \bar{y}_{\rm h}$; we assume the latter and denote this family by

$$\mathcal{P} = \left\{\gamma_{\rm p}(\cdot; y) = \left(v_{\rm p}(\cdot; y), w_{\rm p}(\cdot; y)\right) : y \in (\bar{y}_{\rm h}, \bar{y}_{\rm p})\right\} \tag{2.10}$$

for some $\bar{y}_{\rm h} < \bar{y}_{\rm p} < \bar{y}_r$. As a result, we have the following (see, for instance, the discussion in Homburg and Sandstede 2010, §3.6).

(i) The periodic orbits $\{\gamma_{\rm p}(\cdot; y) : y \in (\bar{y}_{\rm h}, \bar{y}_{\rm p})\}$ have corresponding periods $T_{\rm p}(y)$, $y \in (\bar{y}_{\rm h}, \bar{y}_{\rm p})$, where $T_{\rm p}(y)$ is a smooth function of y and $T_{\rm p}(y) \to \infty$ as $y \to \bar{y}_{\rm h}$.
(ii) Each periodic orbit $\gamma_{\rm p}(\cdot; y)$, $y \in (\bar{y}_{\rm h}, \bar{y}_{\rm p})$ admits a single nontrivial Floquet multiplier $e^{-\mu_{\rm p}(y)T_{\rm p}(y)} < 1$, where $\mu_{\rm p}(y) > 0$ is a smooth function of y.

We note that away from the endpoints $y = \bar{y}_{\rm h}, \bar{y}_{\rm p}$, the family $\mathcal{P}$ forms an invariant manifold, which is normally attracting; this manifold is shaped as a cylinder which surrounds the upper branch $\mathcal{M}_0^u$ (Fig. 4).

The next hypothesis concerns the existence of heteroclinic orbits connecting the middle branch $\mathcal{M}_0^m$ to the bottom branch $\mathcal{M}_0^b$ as well as heteroclinic orbits between $\mathcal{M}_0^m$ and $\mathcal{P}$ (Fig. 7).

Hypothesis 5 (Behavior of $\mathcal{W}^{\rm u}(\mathcal{M}_0^m)$) For each value of $y \in (\bar{y}_\ell, \bar{y}_r)$, the saddle equilibrium $p_m(y)$ has a one-dimensional unstable manifold $\mathcal{W}^{\rm u}(p_m(y))$ which is composed of two orbits W_-^m, W_+^m.

(i) For each $y \in (\bar{y}_\ell, \bar{y}_r)$, W_-^m is given by a heteroclinic orbit $\phi^b(y)$ which limits onto the stable equilibrium $p_b(y)$ on the bottom branch $\mathcal{M}_0^b$.

(ii) The behavior of W^m_+ varies: For $y = \bar{y}_\mathrm{h}$, W^m_+ is precisely the homoclinic orbit γ_h. For $y \in (\bar{y}_\ell, \bar{y}_\mathrm{h})$, W^m_+ is given by a second heteroclinic orbit $\phi^u(y)$ which limits onto the stable equilibrium $p_b(y)$ on the bottom branch $\mathcal{M}^b_0$, while for $y \in (\bar{y}_\mathrm{h}, \bar{y}_\mathrm{p})$, W^m_+ is a heteroclinic orbit $\phi^\mathrm{p}(y)$ which limits onto the attracting periodic orbit $\gamma_\mathrm{p}(\cdot; y)$. The behavior of W^m_+ for $y \geq \bar{y}_\mathrm{p}$ is not relevant.

2.2 Reduced Problem

Taking $\varepsilon = 0$ in (2.2) results in the associated *reduced problem*

$$\begin{aligned} 0 &= f_1(v, w, y, k, 0) \\ 0 &= f_2(v, w, y, k, 0) \\ y' &= g(v, w, y, k, 0), \end{aligned} \tag{2.11}$$

which is a differential–algebraic system in which the flow is restricted to the critical manifold $\mathcal{M}_0$. Regarding the slow flow, we have the following.

Hypothesis 6 (Slow flow) The function $g_0(v, w, y) = g(v, w, y, 0, 0)$ satisfies

$$g_0|_{\mathcal{M}^m_0} < 0, \qquad g_0|_{\mathcal{M}^b_0} > 0, \qquad g_0(\bar{v}_r, \bar{w}_r, \bar{y}_r) = 0, \qquad g_0(\bar{v}_\ell, \bar{w}_\ell, \bar{y}_\ell) < 0 \tag{2.12}$$

and

$$\frac{1}{T_\mathrm{p}(y)} \int_0^{T_\mathrm{p}(y)} g_0(v_\mathrm{p}(t; y), w_\mathrm{p}(t; y), y)\mathrm{d}t < 0, \qquad y \in (\bar{y}_\mathrm{h}, \bar{y}_\mathrm{p}). \tag{2.13}$$

2.3 Fold Points

Finally, we discuss hypotheses regarding the fold points $\mathcal{F}^{\ell,r}$. At each of the folds, the linearization of (2.1) for $\varepsilon = 0$ admits a double-zero eigenvalue due to the loss of normal hyperbolicity occurring along the critical manifold. There is one remaining hyperbolic direction, which we assume is repelling in the case of $\mathcal{F}^\ell$ and attracting in the case of $\mathcal{F}^r$. Hence, near the fold points, there exist local two-dimensional center manifolds, on which we assume that $\mathcal{F}^\ell$ and $\mathcal{F}^r$ take the form of nondegenerate planar fold and canard points (in the sense of Krupa and Szmolyan 2001a), respectively. The corresponding center manifold is repelling in the case of $\mathcal{F}^\ell$ and attracting in the case of $\mathcal{F}^r$, and hence, we refer to $\mathcal{F}^\ell$ as a normally repelling fold point and $\mathcal{F}^r$ as a normally attracting canard point.

This is the content of the following.

Hypothesis 7 The fold points $\mathcal{F}^\ell$, $\mathcal{F}^r$ satisfy the following.

(i) (Normally repelling nondegenerate fold point) The point $\mathcal{F}^\ell$ is a normally repelling fold point, in the sense that

$$D_{(v,w)}F(\bar{v}_\ell, \bar{w}_\ell, \bar{y}_\ell, k, 0) \tag{2.14}$$

has one positive eigenvalue for $k \in [-k_0, k_0]$. The full system (2.1) therefore admits a two-dimensional local center manifold $\mathcal{W}^c(\mathcal{F}^\ell)$, on which we assume the point $\mathcal{F}^\ell$ is a nondegenerate fold (or jump) point in the sense of Krupa and Szmolyan (2001a, §2.1).

(ii) (Normally attracting nondegenerate canard point) The point $\mathcal{F}^r$ is a normally attracting canard point, i.e.,

$$D_{(v,w)}F(\bar{v}_r, \bar{w}_r, \bar{y}_r, k, 0) \tag{2.15}$$

has one negative eigenvalue for $k \in [-k_0, k_0]$. The full system (2.1) therefore admits a two-dimensional local center manifold $\mathcal{W}^c(\mathcal{F}^r)$, on which we assume the point $\mathcal{F}^r$ is a nondegenerate canard point with unfolding parameter k in the sense of Krupa and Szmolyan (2001a, §3.1). This two-dimensional system therefore admits a singular Hopf bifurcation for $k = \varepsilon = 0$, which we assume is nondegenerate, in the sense of Krupa and Szmolyan (2001b, §3.4).

Remark 2.1 The nondegeneracy condition for the singular Hopf bifurcation can be determined from the normal form of the reduced equations on $\mathcal{W}^c(\mathcal{F}^r)$; we refer to Theorem 3.2.

2.4 Statement of the Main Result

We are now able to state our main result.

We define an N-spike bursting solution to be a periodic orbit which completes N excursions around the upper branch $\mathcal{M}^u$. We have the following.

Theorem 2.2 *Consider system (2.1) satisfying Hypotheses 1–7. Then, there exist $\rho, \eta, \varepsilon_0 > 0$ such that for each $\varepsilon \in (0, \varepsilon_0)$, there exists a continuous one-parameter family*

$$\theta \mapsto (k^{\mathrm{sa}}(\theta, \sqrt{\varepsilon}), \mathcal{B}(\theta, \sqrt{\varepsilon})), \qquad \theta \in (0, \Theta(\varepsilon)) \tag{2.16}$$

of periodic orbits $\mathcal{B}(\theta, \sqrt{\varepsilon})$ originating at a Hopf bifurcation near the fold point $\mathcal{F}^r$, where $k^{\mathrm{sa}}, \mathcal{B}$ are C^1 in $(\theta, \sqrt{\varepsilon})$. For $\theta \in (N, N+1)$, the periodic orbit $\mathcal{B}(\theta, \sqrt{\varepsilon})$ is an N-spike bursting solution, and the quantity $\Theta(\varepsilon)$ satisfies $\lim_{\varepsilon \to 0} \varepsilon \Theta(\varepsilon) = \theta_0 > 0$. Further, for $\theta \in (\rho, \Theta(\varepsilon))$, the parameter $k^{\mathrm{sa}}(\theta, \sqrt{\varepsilon})$ satisfies

$$|k^{\mathrm{sa}}(\theta, \sqrt{\varepsilon}) - k^{\mathrm{mc}}(\sqrt{\varepsilon})| = \mathcal{O}(e^{-\eta/\varepsilon}) \tag{2.17}$$

for a C^r function $k^{\mathrm{mc}}(\sqrt{\varepsilon}) = \mathcal{O}(\varepsilon)$.

Theorem 2.2 guarantees the existence of a single connected branch of bursting solutions which encompasses the transition from canard explosion (i.e., small-amplitude Hopf cycles local to the fold point $\mathcal{F}^r$) to large-amplitude bursting oscillations with an $\mathcal{O}(1/\varepsilon)$ number of spikes. Each spike is added sequentially throughout the spike-adding process as the single bifurcation parameter k varies on an interval of size $\mathcal{O}(e^{-\eta/\varepsilon})$.

The remainder of this paper is concerned with the proof of Theorem 2.2.

3 Construction of Spike-Adding Sequence

In this section, we present the proof of Theorem 2.2 by constructing the entire spike-adding sequence of bursting solutions for small $\varepsilon > 0$. We begin in Sect. 3.1 by collecting facts regarding the perturbation of normally hyperbolic portions of the critical manifold $\mathcal{M}_0$ and their (un)stable manifolds, which follow from standard results of geometric singular perturbation theory (Fenichel 1979). In Sects. 3.2 and 3.3, we analyze the fold point $\mathcal{F}^r$ and the canard explosion which occurs in a local two-dimensional center manifold $\mathcal{W}^{\mathrm{c}}(\mathcal{F}^r)$ containing the fold.

We then proceed by constructing bursting solutions which complete large excursions in phase space, that is, periodic orbits which do not remain in a small neighborhood of the fold point $\mathcal{F}^r$. We describe in Sect. 3.4 the general strategy for constructing such solutions, and in Sects. 3.5–3.7, we construct the transition from 0-spike solutions to 1-spike solutions. To understand how additional spikes are generated, a detailed understanding of the flow near the saddle homoclinic bifurcation is needed, which we present in Sect. 3.8, and the proof of the key technical result is given in Sect. 3.9. In Sects. 3.10–3.11, we construct N-spike solutions for any N and show how the branches of N-spike solutions and $(N+1)$-spike solutions are connected. Finally, the proof of Theorem 2.2 is briefly concluded in Sect. 3.12.

3.1 Persistence of Invariant Manifolds

We collect several preliminary results which follow from standard geometric singular perturbation theory and center manifold theory. For sufficiently small ε_0, k_0, we have the following:

1. Away from the fold points $\mathcal{F}^{\ell,r}$, the three branches $\mathcal{M}_0^{b,m,u}$ are normally hyperbolic and persist for $(k,\varepsilon) \in (-k_0,k_0)\times(0,\varepsilon_0)$ as locally invariant slow manifolds $\mathcal{M}_\varepsilon^{b,m,u}$. The middle branch $\mathcal{M}_0^m$ has two-dimensional stable and unstable manifolds $\mathcal{W}^{\mathrm{s}}(\mathcal{M}_0^m)$, $\mathcal{W}^{\mathrm{u}}(\mathcal{M}_0^m)$ which persist as locally invariant manifolds $\mathcal{W}^{\mathrm{s}}(\mathcal{M}_\varepsilon^m)$, $\mathcal{W}^{\mathrm{u}}(\mathcal{M}_\varepsilon^m)$ for $(k,\varepsilon)\in(-k_0,k_0)\times(0,\varepsilon_0)$. Similarly, the bottom branch $\mathcal{M}_0^b$ has a three-dimensional stable manifold $\mathcal{W}^{\mathrm{s}}(\mathcal{M}_0^b)$ which persists as a locally invariant manifold $\mathcal{W}^{\mathrm{s}}(\mathcal{M}_\varepsilon^b)$ for $(k,\varepsilon)\in(-k_0,k_0)\times(0,\varepsilon_0)$.
2. Near the fold point $\mathcal{F}^r$, there is a local two-dimensional attracting C^r-smooth center manifold $\mathcal{W}^{\mathrm{c}}(\mathcal{F}^r)$ which persists for $(k,\varepsilon)\in(-k_0,k_0)\times(0,\varepsilon_0)$. The slow manifolds $\mathcal{M}_\varepsilon^b$ and $\mathcal{M}_\varepsilon^m$ extend into a neighborhood of $\mathcal{F}^r$, where they shadow corresponding basepoint solution orbits $\mathcal{M}_\varepsilon^{b,r}$ and $\mathcal{M}_\varepsilon^{m,r}$ which lie on $\mathcal{W}^{\mathrm{c}}(\mathcal{F}^r)$.
3. Near the fold point $\mathcal{F}^\ell$, there is a local two-dimensional repelling C^r-smooth center manifold $\mathcal{W}^{\mathrm{c}}(\mathcal{F}^\ell)$ which persists for $(k,\varepsilon)\in(-k_0,k_0)\times(0,\varepsilon_0)$.
4. Away from the saddle homoclinic bifurcation at $y=\bar{y}_{\mathrm{h}}$, the periodic manifold $\mathcal{P}$ persists as a two-dimensional normally attracting locally invariant manifold $\mathcal{P}_\varepsilon$ for $(k,\varepsilon)\in(-k_0,k_0)\times(0,\varepsilon_0)$.

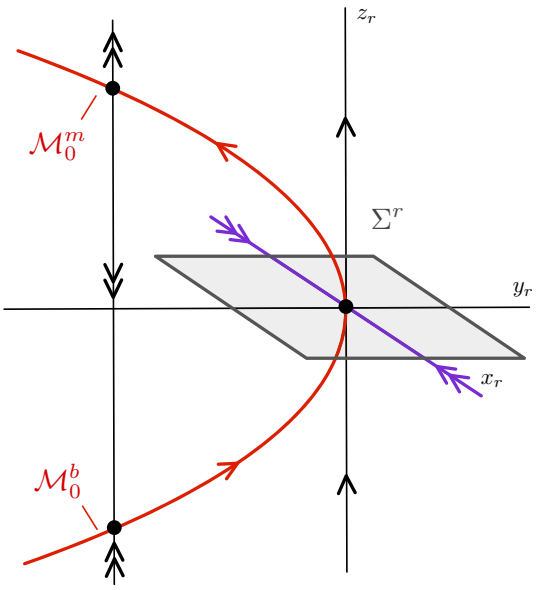

Fig. 8 Pictured is a schematic of the singular flow in a neighborhood of the right fold point $\mathcal{F}^r$. The normally attracting center manifold $\mathcal{W}^c(\mathcal{F}^r)$ corresponds to the plane $\{x_r = 0\}$

3.2 Local Coordinates Near $\mathcal{F}^r$ and Maximal Canards

By Hypothesis 7, in a neighborhood of the fold $\mathcal{F}^r$, after a change of coordinates we obtain the system (see, for instance, Krupa and Szmolyan 2001a; or Carter and Sandstede 2015, §6)

$$\begin{aligned}
\dot{x}_r &= x_r\left(-c_r(k) + \mathcal{O}(x_r, y_r, z_r, \varepsilon)\right)\\
\dot{z}_r &= y_r h_1(y_r, z_r, k, \varepsilon) + z_r^2 h_2(y_r, z_r, k, \varepsilon) + \varepsilon h_3(y_r, z_r, k, \varepsilon)\\
\dot{y}_r &= \varepsilon\left(-z_r h_4(y_r, z_r, k, \varepsilon) + k h_5(y_r, z_r, k, \varepsilon) + y_r h_6(y_r, z_r, k, \varepsilon)\right)\\
\dot{k} &= 0\\
\dot{\varepsilon} &= 0\,,
\end{aligned} \tag{3.1}$$

where $c_r(k) > 0$, and the functions h_j, $j = 1, \ldots, 6$ are C^r and satisfy

$$\begin{aligned}
h_3(y_r, z_r, k, \varepsilon) &= \mathcal{O}(y_r, z_r, k, \varepsilon)\\
h_j(y_r, z_r, k, \varepsilon) &= 1 + \mathcal{O}(y_r, z_r, k, \varepsilon), \quad j = 1, 2, 4, 5.
\end{aligned} \tag{3.2}$$

At the linear level, the slow variable y_r in these local coordinates corresponds to a rescaling of the original slow variable $(y - \bar{y}_r)$. Here, the variables (z_r, y_r) parameterize the center manifold $\mathcal{W}^c(\mathcal{F}^r)$, while x_r parameterizes the strong stable fibers, which have been straightened so that the (z_r, y_r) center dynamics are decoupled from x_r. See Fig. 8 for a schematic of the singular $\varepsilon = 0$ flow near $\mathcal{F}^r$.

The manifold $\mathcal{W}^c(\mathcal{F}^r)$ is given by $x_r = 0$; we recall that by construction $\mathcal{W}^c(\mathcal{F}^r)$ contains the one-dimensional (shadowed) slow manifolds $\mathcal{M}_\varepsilon^{b,r}$ and $\mathcal{M}_\varepsilon^{m,r}$. We note

that the (z_r, y_r) coordinates are in the canonical form for a canard point (compare Krupa and Szmolyan 2001a). Canard points are characterized by canard trajectories which follow a strongly attracting manifold (in this case $\mathcal{M}_\varepsilon^{b,r}$), pass near the equilibrium and continue along a strongly repelling manifold (in this case $\mathcal{M}_\varepsilon^{m,r}$) for some time. To understand the flow near this point, we use blow-up methods as in Krupa and Szmolyan (2001a). Restricting to the center manifold $x_r = 0$, the blow-up transformation is given by

$$y_r = \bar{r}^2 \bar{y}, \quad z_r = \bar{r}\bar{z}, \quad k = \bar{r}\bar{k}, \quad \varepsilon = \bar{r}^2 \bar{\varepsilon}\ , \tag{3.3}$$

defined on the manifold $B = S^2 \times [0, \bar{r}_0] \times [-\bar{k}_0, \bar{k}_0]$ for sufficiently small $\bar{r}_0, \bar{k}_0$ with $(\bar{y}, \bar{z}, \bar{\varepsilon}) \in S^2$. There is one relevant coordinate chart which will be needed for the matching analysis; in the literature, this is frequently referred to as the "family rescaling" chart, which corresponds to an ε-rescaling of the variables and parameters. Keeping the same notation as in Krupa and Szmolyan (2001a) and Krupa and Szmolyan (2001b), the family rescaling chart $\mathcal{K}_2$ uses the coordinates

$$y_r = r_2^2 y_2, \quad z_r = r_2 z_2, \qquad k = r_2 k_2, \quad \varepsilon = r_2^2. \tag{3.4}$$

Using these blow-up charts, the authors of Krupa and Szmolyan (2001a) studied the behavior of the manifolds $\mathcal{M}_\varepsilon^{b,r}$ and $\mathcal{M}_\varepsilon^{m,r}$ and determined conditions under which these manifolds coincide along a canard trajectory. We place a section $\Sigma^r = \{z_r = 0, |x_r| \le \delta_x, |y_r| < \rho\}$ for small fixed δ_x, ρ which will serve as a Poincaré section for constructing the periodic orbits.

In the chart $\mathcal{K}_2$, the section Σ^r is given by $\Sigma^r = \left\{z_2 = 0, |x_r| \le \delta_x, |r_2^2 y_2| < \rho\right\}$. It was shown in Krupa and Szmolyan (2001a) that for all sufficiently small r_2, k_2, the manifolds $\mathcal{M}_\varepsilon^{b,r}$ and $\mathcal{M}_\varepsilon^{m,r}$ reach Σ^r at $y_2 = y_2^b(k_2, r_2)$ and $y_2 = y_2^m(k_2, r_2)$, respectively. We have the following result which describes the distance between $\mathcal{M}_\varepsilon^{b,r}$ and $\mathcal{M}_\varepsilon^{m,r}$ in Σ^r.

Proposition 3.1 (Krupa and Szmolyan 2001a, Proposition 3.5) *The distance between the slow manifolds $\mathcal{M}_\varepsilon^{b,r}$ and $\mathcal{M}_\varepsilon^{m,r}$ in Σ^r is given by*

$$y_2^b - y_2^m = \mathcal{D}_0(k_2, r_2) = d_{k_2} k_2 + d_{r_2} r_2 + \mathcal{O}(r_2^2 + k_2^2)\ , \tag{3.5}$$

where the coefficients d_{k_2}, d_{r_2} are constants, bounded away from zero independently of k_2, r_2. Hence, we can solve for the existence of a maximal canard trajectory within $\mathcal{W}^c(\mathcal{F}^r)$, corresponding to a zero of the distance function $\mathcal{D}_0(k_2, r_2)$, which occurs when

$$k_2 = k_2^{\mathrm{mc}} = \mu r_2 + \mathcal{O}(r_2^2), \tag{3.6}$$

where $\mu = -\frac{d_{r_2}}{d_{k_2}} \neq 0$.

This proposition describes the splitting of the manifolds $\mathcal{M}_\varepsilon^{b,r}$ and $\mathcal{M}_\varepsilon^{m,r}$ as a function of k_2, r_2, and in particular ensures that this splitting occurs in a transverse fashion as the parameter $k = k_2 r_2$ is varied near $k \approx k^{\mathrm{mc}}(\sqrt{\varepsilon})$, where the function

$$k^{\mathrm{mc}}(\sqrt{\varepsilon}) = k_2^{\mathrm{mc}}\sqrt{\varepsilon} = \mu\varepsilon + \mathcal{O}(\varepsilon^{3/2}) \tag{3.7}$$

denotes the location of the maximal canard solution.

Further, it was shown in Krupa and Szmolyan (2001a) that the system (3.1) undergoes a singular Hopf bifurcation, which also occurs near the location of the maximal canard. The sub/supercriticality of the Hopf bifurcation is determined via the quantity

$$A_H = -a_1 + 3a_2 - 2a_4 - 2a_5, \tag{3.8}$$

where

$$a_1 = \frac{\partial h_1}{\partial z_r}(0,0,0,0), \quad a_2 = \frac{\partial h_2}{\partial z_r}(0,0,0,0), \quad a_3 = \frac{\partial h_3}{\partial z_r}(0,0,0,0)$$
$$a_4 = \frac{\partial h_4}{\partial z_r}(0,0,0,0), \quad a_5 = h_6(0,0,0,0).$$

We have the following.

Theorem 3.2 (Krupa and Szmolyan 2001a, Theorem 3.1) *There exist $\varepsilon_0, k_0 > 0$ such that for $(k,\varepsilon) \in (-k_0, k_0) \times (0, \varepsilon_0)$ system (3.1) admits a single equilibrium. The equilibrium is stable for $k < k^H(\sqrt{\varepsilon})$, where*

$$k^H(\sqrt{\varepsilon}) = -\frac{a_3 + a_6}{2}\varepsilon + \mathcal{O}(\varepsilon^{3/2}) \tag{3.9}$$

and loses stability through a Hopf bifurcation as k passes through $k^H(\sqrt{\varepsilon})$. The Hopf bifurcation is nondegenerate if the quantity A_H defined in (3.8) is nonzero. It is supercritical if $A_H < 0$ and subcritical if $A_H > 0$.

3.3 Local Canard Explosion

Within the center manifold $\mathcal{W}^{\mathrm{c}}(\mathcal{F}^r)$, we refer to Krupa and Szmolyan (2001b) for the bifurcation of local canard orbits from the singular Hopf bifurcation at the equilibrium at the origin. Upon varying the parameter $k \approx k^{\mathrm{mc}}(\sqrt{\varepsilon})$, these orbits grow to small, but $\mathcal{O}(1)$, size within $\mathcal{W}^{\mathrm{c}}(\mathcal{F}^r)$. We quote the following from Krupa and Szmolyan (2001b).

Theorem 3.3 (Krupa and Szmolyan 2001b, Theorems 4.1, 4.2, Proposition 4.3) *Assume that $A_H \neq 0$ and that $\rho > 0$ is sufficiently small. Then, there exists $\varepsilon_0 > 0$ such that for $\varepsilon \in (0, \varepsilon_0)$, system (3.1) undergoes a Hopf bifurcation at $k = k^H(\sqrt{\varepsilon})$, from which bifurcates a continuous family of periodic orbits*

$$s \mapsto (k^{\mathrm{sc}}(s, \sqrt{\varepsilon}), \Gamma^{\mathrm{sc}}(s, \sqrt{\varepsilon})), \qquad s \in (0, \rho], \tag{3.10}$$

where $k^{\mathrm{sc}}(s, \sqrt{\varepsilon})$ is C^r in $(s, \sqrt{\varepsilon})$ with $k^{\mathrm{sc}}(s, \sqrt{\varepsilon}) \to k^H(\sqrt{\varepsilon})$ as $s \to 0$, and

$$|k^{\mathrm{sc}}(\rho, \sqrt{\varepsilon}) - k^{\mathrm{mc}}(\sqrt{\varepsilon})| = \mathcal{O}(e^{-q/\varepsilon}). \tag{3.11}$$

For each $s \in (0, \rho]$, *the orbit* $\Gamma^{sc}(s, \sqrt{\varepsilon})) \subset \mathcal{W}^c(\mathcal{F}^r)$ *passes through the point* $(x_r, y_r, z_r) = (0, -s, 0)$.

This theorem guarantees the existence of a singular Hopf bifurcation and the bifurcation of a continuous family of periodic orbits within the center manifold $\mathcal{W}^c(\mathcal{F}^r)$ which grow to $\mathcal{O}(1)$ amplitude for all sufficiently small ε (determined via the small parameter ρ which, in general, satisfies $0 < \varepsilon \ll \rho$).

3.4 General Strategy of Constructing $\mathcal{O}(1)$-Amplitude Periodic Orbits

In this section, we describe a general strategy for constructing a periodic orbit which completes an $\mathcal{O}(1)$ excursion in phase space before returning to a neighborhood of the fold $\mathcal{F}^r$. The idea is to determine an appropriate one-dimensional curve $\mathcal{I}$ of initial conditions which can be evolved both forward and backward in time, spanning a two-dimensional manifold $\overline{\mathcal{I}}$ of candidate solution orbits. This manifold is tracked forward and backward until it first intersects the section Σ^r; this intersection is therefore given by two curves $\mathcal{I}^+, \mathcal{I}^-$, resulting from the forward and backward evolution, respectively. The geometric setup for the construction strategy is shown in Fig. 9.

We then consider the Poincaré map $\Pi^r : \Sigma^r \to \Sigma^r$ and search for solutions with initial conditions on $\mathcal{I}^-$ which return to Σ^r, meeting the curve $\mathcal{I}^+$. The desired periodic orbit is then given by a fixed point of this map, corresponding to an intersection of the curves $\mathcal{I}^+, \mathcal{I}^-$ which occurs along a single solution orbit, lying entirely within the manifold $\overline{\mathcal{I}}$.

We now describe this procedure in more detail and determine conditions on the initial curve $\mathcal{I}$ which guarantee that this strategy results in a unique solution. We assume the following.

(i) The curve $\mathcal{I}$ lies outside a small Δ-neighborhood of $\mathcal{F}^r$.
(ii) Under the forward evolution of (2.1), the manifold $\overline{\mathcal{I}}$ is contained in $\mathcal{W}^s(\mathcal{M}_\varepsilon^b)$.
(iii) Under the backward evolution of (2.1), the manifold $\overline{\mathcal{I}}$ transversely intersects $\mathcal{W}^u(\mathcal{M}_\varepsilon^m)$.

Under these conditions, we can construct a periodic orbits as follows. When evolving forward, since the manifold $\overline{\mathcal{I}}$ is contained in $\mathcal{W}^s(\mathcal{M}_\varepsilon^b)$, we can track $\overline{\mathcal{I}}$ as it is exponentially contracted to $\mathcal{M}_\varepsilon^b$ until reaching a small neighborhood of $\mathcal{F}^r$, whereby $\overline{\mathcal{I}}$ intersects Σ^r in a curve $\mathcal{I}^+$ which is $\mathcal{O}(e^{-\eta/\varepsilon})$-close to $\mathcal{M}_\varepsilon^b \cap \Sigma^r$. On the other hand, since $\overline{\mathcal{I}}$ transversely intersects $\mathcal{W}^u(\mathcal{M}_\varepsilon^m)$ under the backward evolution of (2.1), by the exchange lemma (Schecter 2008b), in backward time $\overline{\mathcal{I}}$ intersects Σ^r in a curve $\mathcal{I}^-$ which is aligned C^1-$\mathcal{O}(e^{-\eta/\varepsilon})$-close to the strong stable fibers of the manifold $\mathcal{W}^c(\mathcal{F}^r)$. In particular, $\mathcal{I}^-$ intersects $\mathcal{W}^c(\mathcal{F}^r) \cap \Sigma^r$ at a basepoint which is $\mathcal{O}(e^{-\eta/\varepsilon})$-close to $\mathcal{M}_\varepsilon^m \cap \Sigma^r$, and $\mathcal{I}^-$ is thus aligned C^1-$\mathcal{O}(e^{-\eta/\varepsilon})$-close to the strong stable fiber of that basepoint.

The Poincaré map $\Pi^r : \Sigma^r \to \Sigma^r$ by construction satisfies $\Pi^r(\mathcal{I}^-) \subseteq \mathcal{I}^+$. We use the blow-up coordinates (3.4) to set up fixed point matching conditions in the section Σ^r. Within Σ^r, it is most natural to parameterize solutions using the coordinates (x_r, y_2).

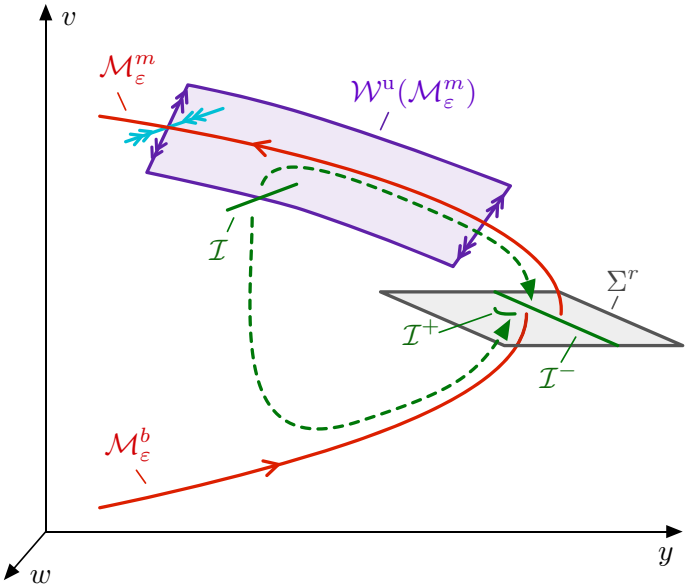

Fig. 9 Shown is a schematic of the strategy for constructing large-amplitude bursting oscillations outlined in Sect. 3.4. A one-dimensional manifold $\mathcal{I}$ of candidate solutions is evolved forward and backward under the flow of (2.1) until intersecting the section Σ^r. This intersection consists of two curves: $\mathcal{I}^{\pm}$ (corresponding to the forward and backward evolution, respectively); matching conditions are then determined within the section Σ^r which guarantee the existence of a periodic orbit

3.5 (Lower) 0-Spike Orbits

In this section, we construct 0-spike orbits, which encompass the transition from the local canard explosion occurring within the center manifold $\mathcal{W}^{\mathrm{c}}(\mathcal{F}^r)$ to large canard orbits which complete a global excursion. This excursion is characterized by a long canard trajectory, which consists of first following $\mathcal{M}_\varepsilon^b$, then $\mathcal{M}_\varepsilon^m$, and then finally returning to $\mathcal{M}_\varepsilon^b$ via one of the heteroclinic orbits $\phi^b(y)$ (Fig. 10). We refer to these orbits as "lower" 0-spike orbits as they traverse one of the heteroclinic orbits $\phi^b(y)$, as opposed to one of the upper heteroclinics $\phi^u(y)$. These orbits are most naturally parameterized by which heteroclinic connection $\phi^b(y)$ is followed, or equivalently, the minimum y-value achieved along the orbit. Hence, for $s \in [\bar{y}_\ell + \Delta, \bar{y}_r - \Delta]$, we search for a 0-spike periodic orbit which achieves a minimum y-value of $y = s$, and is obtained as a perturbation from the singular orbit

$$\Gamma_0(s) := \mathcal{M}_0^b(s, \bar{y}_r) \cup \mathcal{M}_0^m(s, \bar{y}_r) \cup \phi^b(s). \tag{3.12}$$

Following the strategy of the previous section, we choose an appropriate one-dimensional curve $\mathcal{I}^b(s)$ of candidate initial conditions. For this, we denote by w^b the w-coordinate at which the orbit $\phi^b(s)$ intersects the set $\{v = \bar{v}_r\}$. For sufficiently small $\delta > 0$, we then define $\mathcal{I}^b(s)$ to be an interval of width δ which lies in the plane $\{y = s\}$ and is transverse to the fast layer dynamics, and which intersects $\phi^b(s)$ at

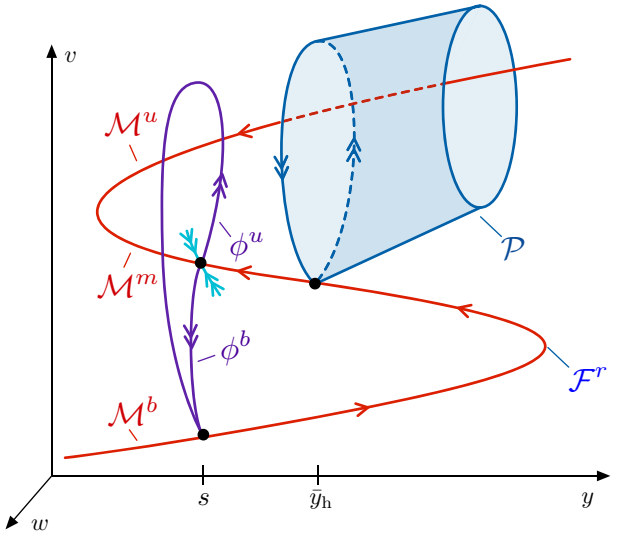

Fig. 10 Shown are singular periodic orbits in the case of lower 0-spike orbits and upper 1-spike orbits. The lower/upper descriptor refers to which of the heteroclinic orbits ϕ^b, ϕ^u is followed. A lower 0-spike orbit follows $\mathcal{M}^b$, then $\mathcal{M}^m$, then the heteroclinic orbit ϕ^b. An upper 1-spike orbit follows $\mathcal{M}^b$, then $\mathcal{M}^m$, then the heteroclinic orbit ϕ^u; the fast increase then decrease in the v-variable along the orbit ϕ^u constitutes the "spike"

$w = w^b$. We now determine the behavior of $\mathcal{I}^b(s)$ under the forward and backward evolution of (2.1).

Since $\phi^b(s)$ lies in the intersection $\mathcal{W}^{\mathrm{s}}(\mathcal{M}_0^b) \cap \mathcal{W}^{\mathrm{u}}(\mathcal{M}_0^m)$ for $\varepsilon = 0$, we see that for all sufficiently small $\varepsilon > 0$, the forward evolution of $\mathcal{I}^b(s)$ must also lie in $\mathcal{W}^{\mathrm{s}}(\mathcal{M}_\varepsilon^b)$. On the other hand, the backward evolution of $\mathcal{I}^b(s)$ transversely intersects the manifold $\mathcal{W}^{\mathrm{u}}(\mathcal{M}_\varepsilon^m)$. By the exchange lemma, the backward evolution of $\mathcal{I}^b(s)$ traces out a two-dimensional manifold $\overline{\mathcal{I}}^b(s)$ which intersects Σ^r in a curve $\mathcal{I}^-(s)$ which is aligned C^1-$\mathcal{O}(e^{-\eta/\varepsilon})$-close to the stable fiber of a basepoint on $\mathcal{W}^{\mathrm{c}}(\mathcal{F}^r)$ which itself is $\mathcal{O}(e^{-\eta/\varepsilon})$-close to $\mathcal{M}_\varepsilon^{m,r} \cap \Sigma^r$ (Fig. 11).

We sum this up in the following

Lemma 3.4 *Within Σ^r, the curve $\mathcal{I}^-(s)$ is given as a graph*

$$\mathcal{I}^-(s) = \{(x_r, y_2) : y_2 = y_2^m + I^-(x_r, s, k, \varepsilon), |x_r| \leq \delta_x\}, \tag{3.13}$$

where

$$I^-(0, s, k, \varepsilon) = \mathcal{O}(e^{-\eta/\varepsilon}), \qquad \partial_v I^-(0, s, k, \varepsilon) = \mathcal{O}(e^{-\eta/\varepsilon}) \tag{3.14}$$

for $v = x_r, s, k$.

We now consider the forward evolution of $\mathcal{I}^-(s)$, which is contained in the two-dimensional manifold $\overline{\mathcal{I}}^b(s)$. By construction and by the above discussion, we have

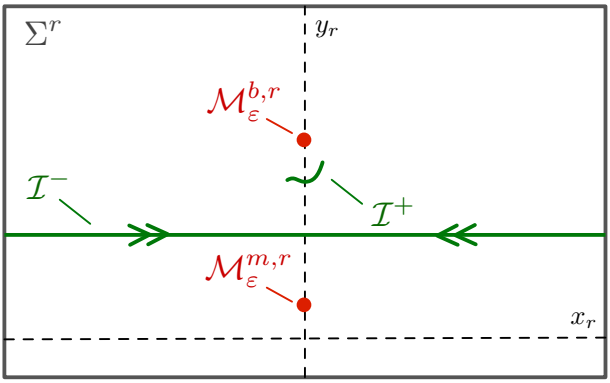

Fig. 11 Shown are the matching conditions within the Poincaré section Σ^r. Note that under the Poincaré map $\Pi^r : \Sigma^r \to \Sigma^r$, we have that $\Pi(\mathcal{I}^-) \subseteq \mathcal{I}^+$. A periodic orbit can be therefore be found when the curves $\mathcal{I}^\pm$ intersect along a single solution orbit

that $\overline{\mathcal{I}}^b(s) \subset \mathcal{W}^s(\mathcal{M}_\varepsilon^b)$, and therefore $\overline{\mathcal{I}}^b(s)$ will be C^1-exponentially contracted to $\mathcal{M}_\varepsilon^b$ and thus meets the section Σ^r in a curve $\mathcal{I}^+(s)$ which is C^1-$\mathcal{O}(e^{-\eta/\varepsilon})$-close to $\mathcal{M}_\varepsilon^{b,r} \cap \Sigma^r$ (Fig. 11). We have the following

Lemma 3.5 *Consider the Poincaré map $\Pi^r : \Sigma^r \to \Sigma^r$. We have that $\Pi^r(\mathcal{I}^-(s)) \subseteq \mathcal{I}^+(s)$; parameterizing points on $\mathcal{I}^-(s)$ by their initial x_r coordinate given by $x_r = x^-$ for $|x^-| \leq \delta_x$, we have that the curve $\Pi^r(\mathcal{I}^-(s))$ is given by*

$$\Pi^r(\mathcal{I}^-(s)) = \left\{ \begin{pmatrix} x_r \\ y_2 \end{pmatrix} = \begin{pmatrix} x^+(x^-, s, k, \varepsilon) \\ y_2^b + I^+(x^-, s, k, \varepsilon) \end{pmatrix}, |x^-| \leq \delta_x \right\}, \tag{3.15}$$

where

$$\begin{aligned} I^+(x^-, s, k, \varepsilon) &= \mathcal{O}(e^{-\eta/\varepsilon}), \qquad \partial_\nu I^+(x^-, s, k, \varepsilon) = \mathcal{O}(e^{-\eta/\varepsilon}) \\ x^+(x^-, s, k, \varepsilon) &= \mathcal{O}(e^{-\eta/\varepsilon}), \qquad \partial_\nu x^+(x^-, s, k, \varepsilon) = \mathcal{O}(e^{-\eta/\varepsilon}) \end{aligned} \tag{3.16}$$

for $\nu = x^-, s, k$.

It remains to solve for a fixed point of Π^r which lies on the intersection of the curves $\mathcal{I}^\pm(s)$; this corresponds to a periodic orbit which is a perturbation of the singular orbit $\Gamma_0(s)$. An intersection of $\mathcal{I}^\pm(s)$ occurs along a single solution orbit if

$$\begin{aligned} x^- &= x^+(x^-, s, k, \varepsilon) \\ y_2^m + I^-(x^-, s, k, \varepsilon) &= y_2^b + I^+(x^-, s, k, \varepsilon) \end{aligned} \tag{3.17}$$

for some value of $|x^-| \leq \delta_x$. Using estimates (3.16), the first equation can be solved for

$$x^- = x^-(s, k, \varepsilon) = \mathcal{O}(e^{-\eta/\varepsilon}), \qquad \partial_k x^-(s, k, \varepsilon) = \mathcal{O}(e^{-\eta/\varepsilon}). \tag{3.18}$$

Plugging this into the second equation and rearranging results in the equation

$$y_2^b - y_2^m + I^+(x^-(s,k,\varepsilon),s,k,\varepsilon) - I^-(x^-(s,k,\varepsilon),s,k,\varepsilon) = 0, \tag{3.19}$$

which by Proposition 3.1 can be rewritten as

$$\mathcal{D}_0(k_2,r_2) + I^+(x^-(s,k,\varepsilon),s,k,\varepsilon) - I^-(x^-(s,k,\varepsilon),s,k,\varepsilon) = 0. \tag{3.20}$$

Using estimates (3.14), (3.16), (3.18), and the implicit function theorem, this equation can be solved for a unique solution when

$$k = k_0^{\mathrm{sa}}(s,\varepsilon) = k^{\mathrm{mc}}(\sqrt{\varepsilon}) + \mathcal{O}(e^{-\eta/\varepsilon}). \tag{3.21}$$

3.6 Upper 1-Spike Orbits

In this section, we construct 1-spike orbits which complete an excursion around the upper branch $\mathcal{M}_\varepsilon^u$, corresponding to a single spike. We first consider the simpler case of orbits which stay away from the upper left fold $\mathcal{F}^\ell$ and the saddle homoclinic bifurcation occurring along $\mathcal{M}_\varepsilon^m$, as these orbits can be constructed in a very similar manner to the 0-spike orbits from Sect. 3.5.

These solutions are again characterized by a long canard trajectory, which consists of first following $\mathcal{M}_\varepsilon^b$, then $\mathcal{M}_\varepsilon^m$, and then finally returning to $\mathcal{M}_\varepsilon^b$; however, in contrast to the solutions constructed in Sect. 3.5, the fast jump down to $\mathcal{M}_\varepsilon^b$ instead follows one of the heteroclinic orbits $\phi^u(y)$ (Fig. 10). Similarly, these orbits are most naturally parameterized by which heteroclinic connection $\phi^u(y)$ is followed, or equivalently, the minimum y-value achieved along the orbit. Hence, for each $s \in [\bar{y}_\ell + \Delta, \bar{y}_\mathrm{h} - \Delta]$ we search for a 1-spike periodic orbit which achieves a minimum y-value of $y = s$ and is obtained as a perturbation from the singular orbit

$$\mathcal{M}_0^b(s,\bar{y}_r) \cup \mathcal{M}_0^m(s,\bar{y}_r) \cup \phi^u(s). \tag{3.22}$$

Following the strategy of Sect. 3.5, we choose an appropriate one-dimensional curve $\mathcal{I}^u(s)$ of candidate initial conditions. For this, we denote by w^u the w-coordinate at which the orbit $\phi^u(s)$ intersects the set $\{v = \bar{v}_\ell\}$. For sufficiently small $\delta > 0$, we then define $\mathcal{I}^u(s)$ to be an interval of width δ which lies in the plane $\{y = s\}$ and is transverse to the fast layer dynamics, and which intersects $\phi^u(s)$ at $w = w^u$. Since $\phi^u(s)$ lies in the intersection $\mathcal{W}^{\mathrm{s}}(\mathcal{M}_0^b) \cap \mathcal{W}^{\mathrm{u}}(\mathcal{M}_0^m)$ for $\varepsilon = 0$, the remainder of the analysis follows identically to that in Sect. 3.5, with the periodic orbit occurring for

$$k = k_1^{\mathrm{sa,upper}}(s,\varepsilon) = k^{\mathrm{mc}}(\sqrt{\varepsilon}) + \mathcal{O}(e^{-\eta/\varepsilon}), \tag{3.23}$$

and we omit the details.

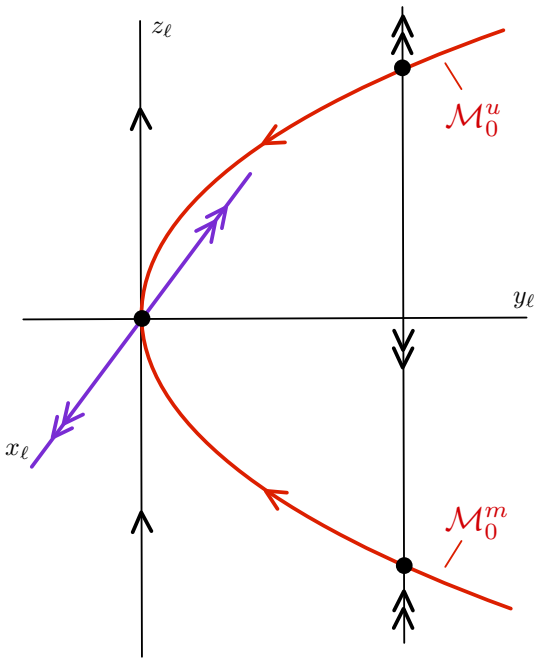

Fig. 12 Shown is a schematic of the singular $\varepsilon = 0$ flow near the upper left fold point $\mathcal{F}^\ell$. The locally invariant attracting center manifold $\mathcal{W}^c(\mathcal{F}^\ell)$ is given by the set $\{x_\ell = 0\}$

3.7 Overlap of 0-Spike Orbits and Upper 1-Spike Orbits: Analysis of Upper Left Fold Point $\mathcal{F}^\ell$

We consider the upper left fold $\mathcal{F}^\ell$. We note that the geometry near the fold is similar to that considered in Carter and Sandstede (2015, §4), and hence, we draw on the local analysis as presented in Carter and Sandstede (2015). We first move to a local coordinate system in a neighborhood of $\mathcal{F}^\ell$, in which the equations take the form

$$\begin{aligned} \dot{x}_\ell &= x_\ell \left(c_\ell(k) + \mathcal{O}(x_\ell, y_\ell, z_\ell, \varepsilon)\right) \\ \dot{z}_\ell &= -y_\ell + z_\ell^2 + h_\ell(y_\ell, z_\ell, k, \varepsilon) \\ \dot{y}_\ell &= \varepsilon g_\ell(y_\ell, z_\ell, k, \varepsilon), \end{aligned} \tag{3.24}$$

where $c_\ell(k) > 0$, and h_ℓ, g_ℓ are C^r-functions satisfying

$$\begin{aligned} h_\ell(y_\ell, z_\ell, k, \varepsilon) &= \mathcal{O}(\varepsilon, y_\ell z_\ell, y_\ell^2, z_\ell^3), \\ g_\ell(y_\ell, z_\ell, k, \varepsilon) &= -1 + \mathcal{O}(y_\ell, z_\ell, \varepsilon), \end{aligned}$$

uniformly in $k \in (-k_0, k_0)$. The geometry of (3.24) for $\varepsilon = 0$ is depicted in Fig. 12. In the transformed system (3.24), the (z_ℓ, y_ℓ)-dynamics are decoupled from the dynamics in the hyperbolic x_ℓ-direction along the straightened strong unstable fibers. At the linear level, the slow variable y_ℓ in these local coordinates corresponds to a rescaling of the original slow variable $(y - \bar{y}_\ell)$.

We consider the flow of (3.24) on the invariant manifold $x_\ell = 0$. We append an equation for ε, arriving at the system

$$\begin{aligned} \dot{z}_\ell &= -y_\ell + z_\ell^2 + h_\ell(y_\ell, z_\ell, k, \varepsilon) \\ \dot{y}_\ell &= \varepsilon g_\ell(y_\ell, z_\ell, k, \varepsilon) \\ \dot{\varepsilon} &= 0. \end{aligned} \tag{3.25}$$

For $\varepsilon = 0$, this system possesses a critical manifold given by $\{(y_\ell, z_\ell) : -y_\ell + z_\ell^2 + h_\ell(y_\ell, z_\ell, k, 0) = 0\}$, which in a sufficiently small neighborhood of the origin is shaped as a parabola opening to the right (Fig. 12). The branch of this parabola for $z_\ell < 0$ is attracting and corresponds to the manifold $\mathcal{M}_0^m$. We define $\mathcal{M}_0^{m,+}$ to be the singular trajectory obtained by appending the fast trajectory given by the line segment $\{(y_\ell, z_\ell) : y_\ell = 0, 0 \le z_\ell \le \delta_z\}$ to the attracting branch $\mathcal{M}_0^m$ of the critical manifold. We have the following

Proposition 3.6 (Carter and Sandstede 2015, Proposition 4.1) *For all sufficiently small $\varepsilon > 0$, we have the following.*

(i) Within the center manifold $\{x_\ell = 0\}$, the singular trajectory $\mathcal{M}_0^{m,+}$ perturbs to a solution $\mathcal{M}_\varepsilon^{m,+}$, which is C^0-$\mathcal{O}(\varepsilon^{2/3})$-close and C^1-$\mathcal{O}(\varepsilon^{1/3})$-close to $\mathcal{M}_0^{m,+}$, uniformly in $|k| < k_0$. This solution can be represented as a graph

$$\mathcal{M}_\varepsilon^{m,+} = \{(0, y_\ell, z_\ell) : y_\ell = s_{m,+}(z_\ell, k, \varepsilon), |z_\ell| \le \delta_z\}. \tag{3.26}$$

(ii) The manifold $\mathcal{W}^{\mathrm{u}}(\mathcal{M}_0^{m,+})$ composed of the strong unstable fibers of the singular trajectory $\mathcal{M}_0^{m,+}$ also perturbs to a two-dimensional locally invariant manifold $\mathcal{W}^{\mathrm{u}}(\mathcal{M}_\varepsilon^{m,+})$ which is C^0-$\mathcal{O}(\varepsilon^{2/3})$-close and C^1-$\mathcal{O}(\varepsilon^{1/3})$-close to $\mathcal{W}^{\mathrm{u}}(\mathcal{M}_0^{m,+})$, uniformly in $|k| < k_0$.

The results of Proposition 3.6 are depicted in Fig. 13.

We proceed by constructing solutions which pass near the fold. These solutions form a "bridge" between orbits which depart $\mathcal{M}_\varepsilon^m$ along the heteroclinics $\phi^b(y)$ and those which depart along the heteroclinics $\phi^u(y)$, which are constructed in Sects. 3.5 and 3.6, respectively. The geometric intuition is that the fold acts as a means of continuously transitioning from one "side" of $\mathcal{M}_\varepsilon^m$ to the other. The challenge lies in parameterizing these orbits, as the exact orbit $\phi^b(y)$ or $\phi^u(y)$ which is followed when leaving a neighborhood of $\mathcal{F}^\ell$ is not naturally determined.

We choose $0 < \delta \ll \delta_z$ and define the section $\Sigma_{\mathrm{in}}^\ell$ (Fig. 13) by

$$\Sigma_{\mathrm{in}}^\ell = \{(x_\ell, y_\ell, z_\ell) : y_\ell = s_{m,+}(-\delta_z, k, 0), |x_\ell| \le \delta_x, |z_\ell + \delta_z| \le \delta\}. \tag{3.27}$$

We have the following.

Lemma 3.7 *For all sufficiently small $\varepsilon > 0$, we have that $\Sigma_{\mathrm{in}}^\ell \subseteq \mathcal{W}^{\mathrm{s}}(\mathcal{M}_\varepsilon^b)$.*

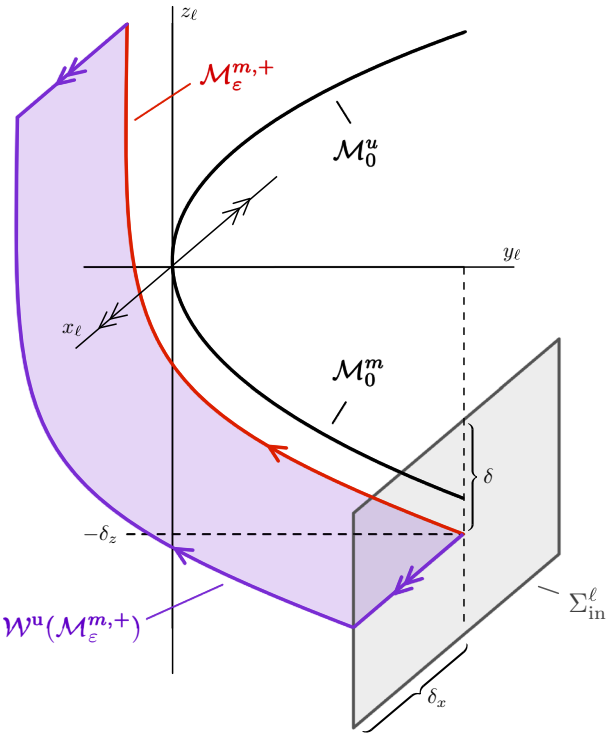

Fig. 13 Depicted are the results of Proposition 3.6. For sufficiently small $\varepsilon > 0$, the singular trajectory $\mathcal{M}_0^{m,+}$ perturbs to a solution $\mathcal{M}_\varepsilon^{m,+}$ within the center manifold $\mathcal{W}^{\text{c}}(\mathcal{F}^\ell) = \{x_\ell = 0\}$. Furthermore, the two-dimensional manifold $\mathcal{W}^{\text{u}}(\mathcal{M}_0^{m,+})$ composed of the strong unstable fibers of $\mathcal{M}_0^{m,+}$ also perturbs to a two-dimensional locally invariant manifold $\mathcal{W}^{\text{u}}(\mathcal{M}_\varepsilon^{m,+})$ depicted by the purple surface. Also shown is the section Σ_{in}^ℓ, transverse to the center manifold $\mathcal{W}^{\text{c}}(\mathcal{F}^\ell)$

Proof We first define a collection of potential "exit" sections for solutions with initial conditions in Σ_{in}^ℓ. The first is given by

$$\Sigma_{\text{out},1}^\ell = \{(x_\ell, y_\ell, \delta_z) : |x_\ell| \leq \delta_x, |y_\ell| \leq \delta\}. \tag{3.28}$$

For the other sections, we first define U^ℓ to be a planar δ-neighborhood of $\mathcal{M}_0^{m,+}$ within the center manifold $\{x_\ell = 0\}$. This neighborhood U^ℓ is bounded by four curves, given by $\Sigma_{\text{in}}^\ell \cap \{x_\ell = 0\}$, $\Sigma_{\text{out},1}^\ell \cap \{x_\ell = 0\}$, as well as two other curves U_{upper}^ℓ and U_{lower}^ℓ, chosen to lie an $\mathcal{O}(\delta)$ distance on either side of $\mathcal{M}_0^{m,+}$, so that the union of these four curves bounds a well-defined planar region U^ℓ within $\{x_\ell = 0\}$ containing $\mathcal{M}_0^{m,+}$, with $\mathcal{O}(\delta)$ thickness.

We now define four additional exit sections

$$\begin{aligned}\Sigma^{\ell}_{\text{out},2} &= \{(\delta_x, y_\ell, z_\ell) : (y_\ell, z_\ell) \in U^{\ell}\}\\ \Sigma^{\ell}_{\text{out},3} &= \{(-\delta_x, y_\ell, z_\ell) : (y_\ell, z_\ell) \in U^{\ell}\}\\ \Sigma^{\ell}_{\text{upper}} &= \{(x_\ell, y_\ell, z_\ell) : |x_\ell| \leq \delta_x, (y_\ell, z_\ell) \in U^{\ell}_{\text{upper}}\}\\ \Sigma^{\ell}_{\text{lower}} &= \{(x_\ell, y_\ell, z_\ell) : |x_\ell| \leq \delta_x, (y_\ell, z_\ell) \in U^{\ell}_{\text{lower}}\}.\end{aligned} \tag{3.29}$$

Previous blow-up analyses (Carter and Sandstede 2015; Krupa and Szmolyan 2001a) of nondegenerate fold points have studied the behavior of basepoint solutions with initial conditions in $\Sigma^{\ell}_{\text{in}} \cap \{x_\ell = 0\}$ for $0 < \varepsilon \ll 1$. In particular, these analyses show that initially such solutions are quickly contracted $\mathcal{O}(e^{-\eta/\varepsilon})$-close to $\mathcal{M}^{m,+}_{\varepsilon}$ and remain $\mathcal{O}(e^{-\eta/\varepsilon})$-close to $\mathcal{M}^{m,+}_{\varepsilon}$ until reaching the set $\Sigma^{\ell}_{\text{out},1} \cap \{x_\ell = 0\}$. Hence, when considering the full dynamics of (3.25), i.e., with the x_ℓ-dynamics included, since solutions on the strong unstable fibers shadow their respective basepoint trajectories, any solution with initial condition in $\Sigma^{\ell}_{\text{in}}$ must pass through one of the three sections $\Sigma^{\ell}_{\text{out},j}$, $j = 1, 2, 3$. In particular, such solutions do not pass through $\Sigma^{\ell}_{\text{upper}}$ or $\Sigma^{\ell}_{\text{lower}}$. It remains to show that $\Sigma^{\ell}_{\text{out},j}$, $j = 1, 2, 3$ are contained in $\mathcal{W}^{\text{s}}(\mathcal{M}^{b}_{\varepsilon})$.

To see this, we first consider solutions within $\Sigma^{\ell}_{\text{out},2} \cap \{y_\ell \geq \delta\}$ and $\Sigma^{\ell}_{\text{out},3} \cap \{y_\ell \geq \delta\}$. Provided $\delta \ll \delta_x$, the fact that such solutions are contained in $\mathcal{W}^{\text{s}}(\mathcal{M}^{b}_{0})$ is clear due to their proximity with the heteroclinic orbits $\phi^u(y), \phi^b(y)$ which lie in $\mathcal{W}^{\text{s}}(\mathcal{M}^{b}_{0})$. For sufficiently small $\varepsilon > 0$, by standard geometric singular perturbation theory, these solutions are contained in $\mathcal{W}^{\text{s}}(\mathcal{M}^{b}_{\varepsilon})$.

For the remaining solutions, i.e., those within $\{|y_\ell| \leq \delta\}$, we first note that due to Hypothesis 7 as well as Hypothesis 5 regarding the layer problem (2.3) for $\varepsilon = 0$, any solution within the plane $\{y_\ell = 0\}$ lying a small fixed distance δ_x from the fold $\mathcal{F}^{\ell}$ must lie in $\mathcal{W}^{\text{s}}(\mathcal{M}^{b}_{0})$. For sufficiently small $\delta \ll \delta_x$, by the smooth dependence of the layer problem on y_ℓ, this also holds for solutions lying distance δ_x from $\mathcal{F}^{\ell}$, which are contained in the region $\{|y_\ell| \leq \delta\}$. Again, the fact that these solutions are contained in $\mathcal{W}^{\text{s}}(\mathcal{M}^{b}_{\varepsilon})$ for small $\varepsilon > 0$ follows from standard geometric singular perturbation theory. Hence, by appropriately choosing $\delta \ll \delta_x, \delta_z$, we obtain the result. □

We note that for $\varepsilon = 0$, we have that

$$\mathcal{W}^{\text{u}}(\mathcal{M}^{m}_{0}) \cap \Sigma^{\ell}_{\text{in}} = \{(x_\ell, y_\ell, \delta_z) : y_\ell = s_{m,+}(\delta_z, k, 0), |x_\ell| \leq \delta_x\}. \tag{3.30}$$

Therefore, for each $|\bar{x}| \leq \delta_x$, we can define the interval

$$\mathcal{I}^{\ell}(\bar{x}) = \Sigma^{\ell}_{\text{in}} \cap \{x_\ell = \bar{x}\}, \tag{3.31}$$

which clearly intersects $\mathcal{W}^{\text{u}}(\mathcal{M}^{m}_{0})$ transversely within $\Sigma^{\ell}_{\text{in}}$. This transversality persists for sufficiently small $\varepsilon > 0$. Combining this with Lemma 3.7, we see that $\mathcal{I}^{\ell}(\bar{x})$ satisfies the conditions outlined in the strategy from Sect. 3.4, and the construction of periodic orbits which pass through $\mathcal{I}^{\ell}(\bar{x})$ follows as in Sect. 3.5.

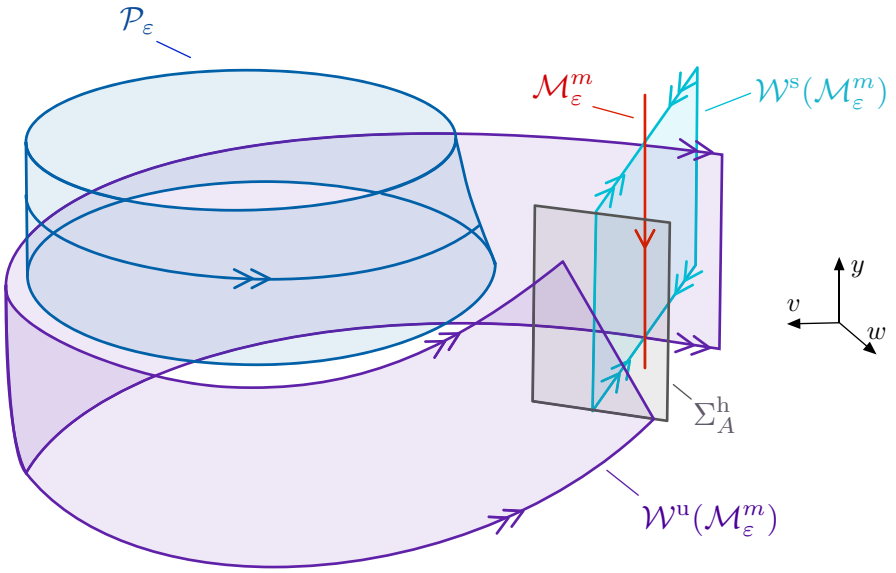

Fig. 14 Shown is the flow near the saddle homoclinic bifurcation for sufficiently small $\varepsilon > 0$. The stable and unstable manifolds $\mathcal{W}^{\rm s,u}(\mathcal{M}_0^m)$ of the critical manifold $\mathcal{M}_0^m$, which intersect transversely for $\varepsilon = 0$, perturb to two-dimensional locally invariant manifolds $\mathcal{W}^{\rm s,u}(\mathcal{M}_\varepsilon^m)$ which again intersect transversely near $y \approx \bar{y}_{\rm h}$ for $0 < \varepsilon \ll 1$. Away from the saddle homoclinic bifurcation, the periodic manifold $\mathcal{P}_0$ persists as a locally invariant manifold $\mathcal{P}_\varepsilon$

3.8 The Flow Near the Saddle Homoclinic Point

Before proceeding to construct N-spike solutions for $N > 1$, it is necessary to understand the passage of solutions the near the saddle homoclinic point $p_{\rm h}$. This analysis is also critical in determining how the different branches of bursting solutions are connected. The main result of this section is Proposition 3.8, which concerns the behavior of solutions which spend long times hear the saddle homoclinic point. The proof of Proposition 3.8 is given in Sect. 3.9.

We continue by considering the flow in a neighborhood of the saddle homoclinic point $p_{\rm h}$. The existence of a saddle homoclinic orbit $\gamma_{\rm h}$ at $p_{\rm h}$ when $\varepsilon = 0$ implies that the manifolds $\mathcal{W}^{\rm u}(\mathcal{M}_0^m)$ and $\mathcal{W}^{\rm s}(\mathcal{M}_0^m)$ intersect transversely along $\gamma_{\rm h}$ in the plane $y = \bar{y}_{\rm h}$. This transverse intersection therefore persists for the manifolds $\mathcal{W}^{\rm u}(\mathcal{M}_\varepsilon^m)$ and $\mathcal{W}^{\rm s}(\mathcal{M}_\varepsilon^m)$ for $\varepsilon > 0$ sufficiently small (Fig. 14).

In a neighborhood of $\mathcal{M}_\varepsilon^m$, there exists a smooth change of coordinates such that the equations can be written in the Fenichel normal form

$$\begin{aligned} \dot{A} &= F_1(A, B, Y, k, \varepsilon)A \\ \dot{B} &= F_2(A, B, Y, k, \varepsilon)B \\ \dot{Y} &= \varepsilon(G_1(Y, k, \varepsilon) + G_2(A, B, Y, k, \varepsilon)), \end{aligned} \tag{3.32}$$

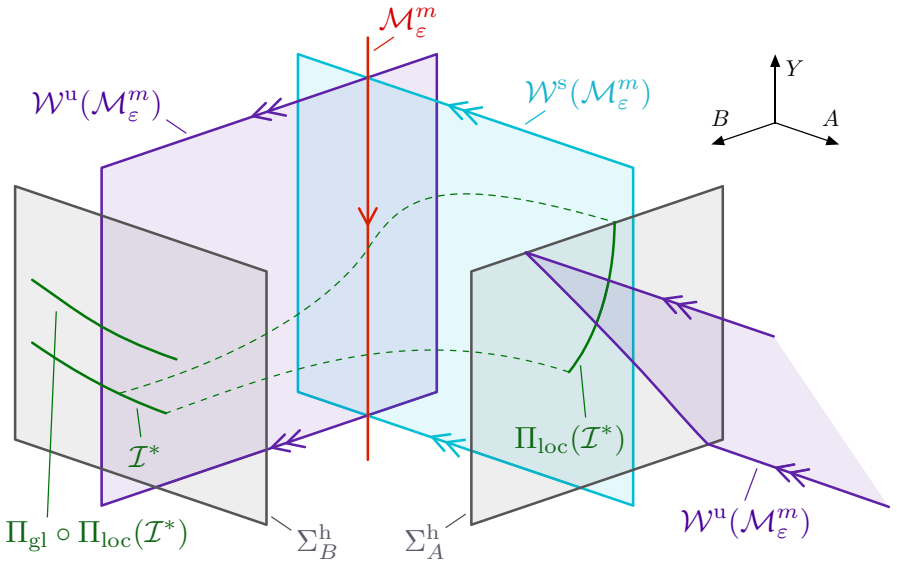

Fig. 15 Shown is the local geometry associated with the flow of the Fenichel normal form (3.32) near the saddle homoclinic bifurcation for sufficiently small $\varepsilon > 0$. The manifolds $\mathcal{W}^{\mathrm{u}}(\mathcal{M}_\varepsilon^m)$ and $\mathcal{W}^{\mathrm{s}}(\mathcal{M}_\varepsilon^m)$ coincide with the sets $A = 0$ and $B = 0$, respectively, and the slow manifold $\mathcal{M}_\varepsilon^m$ is given by $A = B = 0$. The sections $\Sigma_A^{\mathrm{h}}, \Sigma_B^{\mathrm{h}}$ defined in (3.34) are placed at $A = \Delta$ and $B = \Delta$, respectively for small fixed $\Delta > 0$. Due to Hypothesis 4 manifold $\mathcal{W}^{\mathrm{u}}(\mathcal{M}_\varepsilon^m)$ transversely intersects $\mathcal{W}^{\mathrm{s}}(\mathcal{M}_\varepsilon^m)$ in the section Σ_A^{h} for all sufficiently small $\varepsilon > 0$. Also depicted are the results of Lemma 3.13, concerning the return map $\Pi_{\mathrm{gl}} \circ \Pi_{\mathrm{loc}} : \Sigma_B^{\mathrm{h}} \to \Sigma_B^{\mathrm{h}}$ induced by the backward flow of (3.32), applied to a curve $\mathcal{I}^*$ which transversely intersects $\mathcal{W}^{\mathrm{u}}(\mathcal{M}_\varepsilon^m)$ in Σ_B^{h}

where

$$\begin{aligned} F_1(A, B, Y, k, \varepsilon) &= -\alpha(k) + \mathcal{O}(A, B, Y, \varepsilon) \\ F_2(A, B, Y, k, \varepsilon) &= \beta(k) + \mathcal{O}(A, B, Y, \varepsilon) \\ G_1(Y, k, \varepsilon) &= -\gamma(k) + \mathcal{O}(Y, \varepsilon) \\ G_2(A, B, Y, k, \varepsilon) &= \mathcal{O}(AB), \end{aligned} \tag{3.33}$$

where $\alpha(k), \beta(k), \gamma(k) > 0$ uniformly in $|k| < k_0$, and $\alpha(k) > \beta(k)$ due to Hypothesis 4. In the following, we will suppress the dependence on k in the notation. In these coordinates, the set $A = 0$ corresponds to $\mathcal{W}^{\mathrm{u}}(\mathcal{M}_\varepsilon^m)$, the set $B = 0$ coincides with $\mathcal{W}^{\mathrm{s}}(\mathcal{M}_\varepsilon^m)$, and the slow manifold $\mathcal{M}_\varepsilon^m$ is given by $A = B = 0$ (Fig. 15).

We fix the two-dimensional sections

$$\begin{aligned} \Sigma_A^{\mathrm{h}} &= \{A = \Delta, |B| \le \Delta, |Y| \le \delta_Y\} \\ \Sigma_B^{\mathrm{h}} &= \{B = \Delta, |A| \le \Delta, |Y| \le \delta_Y\} \end{aligned} \tag{3.34}$$

for small $\Delta > 0$ to be chosen later (Fig. 15).

By the above discussion, we can track $\mathcal{W}^{\mathrm{u}}(\mathcal{M}_\varepsilon^m)$ along γ_{h} and deduce that this manifold transversely intersects $\mathcal{W}^{\mathrm{s}}(\mathcal{M}_\varepsilon^m)$ in the section Σ_A^{h} for all sufficiently small $\varepsilon > 0$ (Fig. 15). Thus, the intersection of $\mathcal{W}^{\mathrm{u}}(\mathcal{M}_\varepsilon^m)$ with the section Σ_A^{h} is given by a curve which can be represented as a graph over the B-coordinate, that is,

$$\mathcal{W}^{\mathrm{u}}(\mathcal{M}_\varepsilon^m) \cap \Sigma_A^{\mathrm{h}} = \{(\Delta, B, Y_{\mathrm{h}}(B, k, \varepsilon)) : |B| \leq \delta\}, \tag{3.35}$$

for some $0 < \delta \ll \Delta$, where we can assume without loss of generality (by shifting coordinates) that

$$Y_{\mathrm{h}}(0, k, \varepsilon) = 0, \qquad \partial_B Y_{\mathrm{h}}(0, k, \varepsilon) = K(k, \varepsilon, \Delta), \tag{3.36}$$

where $K_1 < K(k, \varepsilon, \Delta) < K_2$ uniformly in $|k| < k_0$ and $0 < \varepsilon \ll 1$ for some $K_j = K_j(\Delta) > 0$ for $j = 1, 2$; note that $Y_{\mathrm{h}}(0, k, 0) = 0$ represents the location of the homoclinic orbit γ_{h} for $\varepsilon = 0$.. In the following, it will also be useful to invert this relation, i.e., represent $\mathcal{W}^{\mathrm{u}}(\mathcal{M}_\varepsilon^m)$ as a graph $B = B_{\mathrm{h}}(Y, k, \varepsilon)$ for $|Y| \leq \delta_Y$, where

$$B_{\mathrm{h}}(0, k, \varepsilon) = 0, \qquad \partial_Y B_{\mathrm{h}}(0, k, \varepsilon) = 1/K(k, \varepsilon, \Delta). \tag{3.37}$$

The primary result of this section is the following proposition, the proof of which is given in Sect. 3.9.

Proposition 3.8 *Consider the backward flow of* (3.32)*. For each sufficiently small* $\Delta > 0$*, there exists* $C, \delta_Y, k_0, \varepsilon_0 > 0$ *such the following holds. For each* $(k, \varepsilon) \in (-k_0, k_0) \times (0, \varepsilon_0)$*, consider a one-dimensional manifold* $\mathcal{I}^* \subset \Sigma_B^{\mathrm{h}}$ *which transversely intersects* $\mathcal{W}^{\mathrm{u}}(\mathcal{M}_\varepsilon^m)$ *in the section* Σ_B^{h} *at some* $Y \in (-\delta_Y, C\varepsilon|\log\varepsilon|)$*. Then, there exists* $\bar{N}(\varepsilon) = \mathcal{O}(1/\varepsilon)$ *such that under the backward flow of* (3.32)*,* $\mathcal{I}^*$ *traces out a two-dimensional manifold* $\overline{\mathcal{I}}$ *which returns to the section* Σ_B^{h} *a total of* $\bar{N}$ *times, each time transversely intersecting the manifold* $\mathcal{W}^{\mathrm{u}}(\mathcal{M}_\varepsilon^m)$*. Furthermore, the transversality is uniform in* $\varepsilon > 0$ *sufficiently small.*

Remark 3.9 The uniformity of the transversality with respect to ε means that this intersection does not approach tangency as $\varepsilon \to 0$. This is important as the manifold $\overline{\mathcal{I}}$ is tracked over $\bar{N} = \mathcal{O}(1/\varepsilon)$ excursions.

Remark 3.10 We also remark briefly on the $\varepsilon|\log\varepsilon|$-bound for the Y-coordinate of intersection with $\mathcal{W}^{\mathrm{u}}(\mathcal{M}_\varepsilon^m)$. For larger values of Y, it is not possible to guarantee that $\overline{\mathcal{I}}$ will intersect $\mathcal{W}^{\mathrm{u}}(\mathcal{M}_\varepsilon^m)$ again on its subsequent returns to Σ_B^{h} under the backward flow of (3.32), unless additional transversality conditions are satisfied. However, we will show that these conditions will be satisfied after an $\mathcal{O}(1)$ number of returns to Σ_B^{h}; see Lemmas 3.13 and 3.14.

3.9 Proof of Proposition 3.8

The proof of Proposition 3.8 involves understanding both the flow near the saddle homoclinic point p_{h} and how solutions leave a neighborhood of the saddle homoclinic

orbit γ_h and interact with the periodic manifold $\mathcal{P}_\varepsilon$. We begin by analyzing the flow near γ_h in Sect. 3.9.1, followed by the flow in a neighborhood of $\mathcal{P}_\varepsilon$ in Sect. 3.9.2. The proof of Proposition 3.8 is briefly concluded in Sect. 3.9.3.

3.9.1 Analysis Near the Saddle Homoclinic Point

The estimates on the flow near the saddle homoclinic orbit γ_h necessary in the proof of Proposition 3.8 are outlined in the following four lemmas. The first two lemmas give estimates on the local map $\Sigma_B^h \to \Sigma_A^h$ under the backward flow of (3.32), and the global map $\Sigma_A^h \to \Sigma_B^h$ in backward time, respectively. The third then combines these to give a precise return estimate $\Sigma_B^h \to \Sigma_B^h$ under the backward flow of (3.32) in the case when $\mathcal{I}^*$ satisfies additional assumptions. The final lemma then shows that any choice of $\mathcal{I}^*$ from Proposition 3.8 will satisfy these extra assumptions after only an $\mathcal{O}(1)$ number of these excursions.

It is essential that the estimates are uniform with respect to the small parameters involved in the analysis, as the two-dimensional manifold $\overline{\mathcal{I}}$, traced out by the one-dimensional manifold $\mathcal{I}^*$ under the backward flow of (3.32), must be tracked over an asymptotically large number of excursions. To this end, we introduce the notation $a \sim b$ for $a, b > 0$ if there exists $C = C(\Delta) > 0$ independent of all sufficiently small δ_Y, ε_0 such that

$$\frac{b}{C} \leq a \leq Cb. \tag{3.38}$$

Here, Δ is the small constant from (3.34). Similarly, we use the notation $a \lesssim b$ for $a, b > 0$ if there exists $C = C(\Delta) > 0$ such that $a \leq C(\Delta)b$. Furthermore, any terms designated by $\mathcal{O}$ notation which do not contain explicit Δ-dependence are understood to be taken up to a constant which may depend on Δ.

We begin with the following Shilnikov-type estimate (Deng 1990; Krupa et al. 1997; Schecter 2008a), the proof of which is given in Appendix A.

Lemma 3.11 *For each sufficiently small $\Delta > 0$, consider the local map $\Pi_{\text{loc}} : \Sigma_B^h \to \Sigma_A^h$ under the backward flow of (3.32). There exists $\delta_Y, \delta > 0$ such that the following holds. Consider $(A, \Delta, Y^*) \in \Sigma_B^h$ satisfying $|A| \leq \delta$. Then, for all sufficiently small $\varepsilon > 0$, we have*

$$\Pi_{\text{loc}} \begin{pmatrix} A \\ \Delta \\ Y^* \end{pmatrix} = \begin{pmatrix} \Delta \\ B_{\text{loc}}(R, Y^*) \\ Y_{\text{loc}}(R, Y^*), \end{pmatrix} \tag{3.39}$$

where $\Delta R^\rho = A$ and

$$\begin{aligned} \rho(R, Y^*; k, \varepsilon) &= \alpha/\beta + \mathcal{O}(\Delta) \\ B_{\text{loc}}(R, Y^*; k, \varepsilon) &= \Delta R(1 + \mathcal{O}(\Delta)) \\ Y_{\text{loc}}(R, Y^*; k, \varepsilon) &= Y^* - \frac{\varepsilon\gamma \log(R)}{\beta}(1 + \mathcal{O}(\Delta)), \end{aligned} \tag{3.40}$$

and the derivatives of these functions with respect to R, Y^* satisfy

$$\begin{aligned} \partial_R \rho &= \mathcal{O}\left(\frac{\Delta}{R \log R}\right), \qquad \partial_{Y^*} \rho = \mathcal{O}(1) \\ \partial_R B_{\text{loc}} &= \Delta(1 + \mathcal{O}(\Delta)), \qquad \partial_{Y^*} B_{\text{loc}} = \mathcal{O}(R \log R) \\ \partial_R Y_{\text{loc}} &= -\frac{\varepsilon}{\beta R}(1 + \mathcal{O}(\Delta)), \qquad \partial_{Y^*} Y_{\text{loc}} = (1 + \mathcal{O}(\Delta)), \end{aligned} \tag{3.41}$$

where the estimates are uniform for all sufficiently small $\delta_Y, \delta, \varepsilon > 0$.

The next lemma concerns the nature of the global map $\Pi_{\text{gl}} : \Sigma_A^{\text{h}} \to \Sigma_B^{\text{h}}$ under the backward flow of (3.32).

Lemma 3.12 *For each sufficiently small $\Delta > 0$, consider the global map $\Pi_{\text{gl}} : \Sigma_A^{\text{h}} \to \Sigma_B^{\text{h}}$ under the backward flow of (3.32). There exists $C_{\text{gl}}, \delta_Y, \delta > 0$ such that the following holds. For all sufficiently small $\varepsilon > 0$, consider a solution $(\Delta, B, Y) \in \Sigma_A^{\text{h}}$ satisfying $|B| \leq \delta$ and $|Y| \leq \delta_Y$. Then,*

$$\Pi_{\text{gl}} \begin{pmatrix} \Delta \\ B \\ Y \end{pmatrix} = \begin{pmatrix} A_{\text{gl}}(B, Y) \\ \Delta \\ Y_{\text{gl}}(B, Y) \end{pmatrix}, \tag{3.42}$$

where

$$\begin{aligned} A_{\text{gl}}(B, Y) &= C_{\text{gl}}(B - B_{\text{h}}(Y, k, \varepsilon)) \\ &\quad + \mathcal{O}\left(|Y||B - B_{\text{h}}(Y, k, \varepsilon)|, \varepsilon|B - B_{\text{h}}(Y, k, \varepsilon)|, |B - B_{\text{h}}(Y, k, \varepsilon)|^2\right) \\ Y_{\text{gl}}(B, Y) &= Y + \mathcal{O}(\varepsilon). \end{aligned} \tag{3.43}$$

The estimates will in general depend on Δ but are uniform with respect to all sufficiently small $\delta, \delta_Y > 0$ provided $\varepsilon > 0$ is taken sufficiently small.

Proof For fixed Δ, the map $\Pi_{\text{gl}} : \Sigma_A^{\text{h}} \to \Sigma_B^{\text{h}}$ for solutions with initial conditions sufficiently close to $\mathcal{W}^{\text{u}}(\mathcal{M}_\varepsilon^m) \cap \Sigma_A^{\text{h}}$ can be determined by a finite time integration. In particular, the set $\mathcal{W}^{\text{u}}(\mathcal{M}_\varepsilon^m) \cap \Sigma_A^{\text{h}}$ will map onto the set $\Sigma_B^{\text{h}} \cap \{A = 0\}$, and the estimates follow from the smoothness of this map. □

The next lemma combines the estimates in Lemmas 3.11 and 3.12 to determine the effect of the return map

$$\Pi_{\text{gl}} \circ \Pi_{\text{loc}} : \Sigma_B^{\text{h}} \to \Sigma_B^{\text{h}} \tag{3.44}$$

under the backward flow of (3.32). In particular, for a manifold which satisfies certain transversality estimates with respect to the manifold $\mathcal{W}^{\text{u}}(\mathcal{M}_\varepsilon^m)$ in the section Σ_B^{h}, these estimates are preserved (in an appropriate sense) under the backward flow of (3.32) (Fig. 16).

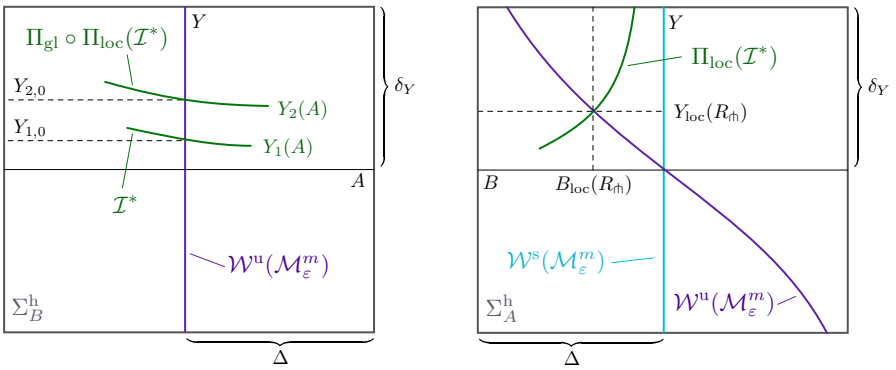

Fig. 16 Depicted is the setup within the sections $\Sigma_B^{\rm h}$ (left) and $\Sigma_A^{\rm h}$ (right) as in Lemma 3.13; see also Fig. 15. Note that in the right panel, the B-coordinate increases to the left in order to preserve the orientation of Fig. 15. The curve $\mathcal{I}^*$, which is given by the graph $Y = Y_1(A, k, \varepsilon)$, transversely intersects $\mathcal{W}^{\rm u}(\mathcal{M}_\varepsilon^m)$ within the section $\Sigma_B^{\rm h}$ at $Y = Y_{1,0}$. Under the reverse flow of (3.32), $\mathcal{I}^*$ is mapped via $\Pi_{\rm loc}$ to $\Sigma_A^{\rm h}$, and the image $\Pi_{\rm loc}(\mathcal{I}^*)$ again transversely intersects $\mathcal{W}^{\rm u}(\mathcal{M}_\varepsilon^m)$ within $\Sigma_A^{\rm h}$ at a point $(B, Y) = (B_{\rm loc}(R_{\pitchfork}), Y_{\rm loc}(R_{\pitchfork}))$, where $R_{\pitchfork}$ is as in (3.55). Further, in backward time, $\Pi_{\rm loc}(\mathcal{I}^*)$ returns to $\Sigma_B^{\rm h}$ via the global map $\Pi_{\rm gl}$, and the image $\Pi_{\rm gl} \circ \Pi_{\rm loc}(\mathcal{I}^*)$ corresponds to the graph of $Y = Y_2(A, k, \varepsilon)$, intersecting $\mathcal{W}^{\rm u}(\mathcal{M}_\varepsilon^m)$ transversely at $Y = Y_{2,0}$

Lemma 3.13 *Fix $\Delta > 0$ sufficiently small. For each $C_1 > 0$ and each sufficiently small $C_2 > 0$, there exists $C, \delta_Y, k_0, \varepsilon_0 > 0$ such that for $(k, \varepsilon) \in (-k_0, k_0) \times (0, \varepsilon_0)$, the following holds. Suppose that the one-dimensional manifold $\mathcal{I}^* \subset \Sigma_B^{\rm h}$ can be represented as a graph $Y = Y_1(A, k, \varepsilon)$ which satisfies*

$$C_1\varepsilon|\log\varepsilon| < Y_{1,0} < \delta_Y, \qquad \sup_{|A|\le C_2|Y_{1,0}|} |\partial_A Y_1(A, k, \varepsilon)| \le \left|\frac{\varepsilon \log|Y_{1,0}|}{Y_{1,0}}\right|, \tag{3.45}$$

where $Y_{1,0} := Y_1(0, k, \varepsilon)$. Then, under the reverse flow of (3.32), $\mathcal{I}^*$ traces out a two-dimensional manifold $\overline{\mathcal{I}}$, which again intersects $\Sigma_B^{\rm h}$ in a curve which can be represented as a graph $Y = Y_2(A, k, \varepsilon)$ satisfying

$$Y_{2,0} > Y_{1,0} + C\varepsilon, \qquad \sup_{|A|\le C_2|Y_{2,0}|} |\partial_A Y_2(A, k, \varepsilon)| \le \left|\frac{\varepsilon \log|Y_{2,0}|}{Y_{2,0}}\right|, \tag{3.46}$$

where $Y_{2,0} := Y_2(0, k, \varepsilon)$.

Proof The strategy of the proof is to combine the results of Lemma 3.11 and Lemma 3.12. Care must be taken to ensure that for fixed Δ, the estimates hold independently of $Y_{1,0} \in (C_1\varepsilon|\log\varepsilon|, \delta_Y)$ for sufficiently small choice of δ_Y, ε_0 with $\varepsilon \in (0, \varepsilon_0)$.

We first use Lemma 3.11 to determine the image of $\mathcal{I}^*$ under the local map $\Pi_{\rm loc} : \Sigma_B^{\rm h} \to \Sigma_A^{\rm h}$. Under the map $\Pi_{\rm loc}$, $\mathcal{I}^*$ is mapped to a curve in $\Sigma_A^{\rm h}$ parameterized by

$R = (A/\Delta)^{1/\rho}$ as

$$\Pi_{\text{loc}} \begin{pmatrix} A \\ \Delta \\ Y_1(A, k, \varepsilon) \end{pmatrix} = \begin{pmatrix} \Delta \\ B_{\text{loc}}(R) \\ Y_{\text{loc}}(R) \end{pmatrix}, \tag{3.47}$$

where the functions

$$\begin{aligned} B_{\text{loc}}(R) &:= B_{\text{loc}}(R, Y_1(\Delta R^\rho, k, \varepsilon)) \\ Y_{\text{loc}}(R) &:= Y_{\text{loc}}(R, Y_1(\Delta R^\rho, k, \varepsilon)). \end{aligned} \tag{3.48}$$

defined as in Lemma 3.11 satisfy

$$\begin{aligned} \rho(R) &= \alpha/\beta + \mathcal{O}(\Delta) \\ B_{\text{loc}}(R) &= \Delta R(1 + \mathcal{O}(\Delta)) \\ Y_{\text{loc}}(R) &= Y_1(\Delta R^\rho, k, \varepsilon) - \frac{\varepsilon\gamma \log R}{\beta}(1 + \mathcal{O}(\Delta)) \end{aligned} \tag{3.49}$$

and

$$\begin{aligned} \partial_R(R^\rho) &= \rho R^{\rho-1}(1 + \mathcal{O}(\Delta)) \\ \partial_R B_{\text{loc}}(R) &= \Delta(1 + \mathcal{O}(\Delta)) \\ \partial_R Y_{\text{loc}}(R) &= \Delta R^{\rho-1} \partial_A Y_1(\Delta R^\rho, k, \varepsilon)(1 + \mathcal{O}(\Delta)) - \frac{\varepsilon\gamma}{\beta R}(1 + \mathcal{O}(\Delta)) \end{aligned} \tag{3.50}$$

by implicitly differentiating the functions $B_{\text{loc}}, Y_{\text{loc}}$ in (3.48) and using estimates (3.41).

We first claim that the curve $(B, Y) = (B_{\text{loc}}, Y_{\text{loc}})(R)$ transversely intersects $\mathcal{W}^{\text{u}}(\mathcal{M}_\varepsilon^m)$ within Σ_B^{h}. The intersection of the manifold $\mathcal{W}^{\text{u}}(\mathcal{M}_\varepsilon^m)$ with Σ_B^{h} is given as a curve $Y = Y_{\text{h}}(B, k, \varepsilon)$. We therefore need to solve the following equation.

$$\begin{aligned} Y_{\text{h}}(B_{\text{loc}}(R), k, \varepsilon) &= Y_{\text{loc}}(R) \\ &= Y_1(\Delta R^\rho, k, \varepsilon) - \frac{\varepsilon\gamma \log R}{\beta}(1 + \mathcal{O}(\Delta)) \\ &= Y_{1,0} + \mathcal{O}(R^\rho) - \frac{\varepsilon\gamma \log R}{\beta}(1 + \mathcal{O}(\Delta)), \end{aligned} \tag{3.51}$$

where we used (3.49). At first, we ignore the last term on the right-hand side and consider the simpler equation

$$Y_{\text{h}}(B_{\text{loc}}(R), k, \varepsilon) = Y_{1,0} + \mathcal{O}(R^\rho). \tag{3.52}$$

Using (3.36) and (3.50), this equation can be solved for $R = R_0 = \frac{Y_{1,0}}{K\Delta}(1 + \mathcal{O}(\Delta))$. We set $R = R_0(1 + R_1)$ and return to the full equation, which becomes

$$K\Delta R_1 R_0(1 + \mathcal{O}(\Delta)) + \mathcal{O}(R_1 R_0^{\nu}) = -\frac{\varepsilon\gamma \log R_0}{\beta}(1 + \mathcal{O}(\Delta)) + \mathcal{O}(\varepsilon R_1), \tag{3.53}$$

where $\nu := \min\{\rho, 2\} > 1$. It is now possible to solve for

$$R_1 = -\frac{\varepsilon\gamma \log R_0}{\beta K\Delta R_0}(1 + \mathcal{O}(\Delta, R_0^{\nu-1})). \tag{3.54}$$

From this, we obtain the solution $R = R_{\pitchfork}(k, \varepsilon) = R_0(1 + R_1)$ given by

$$R_{\pitchfork}(k, \varepsilon) = \frac{Y_{1,0}}{K\Delta}(1 + \mathcal{O}(\Delta)) - \frac{\varepsilon\gamma}{\beta K\Delta} \log\left(\frac{Y_{1,0}}{K\Delta}\right)(1 + \mathcal{O}(\Delta)). \tag{3.55}$$

Provided δ_Y, ε_0 are sufficiently small and since $C_1\varepsilon|\log\varepsilon| < Y_{1,0} < \delta_Y$ by (3.45), we have that $R_{\pitchfork} \sim |Y_{1,0}|$. Note that the lower bound on $Y_{1,0}$ is crucial in order to obtain that $R_{\pitchfork} \sim |Y_{1,0}|$.

We now focus on the global map $\Pi_{\mathrm{gl}} : \Sigma_A^{\mathrm{h}} \to \Sigma_B^{\mathrm{h}}$. Using Lemma 3.12, we have that

$$\Pi_{\mathrm{gl}}\begin{pmatrix} \Delta \\ B_{\mathrm{loc}}(R) \\ Y_{\mathrm{loc}}(R) \end{pmatrix} = \begin{pmatrix} A_{\mathrm{gl}}(B_{\mathrm{loc}}(R), Y_{\mathrm{loc}}(R)) \\ \Delta \\ Y_{\mathrm{gl}}(B_{\mathrm{loc}}(R), Y_{\mathrm{loc}}(R)) \end{pmatrix} \tag{3.56}$$

where

$$\begin{aligned} A_{\mathrm{gl}}(R) &= C_{\mathrm{gl}}(B_{\mathrm{loc}}(R) - B_{\mathrm{h}}(Y_{\mathrm{loc}}(R), k, \varepsilon)) \\ &\quad + \mathcal{O}\left((|Y_{\mathrm{loc}}(R)| + \varepsilon + |B_{\mathrm{loc}}(R)\right. \\ &\quad \left. - B_{\mathrm{h}}(Y_{\mathrm{loc}}(R), k, \varepsilon)|)|B_{\mathrm{loc}}(R) - B_{\mathrm{h}}(Y_{\mathrm{loc}}(R), k, \varepsilon)|\right) \\ Y_{\mathrm{gl}}(R) &= Y_{\mathrm{loc}}(R) + \mathcal{O}(\varepsilon), \end{aligned} \tag{3.57}$$

where we have simplified the notation by writing $A_{\mathrm{gl}}(R) = A_{\mathrm{gl}}(B_{\mathrm{loc}}(R), Y_{\mathrm{loc}}(R))$ and $Y_{\mathrm{gl}}(R) = Y_{\mathrm{gl}}(B_{\mathrm{loc}}(R), Y_{\mathrm{loc}}(R))$. The goal is to express Y_{gl} as a graph $Y_{\mathrm{gl}} = Y_2(A_{\mathrm{gl}}, k, \varepsilon)$ over A_{gl} and verify estimates (3.46) are satisfied. We first determine

$$\begin{aligned} Y_{2,0} &= Y_{\mathrm{gl}}(R_{\pitchfork}) \\ &= Y_1(\Delta R_{\pitchfork}^{\rho}, k, \varepsilon) - \frac{\varepsilon\gamma \log R_{\pitchfork}}{\beta}(1 + \mathcal{O}(\Delta)) + \mathcal{O}(\varepsilon), \end{aligned} \tag{3.58}$$

using (3.49). Using the fact that $R_{\pitchfork} \sim |Y_{1,0}|$, for all sufficiently small δ_Y, ε_0 and $C_1\varepsilon|\log\varepsilon| < Y_{1,0} < \delta_Y$, we have that

$$R_{\pitchfork}^{\rho} \ll |Y_{1,0}|, \tag{3.59}$$

so that

$$0 < (Y_{2,0} - Y_{1,0}) \sim \varepsilon \left|\log |Y_{1,0}|\right| + \mathcal{O}(\varepsilon). \tag{3.60}$$

From this, we obtain

$$Y_{2,0} > Y_{1,0} + C\varepsilon, \tag{3.61}$$

for some $C = C(\Delta)$, and further we note that $|Y_{2,0}| \sim |Y_{1,0}|$.

In order to prove estimate (3.46) regarding the derivative of $Y_2(A, k, \varepsilon)$ on the interval $|A| \leq C_2|Y_{2,0}|$, we first determine the endpoints of this interval in terms of R, which we denote by $R_{\text{start}}, R_{\text{end}}$. To find these endpoints, we must solve for when

$$A_{\text{gl}}(R) = \pm C_2 Y_{2,0} \tag{3.62}$$

in terms of R. By the implicit function theorem, after some manipulations using (3.50) and (3.57), and using the relations (3.51), and (3.58) satisfied by R_{fh}, we find that we can solve for

$$\begin{aligned} R_{\text{start}} &= \left(1 - \frac{C_2 K}{C_{\text{gl}}}\right) R_{\text{fh}}(1 + \mathcal{O}(\Delta)) \\ R_{\text{end}} &= \left(1 + \frac{C_2 K}{C_{\text{gl}}}\right) R_{\text{fh}}(1 + \mathcal{O}(\Delta)), \end{aligned} \tag{3.63}$$

provided C_2 is sufficiently small, and in particular, we have $R_{\text{start}}, R_{\text{end}} \sim R_{\text{fh}}$. Therefore, also $R_{\text{start}}, R_{\text{end}} \sim |Y_{1,0}|$ and hence for all sufficiently small δ_Y, ε_0 and any $C_1\varepsilon|\log\varepsilon| < Y_{1,0} < \delta_Y$, we have

$$R_{\text{end}}^{\rho} < C_2|Y_{1,0}|. \tag{3.64}$$

We now compute

$$\frac{\mathrm{d}Y_{\text{gl}}}{\mathrm{d}R} = \rho\Delta R^{\rho-1}\partial_A Y_1(\Delta R^{\rho}, k, \varepsilon)(1 + \mathcal{O}(\Delta)) - \frac{\varepsilon\gamma}{\beta R}(1 + \mathcal{O}(\Delta)) + \mathcal{O}(\varepsilon) \tag{3.65}$$

whereby

$$\begin{aligned} \left|\frac{\mathrm{d}Y_{\text{gl}}}{\mathrm{d}R}\right| &\leq \rho\Delta R^{\rho-1}\left|\frac{\varepsilon\log|Y_{1,0}|}{Y_{1,0}}\right|(1 + \mathcal{O}(\Delta)) + \frac{\varepsilon\gamma}{\beta R_{\text{start}}}(1 + \mathcal{O}(\Delta)) \\ &\lesssim \left(|Y_{2,0}|^{\rho-1} + \frac{1}{|\log|Y_{2,0}||}\right)\left|\frac{\varepsilon\log|Y_{2,0}|}{Y_{2,0}}\right|. \end{aligned} \tag{3.66}$$

We now use (3.57) and compute the derivative

$$\frac{\mathrm{d}A_{\mathrm{gl}}}{\mathrm{d}R} = C_{\mathrm{gl}}\left(1 + \mathcal{O}\left(\Delta, R, \left|\frac{\mathrm{d}Y_{\mathrm{gl}}}{\mathrm{d}R}\right|\right)\right). \tag{3.67}$$

We can then compute the slope $\frac{\mathrm{d}Y_{\mathrm{gl}}}{\mathrm{d}A_{\mathrm{gl}}}$ as the ratio of (3.66) and (3.67)

$$\begin{aligned}\left|\frac{\mathrm{d}Y_{\mathrm{gl}}}{\mathrm{d}A_{\mathrm{gl}}}\right| &= \frac{\left|\frac{\mathrm{d}Y_{\mathrm{gl}}}{\mathrm{d}R}\right|}{C_{\mathrm{gl}}\left(1 + \mathcal{O}\left(\Delta, R, \left|\frac{\mathrm{d}Y_{\mathrm{gl}}}{\mathrm{d}R}\right|\right)\right)} \\ &\leq \left|\frac{\varepsilon \log|Y_{2,0}|}{Y_{2,0}}\right|\end{aligned} \tag{3.68}$$

independently of the initial $Y_{1,0} \in (C_1\varepsilon|\log\varepsilon|, \delta_Y)$, by choosing δ_Y, ε_0 sufficiently small. It follows that the manifold $\overline{\mathcal{I}}$ intersects Σ_B^{h} in a curve which can be represented as a graph $Y = Y_2(A, k, \varepsilon)$ for values of $|A| \leq C_2|Y_{2,0}|$, satisfying estimates (3.46). □

The final technical lemma ensures that a manifold $\mathcal{I}^*$ which intersects $\mathcal{W}^{\mathrm{u}}(\mathcal{M}_\varepsilon^m)$ transversely in the section Σ_B^{h} as in Proposition 3.8 satisfies the assumptions of Lemma 3.13 after finitely many returns to Σ_B^{h}.

Lemma 3.14 *Consider the backward flow of (3.32). For each sufficiently small $\Delta > 0$ there exist C_1, C_2 and $\delta_Y, \varepsilon_0, k_0 > 0$ such that for each $(k, \varepsilon) \in (-k_0, k_0) \times (0, \varepsilon_0)$, the following holds. Consider a one-dimensional manifold $\mathcal{I}^* \subset \Sigma_B^{\mathrm{h}}$ which can be represented as a graph $Y = Y_1(B, k, \varepsilon)$ with $Y_1(0, k, \varepsilon) =: Y_{1,0} \in (-\delta_Y, C_1\varepsilon|\log\varepsilon|)$, and which transversely intersects $\mathcal{W}^{\mathrm{u}}(\mathcal{M}_\varepsilon^m)$ in the section Σ_B^{h}. Then, under the backward flow of (3.32), $\mathcal{I}^*$ traces out a two-dimensional manifold $\overline{\mathcal{I}}$ which, after finitely many excursions, transversely intersects Σ_B^{h} in a curve which can be represented as a graph $Y = Y_2(A, k, \varepsilon)$ satisfying*

$$C_1\varepsilon|\log\varepsilon| < Y_{2,0} < \delta_Y, \qquad \sup_{|A| \leq C_2|Y_{2,0}|} |\partial_A Y_2(A, k, \varepsilon)| \leq \left|\frac{\varepsilon \log|Y_{2,0}|}{Y_{2,0}}\right|, \tag{3.69}$$

where $Y_{2,0} := Y_2(0, k, \varepsilon)$.

Proof We proceed as in the proof of Lemma 3.13, and we begin by determining the image of $\mathcal{I}^*$ under the local map $\Pi_{\mathrm{loc}} : \Sigma_B^{\mathrm{h}} \to \Sigma_A^{\mathrm{h}}$. Under the map Π_{loc}, $\mathcal{I}^*$ is mapped to a curve in Σ_A^{h} parameterized by $R = (A/\Delta)^{1/\rho}$ as

$$\Pi_{\mathrm{loc}}\begin{pmatrix} A \\ \Delta \\ Y_1(A, k, \varepsilon)\end{pmatrix} = \begin{pmatrix} \Delta \\ B_{\mathrm{loc}}(R) \\ Y_{\mathrm{loc}}(R)\end{pmatrix}, \tag{3.70}$$

where the functions $B_{\mathrm{loc}}(R)$, $Y_{\mathrm{loc}}(R)$ satisfy (3.49) and (3.50). We search for the location of a transverse intersection of the curve $(B, Y) = (B_{\mathrm{loc}}, Y_{\mathrm{loc}})(R)$ with $\mathcal{W}^{\mathrm{u}}(\mathcal{M}_\varepsilon^m)$

within Σ_B^{h}, where $\mathcal{W}^{\mathrm{u}}(\mathcal{M}_\varepsilon^m)$ is given by the graph $Y = Y_{\mathrm{h}}(B, k, \varepsilon)$. As in the proof of Lemma 3.13, we therefore need to solve an equation of the form

$$Y_{\mathrm{h}}(B_{\mathrm{loc}}(R), k, \varepsilon) = Y_{1,0} + \mathcal{O}(R^\rho) - \frac{\varepsilon\gamma \log R}{\beta}(1 + \mathcal{O}(\Delta)), \tag{3.71}$$

where $Y_{1,0} \in (-\delta_Y, C_1\varepsilon|\log\varepsilon|)$. We first focus on the region $|Y_{1,0}| < C_1\varepsilon|\log\varepsilon|$, and we consider the simpler equation

$$Y_{\mathrm{h}}(B_{\mathrm{loc}}(R), k, \varepsilon) = -\frac{\varepsilon\gamma \log R}{\beta}(1 + \mathcal{O}(\Delta)) + \mathcal{O}(R^\rho). \tag{3.72}$$

Proceeding in a similar fashion as in the proof of Lemma 3.13, we set

$$R = \frac{\gamma\varepsilon|\log\varepsilon|}{\beta\Delta K}(1 + R_0), \tag{3.73}$$

which results in the equation

$$R_0(1 + \mathcal{O}(\Delta)) + \mathcal{O}((\varepsilon|\log\varepsilon|)^{\nu-1}R_0) = \mathcal{O}\left(\Delta, \frac{\log(\log\varepsilon)}{\log\varepsilon}, \frac{R_0}{\log\varepsilon}\right), \tag{3.74}$$

which can be solved for

$$R_0 = \mathcal{O}(\Delta) \tag{3.75}$$

for all sufficiently small $\varepsilon > 0$. This gives a solution to (3.72) defined by (3.73), which we denote by R_1. We now return to the full equation (3.71) and set $R = R_1(1 + R_2)$, which results in the equation

$$\begin{aligned} R_2(1 + \mathcal{O}(\Delta)) + \mathcal{O}((\varepsilon|\log\varepsilon|)^{\nu-1}R_2) &= \frac{Y_{1,0}}{\Delta K R_1} + \mathcal{O}\left(\Delta, \frac{\log(\log\varepsilon)}{\log\varepsilon}, \frac{R_0}{\log\varepsilon}\right) \\ &= \frac{\beta Y_{1,0}}{\gamma\varepsilon|\log\varepsilon|} + \mathcal{O}\left(\Delta, \frac{\log(\log\varepsilon)}{\log\varepsilon}, \frac{R_0}{\log\varepsilon}\right), \end{aligned} \tag{3.76}$$

which can be solved in the region $|Y_{1,0}| < C_1\varepsilon|\log\varepsilon|$ for

$$R_2 = \frac{\beta Y_{1,0}}{\gamma\varepsilon|\log\varepsilon|} + \mathcal{O}(\Delta), \tag{3.77}$$

resulting in a solution $R = R_{\text{⫛}} := R_1(1 + R_2)$ of Eq. (3.71) given by

$$R_{\text{⫛}} = \frac{\gamma\varepsilon|\log\varepsilon|}{\beta\Delta K}\left(1 + \frac{\beta Y_{1,0}}{\gamma\varepsilon|\log\varepsilon|} + \mathcal{O}(\Delta)\right). \tag{3.78}$$

We now focus on the global map $\Pi_{\rm gl} : \Sigma_A^{\rm h} \to \Sigma_B^{\rm h}$. Using Lemma 3.12, we have that

$$\Pi_{\rm gl}\begin{pmatrix}\Delta\\ B_{\rm loc}(R)\\ Y_{\rm loc}(R)\end{pmatrix} = \begin{pmatrix}A_{\rm gl}(B_{\rm loc}(R), Y_{\rm loc}(R))\\ \Delta\\ Y_{\rm gl}(B_{\rm loc}(R), Y_{\rm loc}(R))\end{pmatrix}, \tag{3.79}$$

where

$$\begin{aligned} A_{\rm gl}(R) &= C_{\rm gl}(B_{\rm loc}(R) - B_{\rm h}(Y_{\rm loc}(R), k, \varepsilon))\\ &\quad + \mathcal{O}\left((|Y_{\rm loc}(R)| + \varepsilon + |B_{\rm loc}(R)\right.\\ &\quad \left. - B_{\rm h}(Y_{\rm loc}(R), k, \varepsilon)|)|B_{\rm loc}(R) - B_{\rm h}(Y_{\rm loc}(R), k, \varepsilon)|\right)\\ Y_{\rm gl}(R) &= Y_{\rm loc}(R) + \mathcal{O}(\varepsilon). \end{aligned} \tag{3.80}$$

We now show that $Y_{\rm gl}$ can be written as a graph $Y_{\rm gl} = Y_2(A_{\rm gl}, k, \varepsilon)$ over $A_{\rm gl}$ and verify estimates (3.69) are satisfied. We first determine

$$\begin{aligned} Y_{2,0} &= Y_{\rm gl}(R_{\pitchfork})\\ &= Y_1(\Delta R_{\pitchfork}^{\rho}, k, \varepsilon) - \frac{\varepsilon\gamma \log R_{\pitchfork}}{\beta}(1 + \mathcal{O}(\Delta)) + \mathcal{O}(\varepsilon), \end{aligned} \tag{3.81}$$

and using (3.78), we have that

$$Y_{2,0} = Y_{1,0} - \frac{\varepsilon\gamma \log \varepsilon}{\beta}(1 + \mathcal{O}(\Delta)) + \mathcal{O}(\varepsilon), \tag{3.82}$$

so that

$$Y_{2,0} > C_1\varepsilon|\log\varepsilon| \tag{3.83}$$

provided $C_1 = C_1(\Delta)$ is sufficiently small and $|Y_{1,0}| < C_1\varepsilon|\log\varepsilon|$, for all sufficiently small $\varepsilon > 0$. Estimates (3.69) which concern the derivative of $Y_2(A, k, \varepsilon)$ proceed as in the proof of Lemma 3.13, noting that $R_{\pitchfork} \sim \varepsilon|\log\varepsilon|$.

Finally, it remains to consider the region $Y_{1,0} \in (-\delta_Y, -C_1\varepsilon|\log\varepsilon|)$. The strategy is to show that in this case $\mathcal{I}^*$ returns to $\Sigma_B^{\rm h}$ under the backward flow of (3.32), this time intersecting $\mathcal{W}^{\rm u}(\mathcal{M}_\varepsilon^m)$ at a value of $Y > -C_1\varepsilon|\log\varepsilon|$, in which case the above argument can be repeated to complete the proof. We therefore return to Eq. (3.71), which we now aim to solve assuming $Y_{1,0} \in (-\delta_Y, -C_1\varepsilon|\log\varepsilon|)$.

We set $R = R_0R_1$ for some $R_0 \in (0, 1)$ and obtain the equation

$$\begin{aligned} &K\Delta R_0R_1(1 + \mathcal{O}(\Delta, (R_0R_1)^{\nu-1}))\\ &\quad = Y_{1,0} - \frac{\varepsilon\gamma \log R_1}{\beta}(1 + \mathcal{O}(\Delta)) - \frac{\varepsilon\gamma \log R_0}{\beta}(1 + \mathcal{O}(\Delta)). \end{aligned} \tag{3.84}$$

We first solve for R_0 in terms of $R_1, Y_{1,0}$ by solving

$$K\Delta R_0 R_1(1+\mathcal{O}(\Delta,(R_0R_1)^{\nu-1}))=-\frac{\varepsilon\gamma\log R_0}{\beta}(1+\mathcal{O}(\Delta)). \tag{3.85}$$

For $C_3=C_3(\Delta)$ sufficiently large so that

$$C_3>\frac{\gamma}{\beta\Delta K}, \tag{3.86}$$

we separate two cases: $R_1>C_3\varepsilon$ and $R_1<2C_3\varepsilon$. If $R_1>C_3\varepsilon$, proceeding similarly as above, we can solve (3.85) by setting

$$R_0=-\frac{\varepsilon\gamma}{\beta\Delta K R_1}\log\left(\frac{\varepsilon\gamma}{\beta\Delta K R_1}\right)(1+R_2), \tag{3.87}$$

substituting into (3.85), and solving for $R_2=\mathcal{O}(\Delta)$ for all sufficiently small R_1 satisfying $R_1>C_3\varepsilon$.

Substituting back into (3.84), we now determine R_1 by solving

$$0=Y_{1,0}-\frac{\varepsilon\gamma\log R_1}{\beta}(1+\mathcal{O}(\Delta)), \tag{3.88}$$

whereby we obtain

$$R_1=\exp\left(\frac{\beta Y_{1,0}}{\varepsilon\gamma}(1+\mathcal{O}(\Delta))\right), \tag{3.89}$$

and therefore, the full solution $R=R_{\text{fh}}:=R_0R_1$ of (3.71) is given by

$$R_{\text{fh}}=-\frac{\varepsilon\gamma}{\beta\Delta K}\log\left(\frac{\varepsilon\gamma}{\beta\Delta K}\right)(1+\mathcal{O}(\Delta))+\frac{Y_{1,0}}{\Delta K}(1+\mathcal{O}(\Delta)). \tag{3.90}$$

On the other hand, returning to (3.85), in the region $R_1<2C_3\varepsilon$, after some rearranging we obtain the equation

$$R_0=\exp\left(-\frac{\beta K\Delta R_1}{\varepsilon\gamma}R_0(1+\mathcal{O}(\Delta,(R_0R_1)^{\nu-1}))\right). \tag{3.91}$$

For $0<R_1<2C_3\varepsilon$, this relation defines R_0 as a strictly positive, monotone decreasing function of R_1, and in this region, R_0 is confined to the interval $(C_4,1)$ for some $0<C_4(\Delta)<1$, which is independent of δ_Y,ε. In particular, this relation can be solved for

$$R_0=\frac{W[Z]}{Z},\qquad Z=\frac{\beta K\Delta R_1}{\varepsilon\gamma}(1+\mathcal{O}(\Delta)), \tag{3.92}$$

where $W[\cdot]$ denotes the principal branch of the Lambert W-function. Proceeding as above, we substitute back into (3.84), solve for R_1, and obtain the full solution $R = R_{\text{⫛}} := R_0 R_1$ of (3.71), given by

$$R_{\text{⫛}} = R_0 \exp\left(\frac{\beta Y_{1,0}}{\varepsilon\gamma}(1 + \mathcal{O}(\Delta))\right). \tag{3.93}$$

We now determine

$$\begin{aligned} Y_{2,0} &= Y_{\text{gl}}(R_{\text{⫛}}) \\ &= Y_{\text{loc}}(R_{\text{⫛}}) + \mathcal{O}(\varepsilon) \\ &= Y_{\text{h}}(B_{\text{loc}}(R_{\text{⫛}})) + \mathcal{O}(\varepsilon) \\ &= K\Delta R_{\text{⫛}}(1 + \mathcal{O}(\Delta, R_{\text{⫛}})) + \mathcal{O}(\varepsilon). \end{aligned} \tag{3.94}$$

Using (3.84), we have that

$$Y_{2,0} = -\frac{\varepsilon\gamma \log R_0}{\beta}(1 + \mathcal{O}(\Delta)) + \mathcal{O}(\varepsilon, R_{\text{⫛}}^{\nu}). \tag{3.95}$$

In the region $R_1 > C_3\varepsilon$, R_0 is given by (3.87) so that

$$Y_{2,0} > -C_1\varepsilon|\log\varepsilon| \tag{3.96}$$

for all sufficiently small $\varepsilon > 0$. In the region $R_1 < 2C_3\varepsilon$, we have that R_0 is given by (3.92) so that

$$Y_{2,0} = \mathcal{O}(\varepsilon) \tag{3.97}$$

for all sufficiently small $\varepsilon > 0$. Estimates (3.69) which concern the derivative of $Y_2(A, k, \varepsilon)$ are similar as in the proof of Lemma 3.13, though with minor differences outlined below.

Using expressions (3.80), we now compute

$$\frac{\mathrm{d}Y_{\text{gl}}}{\mathrm{d}R} = \rho\Delta R^{\rho-1}\partial_A Y_1(\Delta R^{\rho}, k, \varepsilon)(1 + \mathcal{O}(\Delta)) - \frac{\varepsilon\gamma}{\beta R}(1 + \mathcal{O}(\Delta)) + \mathcal{O}(\varepsilon), \tag{3.98}$$

whereby

$$\frac{\mathrm{d}Y_{\text{gl}}}{\mathrm{d}R} \leq K\Delta \tag{3.99}$$

for all sufficiently small $\varepsilon > 0$. We now use (3.57) and compute the derivative

$$\frac{\mathrm{d}A_{\text{gl}}}{\mathrm{d}R} = C_{\text{gl}}\left(1 + \mathcal{O}(\Delta, R) - \frac{1}{K}\frac{\mathrm{d}Y_{\text{gl}}}{\mathrm{d}R}(1 + \mathcal{O}(\Delta, R))\right). \tag{3.100}$$

We can then compute the slope $\frac{\mathrm{d}Y_{\mathrm{gl}}}{\mathrm{d}A_{\mathrm{gl}}}$ as the ratio of (3.99) and (3.100)

$$\begin{aligned}\left|\frac{\mathrm{d}Y_{\mathrm{gl}}}{\mathrm{d}A_{\mathrm{gl}}}\right| &= \frac{\left|\frac{\mathrm{d}Y_{\mathrm{gl}}}{\mathrm{d}R}\right|}{C_{\mathrm{gl}}\left(1+\mathcal{O}(\Delta,R)-\frac{1}{K}\frac{\mathrm{d}Y_{\mathrm{gl}}}{\mathrm{d}R}\left(1+\mathcal{O}(\Delta,R)\right)\right)} \\ &\leq C_5(\Delta)\end{aligned} \tag{3.101}$$

for some $C_5(\Delta)$ independent of the initial $Y_{1,0} \in (-\delta_Y, -C_1\varepsilon|\log\varepsilon|)$, by choosing δ_Y, ε_0 sufficiently small. □

3.9.2 The Flow Near the Periodic Manifold $\mathcal{P}_\varepsilon$

We now consider the dynamics near the periodic manifold and the interaction with the analysis near the saddle homoclinic point outlined in Sect. 3.9.1.

We consider a compact portion of the periodic manifold $\mathcal{P}_0 \cap \{\bar{y}_{\mathrm{h}} + \delta_Y/2 \leq y \leq \bar{y}_{\mathrm{p}} - \delta_Y\}$, outside a small neighborhood of the saddle homoclinic point. By Hypothesis 4, we note that in this region for $\varepsilon = 0$, the cylindrical singular periodic manifold $\mathcal{P}_0$ is a two-dimensional normally attracting invariant manifold. By Fenichel theory (Fenichel 1971, Theorem 3), this manifold therefore persists for small $\epsilon > 0$ as a two-dimensional normally attracting locally invariant manifold $\mathcal{P}_\varepsilon$ in the region $y \in (\bar{y}_{\mathrm{h}} + \delta_Y/2, \bar{y}_{\mathrm{p}} - \delta_Y)$, which again takes the form of a cylinder which is C^r-close to $\mathcal{P}_0$.

In particular, this cylindrical manifold extends into a small neighborhood of the saddle homoclinic point. As the periodic orbits contained in $\mathcal{P}_0$ bifurcate from the saddle homoclinic orbit γ_{h}, in its region of definition the perturbed manifold $\mathcal{P}_\varepsilon$ lies near the stable/unstable manifolds $\mathcal{W}^{\mathrm{s,u}}(\mathcal{M}_\varepsilon^m)$. We now determine the proximity of $\mathcal{P}_\varepsilon$ and $\mathcal{W}^{\mathrm{u}}(\mathcal{M}_\varepsilon^m)$ within the section Σ_B^{h}, which is given in the next lemma.

Lemma 3.15 *Fix $\Delta > 0$. For all sufficiently small δ_Y and each sufficiently small $\varepsilon > 0$, the following holds. The periodic manifold $\mathcal{P}_\varepsilon$ intersects the section Σ_B^{h} in a curve*

$$\mathcal{P}_\varepsilon \cap \Sigma_B^{\mathrm{h}} = \{(\Delta, B_{\mathrm{p}}(y; k, \varepsilon), Y) : Y \in (\delta_Y/2, \delta_Y)\}, \tag{3.102}$$

where $B_{\mathrm{p}}(Y; k, \varepsilon)$ is a smooth positive function of (Y, k, ε) which satisfies

$$B_{\mathrm{p}}(Y; k, \varepsilon) = \mathcal{O}(Y^{\alpha/\beta}, \varepsilon). \tag{3.103}$$

Proof This estimate is derived from two simpler estimates: first the nature of the bifurcation of the periodic orbits from the saddle homoclinic orbit for $\varepsilon = 0$, and second from the proximity of the perturbed manifold $\mathcal{P}_\varepsilon$ to its $\varepsilon = 0$ counterpart $\mathcal{P}_0$.

We first consider the layer problem (2.3) to determine the proximity of $\mathcal{P}_0$ and $\mathcal{W}^{\mathrm{u}}(\mathcal{M}_0^m)$ for $\varepsilon = 0$. The periodic orbits are obtained by bifurcating from the saddle homoclinic orbit γ_{h} for values of $y > \bar{y}_{\mathrm{h}}$. Here, y acts as the bifurcation parameter which, as outlined in Hypothesis 4, we assume unfolds this bifurcation in a transverse fashion. It then follows from homoclinic bifurcation theory (Homburg and Sandstede

2010) that the periodic orbits which bifurcate from $\gamma_{\rm h}$ for $y \in (\bar{y}_{\rm h}, \bar{y}_{\rm h} + \delta_Y)$ for sufficiently small δ_Y lie at an $\mathcal{O}(|y - \bar{y}_{\rm h}|^{\alpha/\beta})$ distance from $\mathcal{W}^{\rm u}(\mathcal{M}_0^m)$ in the section $\Sigma_B^{\rm h}$. In particular, we have that the manifold $\mathcal{P}_0$ intersects the section $\Sigma_B^{\rm h}$ in a graph $B = B_{\rm p}(Y; k, 0)$, where $B_{\rm p}(Y; k, 0)$ is a smooth positive function of (Y, k) which satisfies

$$B_{\rm p}(Y; k, 0) = \mathcal{O}(Y^{\alpha/\beta}). \tag{3.104}$$

To obtain the full estimate (3.103), we now use the fact that away from the saddle homoclinic point, i.e., for $Y > \delta_Y/2$, the periodic manifold $\mathcal{P}_\varepsilon$ persists as a C^1-$\mathcal{O}(\varepsilon)$ perturbation of its $\varepsilon = 0$ counterpart $\mathcal{P}_0$. □

We now determine the local dynamics in a tubular neighborhood of $\mathcal{P}_\varepsilon$ away from the saddle homoclinic point. See Fig. 17 for a visualization. We have the following.

Lemma 3.16 *For sufficiently small $\delta > 0$ and $\varepsilon_0 > 0$, there exists a smooth change of coordinates $S^1 \times [-\delta, \delta] \times (\bar{y}_{\rm h} + \delta_Y/2, \bar{y}_{\rm p} - \delta_Y) \to \mathbb{R}^3$ in a neighborhood of $\mathcal{P}_\varepsilon$ which transforms (2.1) to the system*

$$\begin{aligned} \dot{x}_c &= \frac{2\pi}{T_{\rm p}(y)} + h_c(x_c, y, \varepsilon) \\ \dot{x}_s &= -(\mu_{\rm p}(y) + h_s(x_c, x_s, y, \varepsilon))x_s \\ \dot{y} &= \varepsilon g_{\rm p}(x_c, y, \varepsilon), \end{aligned} \tag{3.105}$$

where $h_c, h_s, g_{\rm p}$ are smooth functions of $(x_c, x_s, y, \varepsilon)$ which satisfy

$$\begin{aligned} h_c(x_c, y, \varepsilon) &= \mathcal{O}(\varepsilon) \\ h_s(x_c, x_s, y, \varepsilon) &= \mathcal{O}(x_s, \varepsilon) \\ \int_{S^1} g_{\rm p}(x_c, y, \varepsilon) &< 0, \end{aligned} \tag{3.106}$$

uniformly $(x_c, x_s, y, \varepsilon) \in S^1 \times [-\delta, \delta] \times (\bar{y}_{\rm h} + \delta_Y/2, \bar{y}_{\rm p} - \delta_Y) \times [0, \epsilon_0)$.

Proof We consider the variational equation about the periodic orbit $\gamma_{\rm p}(t; y) = (v_{\rm p}(t; y), w_{\rm p}(t; y))$ in the layer problem (2.1), given by

$$\dot{\Phi} = D_{(v,w)} F(v_{\rm p}(t; y), w_{\rm p}(t; y), y, k, 0)\Phi. \tag{3.107}$$

By Hypothesis 4 and standard Floquet theory, there exists a nontrivial solution $\Phi(t) = e^{-\mu_{\rm p}(y)t} p(t; y)$ to (3.107), where $p(t; y) = (p_v, p_w)(t; y) \in \mathbb{R}^2$ is a $T_{\rm p}(y)$-periodic function of t. At the linear level, for small $\delta > 0$, the transformation $S^1 \times [-\delta, \delta] \times (\bar{y}_{\rm h} + \delta_Y/2, \bar{y}_{\rm p} - \delta_Y) \to \mathbb{R}^3$ given by

$$\begin{pmatrix} x_c \\ x_s \\ y \end{pmatrix} \mapsto \begin{pmatrix} v_{\rm p}\left(\frac{T_{\rm p}(y)}{2\pi} x_c, y\right) + x_s p_v\left(\frac{T_{\rm p}(y)}{2\pi} x_c, y\right) \\ w_{\rm p}\left(\frac{T_{\rm p}(y)}{2\pi} x_c, y\right) + x_s p_w\left(\frac{T_{\rm p}(y)}{2\pi} x_c, y\right) \\ y \end{pmatrix} \tag{3.108}$$

maps $(\cdot, 0, y)$ onto $\gamma_{\mathrm{p}}(\cdot; y)$, while x_s parameterizes the tangent space of the stable fiber $\mathcal{W}^{\mathrm{s}}(\gamma_{\mathrm{p}}(\cdot; y))$ of $\gamma_{\mathrm{p}}(\cdot; y)$. In other words, in a plane of fixed y, x_c parameterizes the direction tangent to $\gamma_{\mathrm{p}}(\cdot; y)$, while x_s parameterizes the normal direction.

In particular, the manifold $\mathcal{P}_0$ is given by the set $x_s = 0$; this manifold persists for small $\varepsilon > 0$ as a locally invariant manifold $\mathcal{P}_\varepsilon$, which can be given as a graph $x_s = x_s^{\mathcal{P}}(x_c, y, \varepsilon)$. Setting $\tilde{x}_s = x_s - x_s^{\mathcal{P}}(x_c, y, \varepsilon)$, we arrive at the equations

$$\begin{aligned} \dot{x}_c &= \frac{2\pi}{T_{\mathrm{p}}(y)} + h_c(x_c, \tilde{x}_s, y, \varepsilon) \\ \dot{\tilde{x}}_s &= -(\mu_{\mathrm{p}}(y) + h_s(x_c, \tilde{x}_s, y, \varepsilon))x_s \\ \dot{y} &= \varepsilon g_{\mathrm{p}}(x_c, \tilde{x}_s, y, \varepsilon), \end{aligned} \tag{3.109}$$

where h_c, h_s, g_{p} are C^r functions which satisfy

$$\begin{aligned} h_c(x_c, \tilde{x}_s, y, \varepsilon) &= \mathcal{O}(\tilde{x}_s, \varepsilon) \\ h_s(x_c, \tilde{x}_s, y, \varepsilon) &= \mathcal{O}(\tilde{x}_s, \varepsilon) \\ \int_{S^1} g_{\mathrm{p}}(x_c, 0, y, 0) dx_c &< 0, \end{aligned} \tag{3.110}$$

where the estimate on g_{p} is due to Hypothesis 6. To obtain the form of Eq. (3.105), we apply a final coordinate transformation to straighten the strong stable fibers (see, e.g., (Fenichel 1979, §X)), and abusing notation, we drop the tildes for $\tilde{x}_s$ and continue to denote the (slightly modified) functions on the right-hand side by h_c, h_s, g_{p}. □

The flow in a neighborhood of $\mathcal{P}_\varepsilon$ is shown in Fig. 17. The manifold $\mathcal{P}_\varepsilon$ is given by the set $\{x_s = 0\}$, and we define the section

$$\Sigma^{\mathrm{p}} := \{x_s = \delta\}. \tag{3.111}$$

Solutions in this neighborhood are quickly attracted to $\mathcal{P}_\varepsilon$ and follow the flow of basepoint solutions on $\mathcal{P}_\varepsilon$. These solutions wind around $\mathcal{P}_\varepsilon$ in forward time, slowly drifting downward, in the shape of a helix. Since the y-drift is of $\mathcal{O}(\varepsilon)$, and away from $y \approx \bar{y}_{\mathrm{h}}$ the periods $\{T_{\mathrm{p}}(y)\}$ are bounded from above, given an orbit which starts at $y(0) = y_0$ for some $y_0 > \bar{y}_{\mathrm{h}} + \delta_Y/2$, we can compute the change in y after one rotation around $\mathcal{P}_\varepsilon$ from $x_c = 0$ to $x_c = 2\pi$ to leading order as

$$\int_0^{2\pi} \frac{dy}{dx_c} dx_c = \frac{\varepsilon T_{\mathrm{p}}(y_0)}{2\pi} \int_0^{2\pi} g_{\mathrm{p}}(x_c, y_0, 0) dx_c + \mathcal{O}(\varepsilon^2), \tag{3.112}$$

where the quantity

$$\int_0^{2\pi} g_{\mathrm{p}}(x_c, y_0, 0) dx_c < 0 \tag{3.113}$$

is independent of ε and is bounded away from zero uniformly in $y_0 > \bar{y}_{\mathrm{h}} + \delta_Y/2$ due to Hypothesis 6. That is, after each successive "lap" around $\mathcal{P}_\varepsilon$, the y-coordinate of a

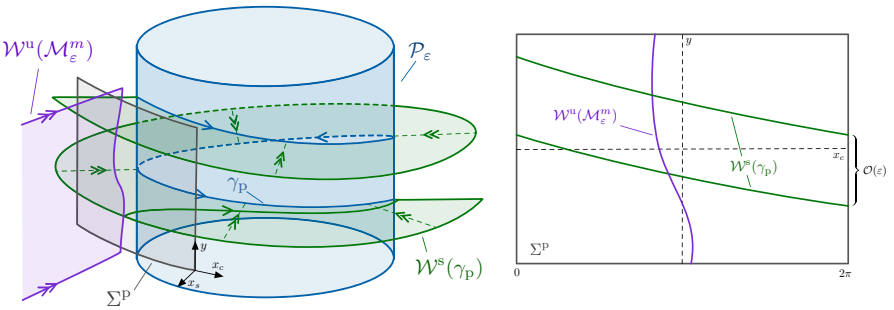

Fig. 17 The left panel depicts the flow near the periodic manifold $\mathcal{P}_\varepsilon$ for sufficiently small $\varepsilon > 0$. Solutions on $\mathcal{P}_\varepsilon$ wind around in forward time, with the y-coordinate decreasing by an $\mathcal{O}(\varepsilon)$ amount after each loop; a sample basepoint solution γ_{p} on $\mathcal{P}_\varepsilon$ is depicted in blue. The strong stable fibers of such a trajectory form a two-dimensional locally invariant manifold $\mathcal{W}^{\mathrm{s}}(\gamma_{\mathrm{p}})$ on which solutions are contracted in forward time toward γ_{p}. The right panel depicts the two-dimensional section Σ^{p} which is placed transverse to the flow at a small fixed distance from the manifold $\mathcal{P}_\varepsilon$. Note that Σ^{p} in fact forms a cylinder which extends all the way around $\mathcal{P}_\varepsilon$, though only a portion is shown in the left panel for clarity. The manifold $\mathcal{W}^{\mathrm{s}}(\gamma_{\mathrm{p}})$ as well as the unstable manifold $\mathcal{W}^{\mathrm{u}}(\mathcal{M}_\varepsilon^m)$ of the slow manifold $\mathcal{M}_\varepsilon^m$ intersect Σ^{p} in smooth curves

given solution decreases by an $\mathcal{O}(\varepsilon)$ amount. Equivalently, under the backward flow of (3.105), solutions on the manifold $\mathcal{P}_\varepsilon$ wind around $\mathcal{P}_\varepsilon$, slowly drifting upward.

We now recall the existence of the heteroclinic orbits $\phi^{\mathrm{p}}(y)$ for $y \in (\bar{y}_{\mathrm{h}}, \bar{y}_{\mathrm{p}})$ for $\varepsilon = 0$ which form connections between $\mathcal{M}_0^m$ and $\mathcal{P}_0$. These orbits form part of $\mathcal{W}^{\mathrm{u}}(\mathcal{M}_0^m)$ in the region $y \in (\bar{y}_{\mathrm{h}}, \bar{y}_{\mathrm{p}})$. Therefore, $\mathcal{W}^{\mathrm{u}}(\mathcal{M}_0^m)$ enters a neighborhood of $\mathcal{P}_\varepsilon$; in particular, $\mathcal{W}^{\mathrm{u}}(\mathcal{M}_0^m)$ transversely intersects the section Σ^{p} in a smooth curve which can be represented as a graph $x_c = x_c(y)$ for $y \in (\bar{y}_{\mathrm{h}} + \delta_Y/2, \bar{y}_{\mathrm{p}} - \delta_Y)$. For sufficiently small $\varepsilon > 0$, the perturbed manifold $\mathcal{W}^{\mathrm{u}}(\mathcal{M}_\varepsilon^m)$ therefore also transversely intersects Σ^{p} in a curve graph $x_c = x_c(y, \varepsilon)$ for $y \in (\bar{y}_{\mathrm{h}} + \delta_Y/2, \bar{y}_{\mathrm{p}} - \delta_Y)$.

We now consider the behavior under the backward flow of (3.105) of a basepoint solution γ_{p} on $\mathcal{P}_\varepsilon$. We refer to Fig. 17 for the relevant geometry. This solution admits a two-dimensional stable manifold $\mathcal{W}^{\mathrm{s}}(\gamma_{\mathrm{p}})$, which forms a surface that winds around $\mathcal{P}_\varepsilon$. Along each "lap" around $\mathcal{P}_\varepsilon$, $\mathcal{W}^{\mathrm{s}}(\gamma_{\mathrm{p}})$ is aligned C^1-$\mathcal{O}(\varepsilon)$-close to a planes $y =$const. Hence, $\mathcal{W}^{\mathrm{s}}(\gamma_{\mathrm{p}})$ repeatedly intersects $\mathcal{W}^{\mathrm{u}}(\mathcal{M}_\varepsilon^m)$ in a transverse fashion on each lap around $\mathcal{P}_\varepsilon$.

3.9.3 Conclusion of the Proof of Proposition 3.8

Combining the results of Sects. 3.9.1 and 3.9.2, we have the following.

Proof of Proposition 3.8 Using Lemma 3.14 and applying Lemma 3.13, the manifold $\overline{\mathcal{I}}$ returns repeatedly to the section Σ_B^{h}, each time transversely intersecting $\mathcal{W}^{\mathrm{u}}(\mathcal{M}_\varepsilon^m)$ and satisfying estimates (3.46).

Eventually $\overline{\mathcal{I}}$ will transversely intersect $\mathcal{W}^{\mathrm{u}}(\mathcal{M}_\varepsilon^m)$ within Σ_B^{h} at some value of $Y > \delta_Y$, whereby Lemma 3.13 is no longer applicable. However, this intersection point now occurs an $\mathcal{O}(\delta_Y)$ distance from the saddle homoclinic bifurcation point, in a region where the periodic manifold $\mathcal{P}_\varepsilon$ is known to persist. Using Lemma 3.15 in combination with Lemma 3.13, we deduce that $\overline{\mathcal{I}}$ transversely intersects $\mathcal{P}_\varepsilon$ in the

section Σ_B^{h}. Further, in backward time $\overline{\mathcal{I}}$ quickly aligns along the strong stable fibers of $\mathcal{P}_\varepsilon$, tracking a solution which winds repeatedly around $\mathcal{P}_\varepsilon$. The results of Sect. 3.9.2 imply that $\overline{\mathcal{I}}$ continues to repeatedly transversely intersect $\mathcal{W}^{\mathrm{u}}(\mathcal{M}_\varepsilon^m)$ after each time around $\mathcal{P}_\varepsilon$, until nearing $y = \bar{y}_{\mathrm{p}}$. The total number of intersections is of $\mathcal{O}(1/\varepsilon)$ as the y coordinate changes by an $\mathcal{O}(\varepsilon)$ amount on each lap around $\mathcal{P}_\varepsilon$. □

3.10 Upper and Lower *N*-Spike Orbits

Using the results of the previous section, it is possible to construct N-spike bursting orbits for any $N < \bar{N}$ for some $\bar{N}(\varepsilon) = \mathcal{O}(1/\varepsilon)$. With the help of Proposition 3.8, the construction is nearly identical to the construction of lower 0-spike orbits and upper 1-spike orbits in Sects. 3.5 and 3.6.

The N-spike orbits are still characterized by a long canard trajectory, which consists of first following $\mathcal{M}_\varepsilon^b$, then $\mathcal{M}_\varepsilon^m$. The orbit then completes N spikes, or excursions, around the upper branch $\mathcal{M}_\varepsilon^u$ before returning to $\mathcal{M}_\varepsilon^m$, then finally returning to $\mathcal{M}_\varepsilon^b$ via one of the heteroclinic connections, either $\phi^u(y)$ in the case of an upper N-spike orbit, or $\phi^b(y)$ for a lower N-spike orbit.

Again, these orbits are most naturally parameterized by which heteroclinic connection ϕ^u or ϕ^b is followed, in addition to the minimum y-value achieved along the orbit, i.e., the y-value of $\phi^u(y)$ or $\phi^b(y)$. Hence, for each $s \in [\bar{y}_\ell + \Delta, \bar{y}_{\mathrm{h}} - \Delta]$ we search for an N-spike periodic orbit which achieves a minimum y-value of $y = s$, and passes near $\phi^j(s)$, for $j = u, b$.

Following the general strategy in Sect. 3.4, in order to construct a periodic orbit, it is necessary to find a one-dimensional manifold of initial conditions $\mathcal{I}$ which lies in $\mathcal{W}^{\mathrm{s}}(\mathcal{M}_\varepsilon^b)$, and which in backward time traces out a two-dimensional manifold $\bar{\mathcal{I}}$ which transversely intersects $\mathcal{W}^{\mathrm{u}}(\mathcal{M}_\varepsilon^m)$. Whenever these conditions hold, then using the exchange lemma, it is possible to set up and solve matching conditions near the fold $\mathcal{F}^r$ for a periodic orbit as in Sect. 3.5. Hence, to construct an N-spike orbit, we aim to find a manifold which satisfies these conditions which also completes N excursions around the upper branch, which we will accomplish through the use of Proposition 3.8.

For lower N-spike orbits, we therefore follow the strategy of Sect. 3.5 by choosing an appropriate one-dimensional curve of candidate initial conditions. As before, we denote by w^b the w-coordinate at which the heteroclinic orbit $\phi^b(s)$ intersects the set $\{v = \bar{v}_r\}$. For sufficiently small $\delta > 0$, we then define $\mathcal{I}^b(s)$ to be an interval of width δ which lies in the plane $\{y = s\}$ and is transverse to the fast layer dynamics, and which intersects $\phi^b(s)$ at $w = w^b$.

In particular, $\mathcal{I}^b(s)$ transversely intersects $\mathcal{W}^{\mathrm{u}}(\mathcal{M}_\varepsilon^m)$, and therefore in backward time $\mathcal{I}^b(s)$ traces out a two-dimensional manifold $\overline{\mathcal{I}}^b(s)$ which, by the exchange lemma, quickly aligns C^1-$\mathcal{O}(e^{-\eta/\varepsilon})$-close to $\mathcal{W}^{\mathrm{s}}(\mathcal{M}_\varepsilon^m)$.

In particular, now transitioning to the local coordinates of Sect. 3.8, we have $\overline{\mathcal{I}}^b(s)$ reaches the section Σ_A^{h} aligned C^1-$\mathcal{O}(e^{-\eta/\varepsilon})$-close to $\mathcal{W}^{\mathrm{s}}(\mathcal{M}_\varepsilon^m)$ and therefore transversely intersects $\mathcal{W}^{\mathrm{u}}(\mathcal{M}_\varepsilon^m)$ within Σ_A^{h} at a value of $Y = \mathcal{O}(e^{-\eta/\varepsilon})$. Using the global map Π_{gl}, this transverse intersection persists as $\overline{\mathcal{I}}^b(s)$ completes an excursion fol-

lowing the singular homoclinic orbit $\gamma_{\rm h}$, and therefore $\overline{\mathcal{I}}^b(s)$ transversely intersects $\mathcal{W}^{\rm u}(\mathcal{M}_\varepsilon^m)$ within $\Sigma_B^{\rm h}$ at a value of $Y = \mathcal{O}(\varepsilon)$.

We now use the results of Proposition 3.8, which guarantee that $\overline{\mathcal{I}}^b(s)$ completes $\bar{N}(\varepsilon) = \mathcal{O}(1/\varepsilon)$ excursions around the upper branch in backward time, transversely intersecting $\mathcal{W}^{\rm u}(\mathcal{M}_\varepsilon^m)$ after each such excursion. Therefore, for each fixed N, by construction the set of initial conditions $\mathcal{I}^b(s)$ lies in the stable manifold $\mathcal{W}^{\rm s}(\mathcal{M}_\varepsilon^b)$, and by the above argument $\mathcal{I}^b(s)$ traces out a two-dimensional manifold $\overline{\mathcal{I}}^b(s)$ which completes N excursions around the upper branch in backward time before transversely intersecting $\mathcal{W}^{\rm u}(\mathcal{M}_\varepsilon^m)$.

Hence, $\mathcal{I}^b(s)$ completes N excursions around $\mathcal{M}_\varepsilon^u$ and satisfies the conditions outlined in Sect. 3.4. We may therefore proceed identically as in Sect. 3.5 to set up matching conditions in order to construct the periodic orbit, which occurs for

$$k = k_N^{\rm sa,lower}(s,\varepsilon) = k^{\rm mc}(\sqrt{\varepsilon}) + \mathcal{O}(e^{-\eta/\varepsilon}). \tag{3.114}$$

For upper N-spike orbits, we follow the strategy of Sect. 3.6, again choosing an appropriate one-dimensional curve of candidate initial conditions. As before, we denote by w^u the w-coordinate at which the heteroclinic orbit $\phi^u(s)$ intersects the set $\{v = \bar{v}_\ell\}$. For sufficiently small $\delta > 0$, we define $\mathcal{I}^u(s)$ to be an interval of width δ which lies in the plane $\{y = s\}$ and is transverse to the fast layer dynamics, and which intersects $\phi^u(s)$ at $w = w^u$. The remainder of the analysis is identical to the above construction of lower N-spike orbits, and we obtain a solution for

$$k = k_N^{\rm sa,upper}(s,\varepsilon) = k^{\rm mc}(\sqrt{\varepsilon}) + \mathcal{O}(e^{-\eta/\varepsilon}). \tag{3.115}$$

Finally, for N-spike orbits which pass near the upper left fold $\mathcal{F}^\ell$, the analysis is identical to that in Sect. 3.7, in combination with the application of Proposition 3.8 as above. Additionally, arguing similarly as with the overlap of lower 0-spike orbits and upper 1-spike orbits, this guarantees the overlap of lower N spike orbits and upper $(N+1)$-spike orbits as one continuous family.

3.11 Orbits Which Pass Near the Saddle Homoclinic Point

In Sect. 3.10, we constructed upper and lower N spike orbits, and we argued that the branch of lower N-spike orbits and the branch of upper $(N+1)$-spike orbits are connected via orbits which pass near the upper left fold $\mathcal{F}^\ell$. However, in order to show that all of these bursting solutions (i.e., N-spike solutions for any N) lie on the same branch, it remains to show that the branches of lower N-spike orbits and upper N-spike orbits are connected. These two families are constructed in different ways, based on either following $\phi^u(y)$ or $\phi^b(y)$ for values of $y \in [\bar{y}_\ell + \Delta, \bar{y}_{\rm h} - \Delta]$; we must show that these two separate constructions can be extended in such a way that they have an overlapping description for values of $y \approx \bar{y}_{\rm h}$, that is, near the saddle homoclinic point.

3.11.1 Upper and Lower Families of *N*-Spike Orbits Near the Saddle Homoclinic Point

We use the coordinate system from Sect. 3.8, and Taking $\delta > 0$ sufficiently small and $Y^* \in [-\Delta, -\delta_Y/2]$, we consider the set

$$\mathcal{I}_+^*(Y^*) = \{(A, \Delta, Y^*) : |A| \leq \delta\} \tag{3.116}$$

within the section $\{B = \Delta\}$. It is clear that $\mathcal{I}_+^*(Y^*)$ transversely intersects $\mathcal{W}^{\rm u}(\mathcal{M}_\varepsilon^m)$ within this section nearby one of the singular orbits $\phi^u(y)$ for some value of $y < \bar{y}_{\rm h} - \delta_Y/2$. In particular, if δ is sufficiently small, then every solution which crosses $\mathcal{I}_+^*(Y^*)$ also lies in the stable manifold $\mathcal{W}^{\rm s}(\mathcal{M}_\varepsilon^b)$. Following a similar construction in 3.10, we see that for each N and each $Y^* \in [-\Delta, -\delta_Y/2]$, the manifold $\mathcal{I}_+^*(Y^*)$ can be used as the basis for constructing an upper N-spike orbit, and in particular, this construction forms an overlapping family with the construction of upper N-spike orbits from 3.10.

On the other hand, if we likewise consider the section $\{B = -\Delta\}$, we can perform an analogous procedure. Taking $\delta > 0$ sufficiently small and $Y^* \in [-\Delta, -\delta_Y/2]$, we consider the set

$$\mathcal{I}_-^*(Y^*) = \{(A, -\Delta, Y^*) : |A| \leq \delta\} \tag{3.117}$$

within the section $\{B = -\Delta\}$. Again it is clear that $\mathcal{I}_-^*(Y^*)$ transversely intersects $\mathcal{W}^{\rm u}(\mathcal{M}_\varepsilon^m)$ within this section. However, this now occurs nearby one of the singular orbits $\phi^b(y)$ for some value of $y < \bar{y}_{\rm h} - \delta_Y/2$. We again see that every solution on $\mathcal{I}_-^*(Y^*)$ also lies in the stable manifold $\mathcal{W}^{\rm s}(\mathcal{M}_\varepsilon^b)$, and for each N, the manifold $\mathcal{I}_-^*(Y^*)$ can be used as the basis for constructing a lower N-spike orbit, and this construction similarly forms an overlapping family with the construction of lower N-spike orbits from 3.10.

3.11.2 Extending the Upper and Lower Families of Orbits

We now work to extend the two families of N-spike solutions defined through the above constructions involving either $\mathcal{I}_-^*$ (the lower family) or $\mathcal{I}_+^*$ (the upper family) in such a way that they form a single overlapping family of N-spike orbits.

We begin with the upper family. We recall from §3.8 the definition of the sections

$$\begin{aligned} \Sigma_A^{\rm h} &= \{A = \Delta, |B| \leq \Delta, |Y| \leq \delta_Y\} \\ \Sigma_B^{\rm h} &= \{B = \Delta, |A| \leq \Delta, |Y| \leq \delta_Y\}, \end{aligned} \tag{3.118}$$

and we consider the intersection of $\mathcal{W}^{\rm u}(\mathcal{M}_\varepsilon^m)$ with the section $\Sigma_A^{\rm h}$. We recall from Sect. 3.8 that this intersection is given by a curve which can be represented as a graph $Y = Y_{\rm h}(B, k, \varepsilon)$ for $|B| \leq \delta$ which satisfies (3.36). We consider the set of curves

$$\mathcal{J}_+^\dagger := \{\mathcal{I}_+^\dagger(B^\dagger) : B^\dagger \in (-\delta, -\varepsilon^\kappa)\} \tag{3.119}$$

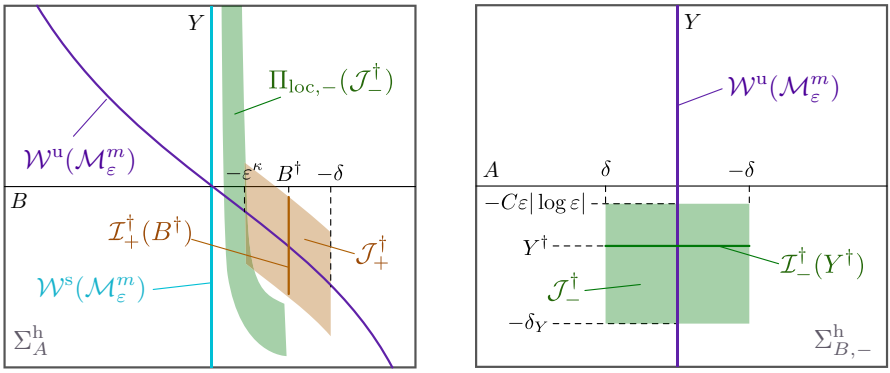

Fig. 18 Depicted is the setup within the sections Σ_A^{h} (left) and $\Sigma_{B,-}^{\mathrm{h}}$ (right) as in Lemma 3.17. Note that in the left (resp. right) panel, the B-coordinate (resp. A-coordinate) increases to the left in order to preserve the orientation of Fig. 15. The two-dimensional set $\mathcal{J}_+^\dagger$, shaded orange in the left panel, consists of the union of the one-dimensional curves $\mathcal{I}_+^\dagger(B^\dagger)$ for $B^\dagger \in (-\delta, -\varepsilon^\kappa)$. Likewise, the two-dimensional set $\mathcal{J}_-^\dagger$, shaded green in the right panel, consists of the union of the one-dimensional curves $\mathcal{I}_-^\dagger(Y^\dagger)$ for $Y^\dagger \in (-\delta_Y, -C\varepsilon|\log\varepsilon|)$. The image of the set $\mathcal{J}_-^\dagger$ under the map $\Pi_{\mathrm{loc},-}$, as in Lemma 3.17, is also shown in the left panel

parameterized by $B^\dagger \in (-\delta, -\varepsilon^\kappa)$, for some $\kappa = \kappa(\Delta) > 0$, where each curve $\mathcal{I}_+^\dagger(B^\dagger)$ within Σ_A^{h} is defined by

$$\mathcal{I}_+^\dagger(B^\dagger) = \{(\Delta, B^\dagger, Y) : |Y - Y_{\mathrm{h}}(B^\dagger, k, \varepsilon)| \leq \delta_Y/2\}. \tag{3.120}$$

We refer to Fig. 18 for an illustration. For each fixed $B^\dagger \in (-\delta, -\varepsilon^\kappa)$, the curve $\mathcal{I}_+^\dagger(B^\dagger)$ clearly intersects $\mathcal{W}^{\mathrm{u}}(\mathcal{M}_\varepsilon^m)$ transversely within the section Σ_A^{h}. Using the global map Π_{gl} for the backward flow of (3.32), $\mathcal{I}_+^\dagger(B^\dagger)$ is mapped to a curve in Σ_B^{h} which also transversely intersects $\mathcal{W}^{\mathrm{u}}(\mathcal{M}_\varepsilon^m)$. Hence, using Proposition 3.8, under the backward flow of (2.1), $\mathcal{I}_+^\dagger(B^\dagger)$ traces out a two-dimensional manifold $\overline{\mathcal{I}}_+^\dagger(B^\dagger)$ in backward time which completes $\bar{N} = \mathcal{O}(1/\varepsilon)$ excursions around the upper branch, transversely intersecting $\mathcal{W}^{\mathrm{u}}(\mathcal{M}_\varepsilon^m)$ after each such excursion. The construction therefore proceeds as in the case of upper N-spike orbits as in Sect. 3.10 provided it can be shown that $\mathcal{I}_+^\dagger(B^\dagger)$ is also contained in the stable manifold $\mathcal{W}^{\mathrm{s}}(\mathcal{M}_\varepsilon^b)$ of the lower branch $\mathcal{M}_\varepsilon^b$, which will be shown below. We first note that orbits constructed in this manner form an overlapping family with those constructed via the sets $\mathcal{I}_+^*$.

We now define the section

$$\Sigma_{B,-}^{\mathrm{h}} = \{B = -\Delta, |A| \leq \Delta, |Y| \leq \delta_Y\}. \tag{3.121}$$

To show $\mathcal{I}_+^\dagger(B^\dagger) \subseteq \mathcal{W}^{\mathrm{s}}(\mathcal{M}_\varepsilon^b)$, we consider the forward evolution of $\mathcal{I}_+^\dagger(B^\dagger)$ from Σ_A^{h} to $\Sigma_{B,-}^{\mathrm{h}}$ under the flow of (3.32). This induces a map $\Sigma_A^{\mathrm{h}} \to \Sigma_{B,-}^{\mathrm{h}}$ under which

points on $\mathcal{I}^\dagger_+(B^\dagger) \in \Sigma^{\mathrm{h}}_A$ are mapped as

$$\begin{pmatrix} \Delta \\ B^\dagger \\ Y \end{pmatrix} \mapsto \begin{pmatrix} (B^\dagger)^\rho \Delta^{1-\rho}(1+\mathcal{O}(\Delta)) \\ \Delta \\ Y + \mathcal{O}(\varepsilon \log B^\dagger) \end{pmatrix}. \tag{3.122}$$

Every point on $\mathcal{I}^\dagger_+(B^\dagger)$ is therefore mapped $\mathcal{O}((B^\dagger)^\rho)$ close to $\mathcal{W}^{\mathrm{u}}(\mathcal{M}^m_\varepsilon)$, and the Y coordinate of each point changes by no more than $\mathcal{O}(\varepsilon \log \varepsilon)$, provided $|B^\dagger|$ is not too small. Since $\mathcal{W}^{\mathrm{u}}(\mathcal{M}^m_\varepsilon)$ is contained in $\mathcal{W}^{\mathrm{s}}(\mathcal{M}^b_\varepsilon)$, we must also have $\mathcal{I}^\dagger_+(B^\dagger) \subseteq \mathcal{W}^{\mathrm{s}}(\mathcal{M}^b_\varepsilon)$, for sufficiently small choice of the constants $\delta_Y, \delta > 0$, and all sufficiently small $\varepsilon > 0$.

Since $\mathcal{I}^\dagger_+(B^\dagger) \subseteq \mathcal{W}^{\mathrm{s}}(\mathcal{M}^b_\varepsilon)$, we can now proceed as in the case of upper N-spike orbits from Sect. 3.10 and construct N-spike orbits passing through $\mathcal{I}^\dagger_+(B^\dagger)$ for each $B^\dagger \in (-\delta, -\varepsilon^\kappa)$, for a constant $\kappa = \kappa(\Delta) > 0$.

We now work to extend the lower family, i.e., those orbits constructed via the sets $\mathcal{I}^*_-(Y^*)$. For each $Y^\dagger \in (-\delta_Y, -C\varepsilon|\log\varepsilon|)$, we consider the curve $\mathcal{I}^\dagger_-(Y^\dagger)$ within $\Sigma^{\mathrm{h}}_{B,-}$ defined by

$$\mathcal{I}^\dagger_-(Y^\dagger) = \{(A, -\Delta, Y^\dagger) : |A| \leq \delta\}. \tag{3.123}$$

We first note that $\mathcal{W}^{\mathrm{u}}(\mathcal{M}^m_\varepsilon) \subset \mathcal{W}^{\mathrm{s}}(\mathcal{M}^b_\varepsilon)$, and in the section $\Sigma^{\mathrm{h}}_{B,-}$, $\mathcal{W}^{\mathrm{u}}(\mathcal{M}^m_\varepsilon)$ is given by the set $\{A = 0\}$; hence, for δ sufficiently small, we have that $\mathcal{I}^\dagger_-(Y^\dagger) \subset \mathcal{W}^{\mathrm{s}}(\mathcal{M}^b_\varepsilon)$. We now aim to show that the backward evolution of $\mathcal{I}^\dagger_-(Y^\dagger)$ under the flow of (3.32) transversely intersects $\mathcal{W}^{\mathrm{u}}(\mathcal{M}^m_\varepsilon)$ within the section Σ^{h}_A, in which case N-spike orbits can be constructed similarly to those constructed via the sets $\mathcal{I}^\dagger_+$ above. We also show that these two constructions have an overlapping region of definition, forming a single continuous family. (We note that it is clear that orbits constructed via the sets $\mathcal{I}^\dagger_-(Y^\dagger)$ have an overlapping region of definition with the lower family constructed via the sets $\mathcal{I}^*_-(Y^*)$.)

We have the following, regarding the local map $\Pi_{\mathrm{loc},-} : \Sigma^{\mathrm{h}}_{B,-} \to \Sigma^{\mathrm{h}}_A$ induced by the backward flow of (3.32), when applied to $\mathcal{I}^\dagger_-(Y^\dagger)$ (Fig. 18).

Lemma 3.17 *For each sufficiently small $\Delta > 0$, there exist $C, \delta_Y, \kappa > 0$ such that the following holds. Consider the set of curves $\mathcal{J}^\dagger_- \subset \Sigma^{\mathrm{h}}_{B,-}$ defined by*

$$\mathcal{J}^\dagger_- := \{\mathcal{I}^\dagger_-(Y^\dagger), Y^\dagger \in (-\delta_Y, -C\varepsilon|\log\varepsilon|)\}. \tag{3.124}$$

This set is mapped by $\Pi_{\mathrm{loc},-}$ onto a set $\{\tilde{\mathcal{I}}^\dagger_-(B^\dagger), B^\dagger \in (-\varepsilon^\kappa, \mathcal{O}(e^{-\eta/\varepsilon}))\} \subset \Sigma^{\mathrm{h}}_A$, where $\tilde{\mathcal{I}}^\dagger_-(B^\dagger)$ is a curve which transversely intersects $\mathcal{W}^{\mathrm{u}}(\mathcal{M}^m_\varepsilon)$ at $B = B^\dagger$.

Proof For a point $(A, -\Delta, Y^\dagger) \in \mathcal{I}_-^\dagger(Y^\dagger)$, we have

$$\Pi_{\mathrm{loc},-}\begin{pmatrix} A \\ -\Delta \\ Y^\dagger \end{pmatrix} \mapsto \begin{pmatrix} \Delta \\ -\Delta R(1+\mathcal{O}(\Delta)) \\ Y^\dagger + \mathcal{O}(\varepsilon \log R) \end{pmatrix}, \tag{3.125}$$

where $A = \Delta R^\rho$.

We proceed similarly as in the proof of Lemma 3.13, solving for when this curve intersects $\mathcal{W}^{\mathrm{u}}(\mathcal{M}_\varepsilon^m)$ within the section Σ_A^{h}. This results in an equation of the form

$$-K\Delta R(1+\mathcal{O}(\Delta, R)) = Y^\dagger - \frac{\varepsilon\gamma \log R}{\beta}(1+\mathcal{O}(\Delta)). \tag{3.126}$$

We use a similar strategy as in the proof of Lemma 3.14 and set $R = R_0R_1$ for some $R_0 > 1$ and obtain the equation

$$-K\Delta R_0R_1(1+\mathcal{O}(\Delta, R_0R_1)) = Y^\dagger - \frac{\varepsilon\gamma \log R_1}{\beta}(1+\mathcal{O}(\Delta)) - \frac{\varepsilon\gamma \log R_0}{\beta}(1+\mathcal{O}(\Delta)). \tag{3.127}$$

We first solve for R_0 in terms of R_1, $Y^\dagger$ by solving

$$-K\Delta R_0R_1(1+\mathcal{O}(\Delta, R_0R_1)) = -\frac{\varepsilon\gamma \log R_0}{\beta}(1+\mathcal{O}(\Delta)). \tag{3.128}$$

After some rearranging, we obtain the equation

$$R_0 = \exp\left(\frac{\beta K\Delta R_1}{\varepsilon\gamma} R_0(1+\mathcal{O}(\Delta, R_0R_1))\right). \tag{3.129}$$

It suffices to solve in the region $0 < R_1 \leq \mathcal{O}(\varepsilon)$, where this relation defines R_0 as a strictly positive, monotone increasing function of R_1; in this region, R_0 is confined to the interval $(1, \tilde{C}(\Delta))$ for some $\tilde{C}(\Delta) > 1$. We substitute back into (3.127), solve for R_1, and obtain the full solution $R = R^\dagger := R_0R_1$ of (3.126), given by

$$R^\dagger = R_0 \exp\left(\frac{\beta Y^\dagger}{\varepsilon\gamma}(1+\mathcal{O}(\Delta))\right). \tag{3.130}$$

Over the interval of $Y^\dagger \in (-\delta_Y, -C\varepsilon|\log\varepsilon|)$ for sufficiently large $C = C(\Delta)$, the locations $R^\dagger$ of intersection span an interval $R^\dagger \in (\varepsilon^\kappa, \mathcal{O}(e^{-\eta/\varepsilon}))$ for some $\kappa = \kappa(\Delta) > 1$. Using (3.125) to determine the corresponding B-coordinate of this intersection, and possibly taking κ slightly larger, we obtain the result. □

Since the choice of $\kappa = \kappa(\Delta) > 0$ in (3.119) was arbitrary, it follows from Lemma 3.17 that N-spike solutions constructed via the sets $\mathcal{I}_-^\dagger(Y^\dagger)$ have an overlapping region of definition with those constructed via $\mathcal{I}_+^\dagger(B^\dagger)$ and thus can be taken to form a single continuous family.

3.12 Proof of Theorem 2.2

In this section, we briefly conclude the proof of the main theorem.

Proof of Theorem 2.2 The transition from the singular Hopf bifurcation and local canard explosion to 1-spike bursting solutions was constructed in Sects. 3.3–3.7.

In Sects. 3.10 and 3.11, upper and lower N-spike bursting solutions were constructed for each $N < \bar{N}$, where $\bar{N} = \mathcal{O}(1/\varepsilon)$. It was also shown that the upper/lower families of N-spike orbits form a continuous family and further that the branch of N-spike orbits is connected to the branch of $(N+1)$-spike orbits via orbits which pass near the upper fold $\mathcal{F}^{\ell}$. Hence, we inductively obtain a single continuous family of orbits beginning with the local canard explosion which contains all of the bursting solutions up to those with $\bar{N}$ spikes.

In order to parameterize the sequence of solutions, by Theorem 3.2, the Hopf bifurcation and local canard explosion occur for $k = k^{\mathrm{sc}}(s, \sqrt{\varepsilon})$ for $s \in (0, \rho]$, and hence, for $\theta \in (0, \rho]$ we set $k^{\mathrm{sa}}(\theta, \sqrt{\varepsilon}) := k^{\mathrm{sc}}(\theta, \sqrt{\varepsilon})$, and we define $\mathcal{B}(\theta, \sqrt{\varepsilon})$ to be the corresponding orbit $\Gamma^{\mathrm{sc}}(s, \sqrt{\varepsilon})$. Next, we recall from Sects. 3.5 that the 0-spike solutions were parameterized by the minimum y-value achieved given by $y = s$ for $s \in [\bar{y}_{\ell} + \Delta, \bar{y}_r - \Delta]$ and

$$|k_0^{\mathrm{sa,lower}}(s, \sqrt{\varepsilon}) - k^{\mathrm{mc}}(\sqrt{\varepsilon})| = \mathcal{O}(e^{-\eta/\varepsilon}). \tag{3.131}$$

We therefore set

$$k^{\mathrm{sa}}(\theta, \sqrt{\varepsilon}) := k_0^{\mathrm{sa,lower}}(\bar{y}_{\ell} + \theta(\bar{y}_r - \bar{y}_{\ell}), \sqrt{\varepsilon}) \tag{3.132}$$

for $\theta \in [\Delta/(\bar{y}_r - \bar{y}_{\ell}), 1 - \Delta/(\bar{y}_r - \bar{y}_{\ell})]$ and we define $\mathcal{B}(\theta, \sqrt{\varepsilon})$ to be the corresponding bursting orbit. Provided Δ is sufficiently small, there will be overlap with the small-amplitude canard orbits from the Hopf bifurcation, in the sense that some orbits could have been constructed as both 0-spike bursting and small-amplitude canard orbits. Since each of these families was constructed using the implicit function theorem, they are locally unique and hence form one continuous family. As these two families were parameterized slightly differently in s, solutions on the overlapping region can be reparameterized if necessary.

For $N \geq 1$, there are two families of N-spike orbits, namely the upper and lower families constructed in Sect. 3.10, which occur for $k = k_N^{\mathrm{sa,upper}}(s, \sqrt{\varepsilon})$ and $k = k_N^{\mathrm{sa,lower}}(s, \sqrt{\varepsilon})$, respectively, where $s \in [\bar{y}_{\ell} + \Delta, \bar{y}_{\mathrm{h}} - \Delta]$ denotes the y-layer of the fast jump $\phi^u(s)$ or $\phi^b(s)$ which is followed.

We therefore set

$$k^{\mathrm{sa}}(\theta, \sqrt{\varepsilon}) := \begin{cases} k_N^{\mathrm{sa,upper}}(\bar{y}_{\ell} + 2(\theta - N)(\bar{y}_{\mathrm{h}} - \bar{y}_{\ell}), \sqrt{\varepsilon}), & \theta \in \left[N + \frac{\Delta}{2(\bar{y}_{\mathrm{h}} - \bar{y}_{\ell})}, N + \frac{1}{2} - \frac{\Delta}{2(\bar{y}_{\mathrm{h}} - \bar{y}_{\ell})}\right] \\ k_N^{\mathrm{sa,lower}}(\bar{y}_{\ell} + 2(N + 1 - \theta)(\bar{y}_{\mathrm{h}} - \bar{y}_{\ell}), \sqrt{\varepsilon}), & \theta \in \left[N + \frac{1}{2} + \frac{\Delta}{2(\bar{y}_{\mathrm{h}} - \bar{y}_{\ell})}, N + 1 - \frac{\Delta}{2(\bar{y}_{\mathrm{h}} - \bar{y}_{\ell})}\right] \end{cases} \tag{3.133}$$

and we define $\mathcal{B}(\theta, \sqrt{\varepsilon})$ to be the corresponding bursting orbit. In Sect. 3.10, it is shown that there exists a family of solutions which pass near the fold $\mathcal{F}^\ell$ which form a bridge between the lower N-spike solutions and upper $(N+1)$-spike solutions. Further, in Sect. 3.11 it is shown that there exists a family of solutions which pass near the saddle homoclinic bifurcation which form a bridge between the upper and lower N-spike solutions, which are not naturally parameterized by the y-jump which was followed, and hence, we may reparameterize $k^{\mathrm{sa}}(\theta, \sqrt{\varepsilon})$ on the intervals

$$\theta \in \left[N + \frac{1}{2} - \frac{\Delta}{2(\bar{y}_{\mathrm{h}} - \bar{y}_\ell)}, N + \frac{1}{2} + \frac{\Delta}{2(\bar{y}_{\mathrm{h}} - \bar{y}_\ell)}\right] \cup \left[N - \frac{\Delta}{2(\bar{y}_{\mathrm{h}} - \bar{y}_\ell)}, N + \frac{\Delta}{2(\bar{y}_{\mathrm{h}} - \bar{y}_\ell)}\right] \tag{3.134}$$

for each N to account for this. We therefore obtain N spike bursting solutions for $N < \bar{N}(\varepsilon)$, corresponding to $\theta \in (0, \Theta(\varepsilon))$, where $\Theta(\varepsilon) := \bar{N}(\varepsilon) = \mathcal{O}(1/\varepsilon)$.

Finally, the estimate

$$|k^{\mathrm{sa}}(\theta, \sqrt{\varepsilon}) - k^{\mathrm{mc}}(\sqrt{\varepsilon})| = \mathcal{O}(e^{-\eta/\varepsilon}) \tag{3.135}$$

for $\theta > \rho$ follows from estimates (3.21) and analogous estimates for the solutions with additional spikes. □

4 Discussion

In this paper, we considered a class of three-dimensional singularly perturbed ODEs under general assumptions which guarantee the existence of a one-parameter family of periodic bursting orbits, encompassing the spike-adding transition from a local canard explosion to large-amplitude bursting oscillations with an $\mathcal{O}(1/\varepsilon)$-number of spikes. Among the geometric features necessary for this construction is a cubic critical manifold, where the middle branch is of saddle type and one of the folds is a canard point (Krupa and Szmolyan 2001a), which allows for a local canard explosion as well as long canard trajectories along the middle branch. The other crucial feature is a saddle homoclinic bifurcation on the middle branch in the fast subsystem, from which bifurcates a family of periodic orbits in the layer problem.

The construction of the spike-adding sequence was obtained by considering the global aspects of the flow via geometric singular perturbation theory as well as calling on prior results for local analyses of the fold points (Carter and Sandstede 2015; Krupa and Szmolyan 2001a). New to this work is a detailed analysis of slow passage through the saddle homoclinic bifurcation, which was essential for guaranteeing the transverse construction of the bursting solutions as well as ensuring that the branches of N-spike and $(N+1)$-spike bursting solutions are in fact connected, so that the entire sequence forms a single uninterrupted branch. The analysis of this bifurcation is based on well known homoclinic bifurcation theory (Homburg and Sandstede 2010) combined with Shilnikov-type estimates (Deng 1990; Krupa et al. 1997; Schecter 2008a). Of particular difficulty is tracking solutions in this region for $\mathcal{O}(1/\varepsilon)$ time,

for which new analysis involving geometric singular perturbation methods is necessary.

We remark on the relation of the bursting solutions constructed here to the classical square-wave-type bursting solutions studied in detail in prior works (Terman 1991, 1992), in which solutions were constructed using similar geometric ideas. However, ultimately the geometry of the classical bursting solutions differs in that they are constructed outside the canard regime and involve trajectories which "fall off" the fold point $\mathcal{F}^r$ onto the periodic manifold $\mathcal{P}_\varepsilon$ (Fig. 6), rather than continue up the middle branch $\mathcal{M}_\varepsilon^m$ along a canard trajectory before doing so. In particular, for such solutions to exist, one must have that the periodic manifold $\mathcal{P}_\varepsilon$ extends to some value of $\bar{y}_{\mathrm{p}} > \bar{y}_r$. Associated with these solutions are rich dynamics and chaotic behavior (Terman 1992), and without further detailed analysis, it is not immediately obvious that these solutions lie on the same branch as those constructed in Theorem 2.2, or whether a continuous spike-adding process persists into this region, though numerical evidence suggests this is the case (Fig. 2). Under additional technical assumptions, we expect that the solutions constructed in Theorem 2.2 should indeed lie on the same branch as the classical solutions, with the spike-adding process continuing upon varying k. While the focus of the current work is on the onset of the spike-adding process as a canard-induced phenomenon, we expect that similar methods will be applicable in this regime. This is beyond the scope of this paper and is the subject of ongoing work.

While the assumptions for system (2.1) are fairly general, in a broader sense the geometric setup is still rather specific. Systems such as the Morris–Lecar–Terman model (1.1) fit directly into such a framework, and other three-dimensional square-wave bursting models, such as the Hindmarsh–Rose model, which admits Hopf bifurcations and an additional saddle homoclinic bifurcation in the layer problem (Desroches et al. 2013), could be analyzed via the same analysis, with some additional steps, to obtain a result analogous to Theorem 2.2. However, systems with more complicated geometry would require the analysis of canard phenomena not treated in this work; for instance, the role of folded saddle canards on a two-dimensional slow manifold has been emphasized in some four-dimensional parabolic bursting oscillation models (Desroches et al. 2016b). Additionally, slow passage through a spike-adding bifurcation has been used to explain the phenomenon of mixed-mode bursting oscillations (Desroches et al. 2013). We note that canards and saddle homoclinic bifurcations are still identified in these contexts as being important for the spike-adding phenomenon, and we emphasize that the techniques used in this current work are general; the fundamental idea involves combining local and global analyses, geometric singular perturbation methods, blow-up, and homoclinic bifurcation theory in such a way that global transitions between different solutions can be captured. These techniques likely have wide applicability into these more complicated bifurcation scenarios, and this will be the subject of future work. Furthermore, we remark that these methods are not limited to the study of bursting solutions or periodic orbits in ODEs; for example, similar methods were used with success in constructing transitions between single and double traveling pulse solutions in the FitzHugh–Nagumo system (Carter and Sandstede 2018).

Acknowledgements The author gratefully acknowledges support through NSF Grant DMS-2016216 (formerly DMS-1815315).

A Estimates Near the Saddle Homoclinic Point

In this section, we present a proof of Lemma 3.11. We first quote the following result regarding the nature of solutions to the boundary value problem with entry/exit conditions in the sections $\Sigma_A^{\mathrm{h}}, \Sigma_B^{\mathrm{h}}$.

Proposition A.1 (Schecter 2008a, Theorem 2.1) *Fix $\Delta > 0$ small. There exists $K_0, \eta > 0$ such that the following holds. For any sufficiently small $\varepsilon > 0$, any $T > 0$ and any $|Y^*| \leq \delta_Y$, there exists a solution $(A, B, Y)(\xi; Y^*, T)$ to (3.32) with $(A, B, Y)(0) \in \Sigma_A^{\mathrm{h}}$ and $(A, B, Y)(T) \in \Sigma_B^{\mathrm{h}}$ with $Y(T; Y^*, T) = Y^*$. Furthermore,*

$$\begin{aligned} |A(\xi; Y^*, T)| &\leq K_0 e^{-\eta\xi} \\ |B(\xi; Y^*, T)| &\leq K_0 e^{\eta(\xi - T)} \\ |Y(\xi; Y^*, T) - \Phi(\xi, Y^*, T)| &\leq K_0 \varepsilon e^{-\eta T}, \end{aligned} \tag{A.1}$$

where $\Phi(\xi, Y^*, T)$ denotes the solution of $\dot{Y} = \varepsilon G_1(Y, k, \varepsilon)$ satisfying $Y(T) = Y^*$. The partial derivatives of $(A, B, Y)(\xi; Y^*, T)$ with respect to ξ, Y^*, T up to order r satisfy the same estimates.

Remark A.2 We remark on the appearance of the factor of ε appearing in estimates (A.1) for the solution $Y(\xi; Y^*, T)$ which is not present in Schecter (2008a, Theorem 2.1). This is due to the fact that the Y-dynamics are of $\mathcal{O}(\varepsilon)$, in contrast to the more general case in Schecter (2008a), where there is no small parameter and hence the center dynamics are $\mathcal{O}(1)$.

Proof of Lemma 3.11 We use the formulation of Proposition A.1 to prove the estimates on the local map Π_{loc}. We fix $\Delta > 0$ and assume $0 < \delta_Y, \delta \ll \Delta$ are taken sufficiently small.

For a solution $(A, B, Y)(\xi; Y^*, T)$ of Proposition A.1, we set $\tilde{A}(Y^*, T) := A(T; Y^*, T)$ and $\tilde{B}(Y^*, T) := B(0; Y^*, T) = \mathcal{O}(e^{-\eta T})$. The map Π_{loc} is then determined by

$$\begin{aligned} B_{\mathrm{loc}}(R, Y^*) &= \tilde{B}(Y^*, T) \\ Y_{\mathrm{loc}}(R, Y^*) &= Y(0; Y^*, T). \end{aligned} \tag{A.2}$$

where R is defined via the relation $\Delta R^\rho = \tilde{A}(Y^*, T)$, and the exponent ρ is as yet to be determined.

Let $\Phi(\xi, Y^*, T)$ denote the solution of $\dot{Y} = \varepsilon G_1(Y, k, \varepsilon)$ satisfying $Y(T) = Y^*$; in particular, $\Phi(\xi, Y^*, T)$ satisfies the integral equation

$$\Phi(\xi, Y^*, T) = Y^* + \int_T^\xi \varepsilon G_1(\Phi(\xi, Y^*, T), k, \varepsilon) \mathrm{d}\xi, \tag{A.3}$$

and we have the estimates

$$\begin{aligned}\Phi(0, Y^*, T) &= Y^* + \varepsilon\gamma T(1 + \mathcal{O}(\Delta))\\ \partial_{Y^*}\Phi(\xi, Y^*, T) &= 1 + \mathcal{O}(\Delta)\\ \partial_T\Phi(\xi, Y^*, T) &= \mathcal{O}(\varepsilon).\end{aligned} \tag{A.4}$$

We now define the functions

$$\begin{aligned}\tilde{\alpha}_0(Y^*, T) &:= \int_0^T F_1(0, 0, \Phi(\xi, Y^*, T), k, \varepsilon)\mathrm{d}\xi\\ &= \int_0^T \alpha + \mathcal{O}(\Phi, \varepsilon)\mathrm{d}\xi\\ \tilde{\beta}_0(Y^*, T) &:= \int_0^T F_2(0, 0, \Phi(\xi, Y^*, T), k, \varepsilon)\mathrm{d}\xi\\ &= \int_0^T \beta + \mathcal{O}(\Phi, \varepsilon)\mathrm{d}\xi,\end{aligned} \tag{A.5}$$

where

$$\begin{aligned}\partial_{Y^*}\tilde{\alpha}_0(Y^*, T) &= \mathcal{O}(T)\\ \partial_T\tilde{\alpha}_0(Y^*, T) &= \alpha + \mathcal{O}(\Delta)\\ \partial_{Y^*}\tilde{\beta}_0(Y^*, T) &= \mathcal{O}(T)\\ \partial_T\tilde{\beta}_0(Y^*, T) &= \beta + \mathcal{O}(\Delta).\end{aligned} \tag{A.6}$$

We further define the functions

$$\begin{aligned}\tilde{\alpha}(Y^*, T) &:= \int_0^T F_1\left(A(\xi; Y^*, T), B(\xi; Y^*, T), Y(\xi; Y^*, T), k, \varepsilon\right)\mathrm{d}\xi\\ \tilde{\beta}(Y^*, T) &:= \int_0^T F_2\left(A(\xi; Y^*, T), B(\xi; Y^*, T), Y(\xi; Y^*, T), k, \varepsilon\right)\mathrm{d}\xi.\end{aligned} \tag{A.7}$$

We use the estimates in Proposition A.1 combined with directly integrating Eq. (3.32) in reverse time and obtain

$$\begin{aligned}\tilde{A} &= \Delta\exp\left(-\tilde{\alpha}(Y^*, T)\right)\\ \tilde{B} &= \Delta\exp\left(-\tilde{\beta}(Y^*, T)\right).\end{aligned} \tag{A.8}$$

Using these expressions along with estimates (A.1), we have that

$$\begin{aligned}|\tilde{\alpha}(Y^*, T) - \tilde{\alpha}_0(Y^*, T)| &= \mathcal{O}(\Delta)\\ |\tilde{\beta}(Y^*, T) - \tilde{\beta}_0(Y^*, T)| &= \mathcal{O}(\Delta)\end{aligned} \tag{A.9}$$

and the partial derivatives of these expressions with respect to Y^*, T are also $\mathcal{O}(\Delta)$.

The ultimate goal is to express the quantities $\tilde{B}$ and $Y(0; Y^*, T)$ in terms of the quantities R, Y^*, where we define

$$R = \left(\frac{\tilde{A}}{\Delta}\right)^{\tilde{\beta}_0/\tilde{\alpha}_0}. \tag{A.10}$$

To achieve this, we recall (A.8) combined with (A.9)

$$\begin{aligned} \tilde{A} &= \Delta \exp\left(-\tilde{\alpha}_0(Y^*, T) + \mathcal{O}(\Delta)\right) \\ &= \Delta \exp\left(-\tilde{\alpha}_0(Y^*, T)\right)(1 + \mathcal{O}(\Delta)), \end{aligned} \tag{A.11}$$

where the derivatives of the $\mathcal{O}(\Delta)$ remainder terms with respect to Y^*, T are also $\mathcal{O}(\Delta)$. Hence,

$$\begin{aligned} R &= \left(\frac{\tilde{A}}{\Delta}\right)^{\tilde{\beta}_0/\tilde{\alpha}_0} \\ &= \exp\left(-\tilde{\beta}_0(Y^*, T)\right)(1 + \mathcal{O}(\Delta))^{\tilde{\beta}_0/\tilde{\alpha}_0}. \end{aligned} \tag{A.12}$$

This relation can be used to solve for $T = T(R, Y^*)$, obtaining

$$T(R, Y^*) = -\frac{\log R}{\beta}(1 + \mathcal{O}(\Delta)). \tag{A.13}$$

Note, due to the exponent $\tilde{\beta}_0/\tilde{\alpha}_0$ appearing in the remainder term of (A.12), the derivatives of the remainder terms in (A.13) with respect to R, Y^* no longer satisfy the same estimates. However, we are still able to estimate the first order partial derivatives

$$\begin{aligned} \partial_R T(R, Y^*) &= -\frac{1}{\beta R}(1 + \mathcal{O}(\Delta)) \\ \partial_{Y^*} T(R, Y^*) &= \mathcal{O}(\log R), \end{aligned} \tag{A.14}$$

by implicitly differentiating (A.12).

We set $B_{\text{loc}}(R, Y^*) := \tilde{B}$ and determine

$$\begin{aligned} \tilde{B} &= \Delta \exp\left(-\tilde{\beta}_0(Y^*, T)\right)(1 + \mathcal{O}(\Delta)) \\ &= \Delta R(1 + \mathcal{O}(\Delta)), \end{aligned} \tag{A.15}$$

where the derivatives of the $\mathcal{O}(\Delta)$ remainder terms with respect to Y^*, T are also $\mathcal{O}(\Delta)$, and using the expressions (A.14), we obtain

$$\begin{aligned} \partial_R B_{\text{loc}}(R, Y^*) &= \Delta(1 + \mathcal{O}(\Delta)) \\ \partial_{Y^*} B_{\text{loc}}(R, Y^*) &= \mathcal{O}(R \log R). \end{aligned} \tag{A.16}$$

Next, using (A.1), (A.4), and (A.14), and setting $Y_{\rm loc}(R, Y^*) := Y(0)$, we have that

$$\begin{aligned} Y_{\rm loc}(R, Y^*) &= Y^* - \frac{\varepsilon\gamma \log R}{\beta}\,(1 + \mathcal{O}(\Delta)) \\ \partial_R Y_{\rm loc}(R, Y^*) &= -\frac{\varepsilon\gamma}{\beta R}\,(1 + \mathcal{O}(\Delta)) \\ \partial_{Y^*} Y_{\rm loc}(R, Y^*) &= 1 + \mathcal{O}(\Delta). \end{aligned} \tag{A.17}$$

Finally, we define $\rho(R, Y^*) := \tilde{\alpha}_0/\tilde{\beta}_0$, and using (A.5) and (A.14), we have

$$\begin{aligned} \rho(R, Y^*) &= \alpha/\beta + \mathcal{O}(\Delta) \\ \partial_R \rho(R, Y^*) &= \mathcal{O}\left(\frac{\Delta}{R \log R}\right) \\ \partial_{Y^*} \rho(R, Y^*) &= \mathcal{O}(1), \end{aligned} \tag{A.18}$$

which completes the proof of estimates (3.41). □

References

Al-Naimee, K., Marino, F., Ciszak, M., Meucci, R., Arecchi, F.T.: Chaotic spiking and incomplete homoclinic scenarios in semiconductor lasers with optoelectronic feedback. New J. Phys. **11**(7), 073022 (2009)

Carter, P., Sandstede, B.: Fast pulses with oscillatory tails in the FitzHugh–Nagumo system. SIAM J. Math. Anal. **47**(5), 3393–3441 (2015)

Carter, P., Sandstede, B.: Unpeeling a homoclinic banana in the FitzHugh–Nagumo system. SIAM J. Appl. Dyn. Syst. **17**(1), 236–349 (2018)

Chay, T.R., Keizer, J.: Minimal model for membrane oscillations in the pancreatic beta-cell. Biophys. J. **42**(2), 181–189 (1983)

Deng, B.: Homoclinic bifurcations with nonhyperbolic equilibria. SIAM J. Math. Anal. **21**(3), 693–720 (1990)

Desroches, M., Kaper, T.J., Krupa, M.: Mixed-mode bursting oscillations: dynamics created by a slow passage through spike-adding canard explosion in a square-wave burster. Chaos **23**(4), 046106 (2013)

Desroches, M., Fernández-García, S., Krupa, M.: Canards in a minimal piecewise-linear square-wave burster. Chaos **26**(7), 073111 (2016)

Desroches, M., Krupa, M., Rodrigues, S.: Spike-adding in parabolic bursters: the role of folded-saddle canards. Physica D **331**, 58–70 (2016)

Dumortier, F., Roussarie, R.H.: Canard cycles and center manifolds, volume 577. American Mathematical Soc (1996)

Eckhaus, W.: Relaxation oscillations including a standard chase on French ducks. In: Asymptotic Analysis II, pp. 449–497. Springer (1983)

Fenichel, N.: Persistence and smoothness of invariant manifolds for flows. Indiana Univ. Math. J. **21**(3), 193–226 (1971)

Fenichel, N.: Geometric singular perturbation theory for ordinary differential equations. J. Differ. Equ. **31**(1), 53–98 (1979)

Guckenheimer, J., Kuehn, C.: Computing slow manifolds of saddle type. SIAM J. Appl. Dyn. Syst. **8**(3), 854–879 (2009)

Hindmarsh, J.L., Rose, R.M.: A model of the nerve impulse using two first-order differential equations. Nature **296**(5853), 162 (1982)

Hindmarsh, J.L., Rose, R.M.: A model of neuronal bursting using three coupled first order differential equations. Proc. R. Soc. Lond. B **221**(1222), 87–102 (1984)

Homburg, A.J., Sandstede, B.: Homoclinic and heteroclinic bifurcations in vector fields. Handb. Dyn. Syst. **3**, 379–524 (2010)
Kinney, W.M.: An application of Conley index techniques to a model of bursting in excitable membranes. J. Differ. Equ. **162**(2), 451–472 (2000)
Kinney, W.M.: Applying the Conley index to fast-slow systems with one slow variable and an attractor. Rocky Mt. J. Math. **38**(4), 1177–1214 (2008)
Krupa, M., Sandstede, B., Szmolyan, P.: Fast and slow waves in the FitzHugh–Nagumo equation. J. Differ. Equ. **133**(1), 49–97 (1997)
Krupa, M., Szmolyan, P.: Extending geometric singular perturbation theory to nonhyperbolic points–fold and canard points in two dimensions. SIAM J. Math. Anal. **33**(2), 286–314 (2001)
Krupa, M., Szmolyan, P.: Relaxation oscillation and canard explosion. J. Differ. Equ. **174**(2), 312–368 (2001)
Lee, E., Terman, D.: Uniqueness and stability of periodic bursting solutions. J. Differ. Equ. **158**(1), 48–78 (1999)
Lin, X.-B.: Using Melnikov's method to solve Silnikov's problems. Proc. R. Soc. Edinb. Sect. A: Math. **116**(3–4), 295–325 (1990)
Linaro, D., Champneys, A., Desroches, M., Storace, M.: Codimension-two homoclinic bifurcations underlying spike adding in the Hindmarsh–Rose burster. SIAM J. Appl. Dyn. Syst. **11**(3), 939–962 (2012)
Morris, C., Lecar, H.: Voltage oscillations in the barnacle giant muscle fiber. Biophys. J. **35**(1), 193–213 (1981)
Nowacki, J., Osinga, H.M., Tsaneva-Atanasova, K.: Dynamical systems analysis of spike-adding mechanisms in transient bursts. J. Math. Neurosci. **2**(1), 1–28 (2012)
Osinga, H.M., Tsaneva-Atanasova, K.T.: Dynamics of plateau bursting depending on the location of its equilibrium. J. Neuroendocrinol. **22**(12), 1301–1314 (2010)
Plant, R.E., Kim, M.: On the mechanism underlying bursting in the Aplysia abdominal ganglion R15 cell. Math. Biosci. **26**(3–4), 357–375 (1975)
Rinzel, J.: Bursting oscillations in an excitable membrane model. In: *Ordinary and partial differential equations*, pp. 304–316. Springer (1985)
Rinzel, J.: A formal classification of bursting mechanisms in excitable systems. In: Mathematical Topics in Population Biology, Morphogenesis and Neurosciences, pp. 267–281. Springer (1987)
Rinzel, J., Troy, W.C.: Bursting phenomena in a simplified oregonator flow system model. J. Chem. Phys. **76**(4), 1775–1789 (1982)
Rinzel, J., Ermentrout, G.B.: Analysis of neural excitability and oscillations. Methods Neuronal. Model. 135–169 (1989)
Ruschel, S., Yanchuk, S.: Chaotic bursting in semiconductor lasers. Chaos Interdiscip. J. Nonlinear Sci. **27**(11), 114313 (2017)
Schecter, S.: Exchange lemmas 1: Deng's lemma. J. Differ. Equ. **245**(2), 392–410 (2008)
Schecter, S.: Exchange lemmas 2: general exchange lemma. J. Differ. Equ. **245**(2), 411–441 (2008)
Terman, D.: Chaotic spikes arising from a model of bursting in excitable membranes. SIAM J. Appl. Math. **51**(5), 1418–1450 (1991)
Terman, D.: The transition from bursting to continuous spiking in excitable membrane models. J. Nonlinear Sci. **2**(2), 135–182 (1992)
Tsaneva-Atanasova, K., Osinga, H.M., Rieß, T., Sherman, A.: Full system bifurcation analysis of endocrine bursting models. J. Theor. Biol. **264**(4), 1133–1146 (2010)